EXPLORING COSMIC STRINGS: OBSERVABLE EFFECTS AND COSMOLOGICAL CONSTRAINTS

A dissertation

submitted by

Eray Sabancilar

In partial fulfilment of the requirements

for the degree of

Doctor of Philosophy

in

Physics

TUFTS UNIVERSITY

May 2011

ADVISOR: Prof. Alexander Vilenkin

To my parents Afife and Erdal,

and to the memory of my grandmother Fadime

Abstract

Observation of cosmic (super)strings can serve as a useful hint to understand the fundamental theories of physics, such as grand unified theories (GUTs) and/or superstring theory. In this regard, I present new mechanisms to produce particles from cosmic (super)strings, and discuss their cosmological and observational effects in this dissertation.

The first chapter is devoted to a review of the standard cosmology, cosmic (super)strings and cosmic rays.

The second chapter discusses the cosmological effects of moduli. Moduli are relatively light, weakly coupled scalar fields, predicted in supersymmetric particle theories including string theory. They can be emitted from cosmic (super)string loops in the early universe. Abundance of such moduli is constrained by diffuse gamma ray background, dark matter, and primordial element abundances. These constraints put an upper bound on the string tension as strong as $G\mu \lesssim 10^{-28}$ for a wide range of modulus mass m. If the modulus coupling constant is stronger than gravitational strength, modulus radiation can be the dominant energy loss mechanism for the loops. Furthermore, modulus lifetimes become shorter for stronger coupling. Hence, the constraints on string tension $G\mu$ and modulus mass m are significantly relaxed for strongly coupled moduli predicted in superstring theory. Thermal production of these particles and their possible effects are also considered.

In the third chapter, moduli emitted from cosmic string cusps are studied. Highly boosted modulus bursts emanating from cusps subsequently decay into gluons and generate hadronic cascades which in turn produce large number of

neutrinos. For reasonable values of the modulus mass and coupling constant, observable ultra high energy neutrino fluxes can be produced for a wide range of string tension $G\mu$.

The fourth chapter discusses cosmic rays produced by the charged particles ejected from cusps of superconducting cosmic strings. In many particle physics theories, cosmic strings respond to external magnetic fields, e.g., in clusters of galaxies, and develop currents. Observable UHE neutrino fluxes can be achieved for a range of symmetry breaking scale of strings. In this model, neutrinos with $E \gtrsim 10^{11}$ GeV are expected in correlation with clusters of galaxies. Another unique signature of the model is simultaneous appearance of several neutrino-produced showers in the field of view of very large detectors, such as JEM-EUSO. The flux of UHE protons from cusps may account for a large fraction of the observed events at the highest energies.

The dissertation ends with overall conclusions.

Acknowledgements

First of all, I would like to thank my advisor and the director of the Tufts Institute of Cosmology Prof. Alexander Vilenkin for his patience, encouragement and helping me generously with any problems I had. Among his many other incredible abilities, I witnessed his intuitive and clear way of thinking as he made a very complicated subject easily understandable during the lectures he taught and our private discussions. Therefore, I think myself as extremely lucky to have a chance to work with him. I was also a close witness of how he could turn a naive enthusiastic mind with unfocused ideas into a theoretical physicist. This work would not be possible without him.

I would like to thank my collaborators and my secondary mentors Prof. Veniamin Berezinsky for the so many things I have learnt while working with him, and Prof. Ken Olum for introducing me my first research project. Prof.Krzysztof Sliwa, you are such a great person and a graduate student advisor. Thank you for giving me a chance to work with the experimental high energy group at CERN, helping me getting over the problems I faced with during my study at Tufts, and providing a stimulating, free research environment for the graduate students. Prof. Larry Ford, Prof. Jose-Juan Blanco-Pillado, Prof. Tony Mann, Prof. Jack Schneps, Prof. Austin Napier and Prof. George Leger, thank you all for the incredible lectures that you taught. Special thanks to Prof. Tanmay Vachaspati for kindly accepting to be in my dissertation committee.

I would like to thank my friends at Tufts graduate physics program, Handhika Ramadhan, Spencer Smith, Doug Urban, Yuji Zhang and Konstantinos Metallinos for their support and close friendship, department manager Shan-

non Landis and our absolutely great secretary Gayle Grant for their help with the administrative issues.

I would like to thank many great friends of mine in Boston: Yavuz Kilic, Yetkin Yilmaz, Hakan Sonmez, Ozan Candogan, Baris Nakiboglu, Leif Eckstrom, and all the members of my music band "On": Ilke Kalcioglu, Yalcin Cayir, Ozgur Amac, Aylin Kentkur and Guner Celik. Thank you all for supporting me, making me feel like home and never feeling alone in a foreign country five thousand miles away from home.

I would also like to thank my Professors at Middle East Technical University, Prof. Namik Kemal Pak, Prof. Atalay Karasu and Prof. Bayram Tekin for providing me the very first knowledge in theoretical physics and encouraging me to continue my career as a Ph.D. student in the US.

My best friends Gokhan Savas, Alper Bese, Onur Yasar, Ozlem Savas, Sinem Kubilay, Ebru Kaya Yasar, and especially Gurdal Sur and Riza Demirbilek, who are responsible for pushing me into the world of physics, thank you all for believing in me and supporting me since I was a little kid. Gokhan Savas, you have been a brother to me since I met you, but especially for the last five years in the US, your support has been lifesaving by any means.

And special thanks go to my mother Afife, my father Erdal and my sister Deniz, who have always believed in me and supported me with their endless love and care. My grandmother Fadime, thank you for raising me up with incredible love and care; rest in peace.

Contents

List of Tables

List of Figures

Chapter 1

Introduction

"The universe is the poor man's accelerator." Yakov Borisovich Zel'dovich

Cosmic (super)strings and other topological defects could serve as traces of the early universe if they exist. They are the *Hieroglyphs* of the universe which carry that information in their very core. *Hieroglyphs* can only tell us about what happened a couple of thousands years ago, whereas topological defects can do a lot better: They can tell us about the very beginning of the universe since they carry the energy densities of the time they are formed, namely energy scales of Grand Unified Theories (GUTs) and/or superstring theory.

Topological defects arise as stable solutions in particle physics models, which include domain walls, cosmic strings, monopoles and textures. The stability of such objects is guaranteed by topological reasons, hence the name. Cosmic superstrings, on the other hand, can be formed at the end of the so called brane inflation –a model of inflation in Type IIB string theory– and

share most of the properties of the ordinary cosmic strings[1].

Monopoles and local domain walls could be disastrous for the universe if they exist. Since monopoles act as nonrelativistic matter, they rapidly dominate the energy density of the universe [5]. Domain walls also dominate the energy density quickly and have unacceptably large gravitational field that cause large anisotropies in the CMB [6, 7]. Cosmic strings, on the other hand, can exist without causing much trouble. They can actually be responsible for the highest energy events occurring in the universe, such as ultra high energy (UHE) cosmic rays [8, 9, 10, 11]. They can also produce a variety of other observational effects, which include gravitational lensing [7, 12], linear discontinuities in the cosmic microwave background (CMB) [13, 14, 15, 16, 17], B-mode polarization of the CMB photons [18], electromagnetic bursts [19, 20, 21, 22] and gravitational radiation, both in the form of a stochastic background and localized bursts [23, 24].

Of particular interest to this dissertation are the UHE particles, especially neutrinos, emanating from cusps –parts of cosmic string loops where extremely large Lorentz factors are achieved momentarily– and observational constraints resulting from string interaction with moduli predicted in supersymmetric theories.

This dissertation is organized as follows: In the following sections of this chapter, a brief history of the universe is given to set the grounds and the notation. Then, various properties of cosmic (super)strings including their formation, evolution and effects on cosmology are discussed. Finally, a review about cosmic rays with a particular emphasis on UHE neutrinos is given.

[1]For an extensive review of the subject, see [1, 2, 3, 4].

In Chapter 2, cosmological constraints on scalar particles emitted from cosmic string loops at earlier epochs are discussed with a special attention given to the strongly coupled moduli. The production mechanism relies on the existence of moduli –relatively light, weakly coupled scalar fields, predicted in supersymmetric particle theories, including string theory. Moduli couple to strings linearly and would be copiously radiated by oscillating loops of string at early cosmic times when the loops are very small and their frequency of oscillation is greater than the modulus mass. The emitted moduli and their decay products can manifest themselves observationally in many different ways. Abundance of such moduli is constrained by diffuse gamma ray background, dark matter, and primordial element abundances if their lifetime is of the order of the relevant cosmic time. This leads to stringent constraints on both the cosmic string tension and modulus mass for the moduli with gravitational-strength couplings to matter [25, 26, 27]. It will be shown that the constraints from modulus radiation are significantly relaxed when the couplings are much stronger [28]. Such strongly coupled moduli appear to be quite generic in superstring theory [29, 30, 31, 32, 33, 34, 35].

In Chapter 3, modulus emission from cosmic string cusps is studied. At late times, moduli can only be emitted from cusps since the characteristic frequency of loop oscillation is much smaller than the mass of a modulus. Therefore, modulus production is suppressed, except in the vicinity of cusps, where extremely high frequencies can be reached. Hence, sharp bursts of high energy moduli are emitted from cosmic string loops and eventually moduli decay into standard model particles. Gravitationally coupled moduli have very long mean lifetimes, thus the cosmic ray fluxes are negligible. On the other

hand, for stronger coupling, moduli production by cosmic strings is enhanced by α^2, where α/m_p is the modulus coupling constant. They also decay faster since their mean lifetime, $\tau \propto \alpha^{-2}$, where $\alpha >> 1$. It will be shown that this way their decay products can yield observable cosmic ray fluxes, in particular UHE neutrinos that can be detected at the future sensitive detectors such as space based neutrino observatory JEM-EUSO.

In Chapter 4, a different mechanism to emit particles from cusps of cosmic string loops is studied. Cosmic strings predicted in many grand unified models respond to external electromagnetic fields as thin superconducting wires. As they move through cosmic magnetic fields, such strings develop electric currents. Oscillating loops of current-carrying string emit highly boosted charged particles from cusps. The emitted particles and their decay products can be observed as UHE cosmic rays. It is found that observable UHE neutrino and proton fluxes can be obtained for a wide range of cosmic string parameters [11].

The dissertation ends with the overall conclusions.

Natural units along with the Gaussian units are used in this dissertation, namely, Planck constant $\hbar = 1$, speed of light $c = 1$, Boltzmann's constant $k_B = 1$, unit electric charge $e = 0.1$. The following conversion relations and quantities will be used quite often: Newton's constant $G = m_p^{-2}$, Planck mass $m_p = 1.2 \times 10^{19}$GeV, Planck time $t_p = 5.4 \times 10^{-44}$s, 1GeV$= 1.8 \times 10^{-24}$g, 1GeV$^{-1} = 2.0 \times 10^{-14}cm= 6.6 \times 10^{-25}$s, 1GeV$= 1.2 \times 10^{13}$K, 1Gauss$= 7.0 \times 10^{-20}$GeV^2, 1Mpc$= 3.1 \times 10^{24}$cm.

1.1 Brief history of the universe

The standard model of the universe is based on the following basic observational facts: Recession of galaxies, homogeneity and isotropy of the cosmic microwave background (CMB) –the relic radiation that propagates to us from the time at which the universe became transparent to photons. This can be summarized as a cosmological principle: The universe is homogeneous and isotropic beyond the scales of order 100 Mpc. In other words, on large scales there is no center to the universe. The isotropy is clearly seen in the CMB data up to accuracy about one part in 10^5 [36]. The expansion along with the CMB suggests that the universe was hot and dense in the beginning. As it cooled down and the initial perturbations grew, structures such as stars, galaxies and clusters were formed.

Friedmann found a solution to the Enstein's equation for an expanding universe in 1922 and showed that the expansion rate can be calculated from the so called Friedman equations [37]. Georges Lemaitre independently found similar solutions and derived what is known as Hubble law in 1927 [38]. In 1929, Edwin Hubble showed the linear relationship between the recession velocities of the galaxies and their distance as [39]

$$v = H_0 r, \tag{1.1}$$

where $H_0 = 100h\,km/s/Mpc$ is the Hubble parameter at the present epoch and $h = 0.7$ [36]. The metric describing the modern cosmology was derived by Robertson and Walker on the basis of homogeneity and isotropy [40, 41].

In the comoving coordinates, the Robertson-Walker (RW) metric is given by

$$ds^2 = -dt^2 + a^2(t)\left(\frac{dr^2}{1-kr^2} + r^2 d\Omega_2\right), \tag{1.2}$$

where $a(t)$ is the scale factor representing the relative size of the spacelike hypersurfaces as a function of coordinate time t and k is the curvature parameter. $k = +1,\ 0,\ -1$ for a closed, flat and open Friedman-Lemaitre-Robertson-Walker (FLRW) universe, respectively. As the universe expands, the frequency of a photon redshifts as its wavelength is stretched by the expansion. Redshift is defined as $1 + z = \lambda_{observed}/\lambda_{emitted}$, where λ is the wavelength of the photon. Since any physical length will scale as $x(t) \propto a(t)$ in this spacetime, the redshift can be related to the scale factor in the following useful relation

$$1 + z = \frac{a_0}{a_{emitted}}. \tag{1.3}$$

Therefore, redshift is a useful measure for the distance and/or time in cosmology.

Using Einstein's equation

$$R_{\mu\nu} - \frac{1}{2}g_{\mu\nu} = 8\pi G T_{\mu\nu}, \tag{1.4}$$

and the energy-momentum tensor for a perfect fluid with the components $T_{00} = \rho$ and $T_{ij} = p g_{ij}$, where ρ is the energy density and p is the pressure of the fluid, and then, substituting RW metric into Einstein's equation, one obtains the Friedmann equations

$$H^2 = \frac{8\pi G\rho}{3} - \frac{k}{a^2}, \tag{1.5}$$

where $H \equiv \dot{a}/a$ is the Hubble parameter and

$$\frac{\ddot{a}}{a} = -\frac{4\pi G}{3}(\rho + 3p). \tag{1.6}$$

Using (1.5) and (1.6), a useful relation for the conservation of energy can be obtained as

$$\dot{\rho} + 3H(\rho + p) = 0. \tag{1.7}$$

The equation of state takes the form $p = \omega\rho$ with $\omega = constant$ for some special cases. For instance, $\omega = -1, 1/3, 0$ for vacuum, radiation and matter, respectively. It can be easily seen from (1.7) that energy density scales as

$$\rho \propto a^{-3(1+\omega)}, \tag{1.8}$$

i.e., $\rho \propto a^0, a^{-4}, a^{-3}$ for vacuum, radiation and matter dominated universe, respectively. Note that vacuum energy is constant by definition, and thus, it remains constant during the expansion. Matter is diluted as the volume increases by a factor of a^3. Radiation is diluted even more since the energy decreases due to the redshift, i.e., $E \propto \lambda^{-1} \propto a^{-1}$, where λ is the wavelength of the particle.

The comoving distance $r(t)$ travelled by light between time t to t_0 in a FLRW universe is

$$r(t) = \int_t^{t_0} \frac{dt'}{a(t')}, \tag{1.9}$$

and the corresponding physical distance is $d(t) = a(t)r(t)$. Comoving volume in the interval $(r, r + dr)$ is $dV_c = 4\pi r^2 dr$ and the physical volume is $dV = a^3 dV_c$.

Density of the universe determines its geometry. The density parameter is defined as

$$\Omega_i = \frac{\rho_i}{\rho_c}, \;\; \Omega \equiv \sum_i \Omega_i, \tag{1.10}$$

where

$$\rho_c \equiv \frac{3H^2}{8\pi G} = 7.8 \times 10^{-47}\, h^2\, GeV^4, \tag{1.11}$$

is called the critical density and the summation is over the different components, such as radiation, matter and the vacuum. The equation (1.5) can be written as

$$\frac{k}{H^2a^2} = \Omega - 1. \tag{1.12}$$

It is easy to see from (1.12) that the universe is open if $\Omega < 1$, closed if $\Omega > 1$, and flat if $\Omega = 1$.

When the universe is dominated by radiation, i.e., $\Omega_r >> \Omega_i$, where i represents the other components, the solution for the scale factor can be found from (1.5) as

$$a(t) = a' \left(\frac{t}{t_0}\right)^{1/2}, \tag{1.13}$$

and when the matter is the dominant component, it is

$$a(t) = \left(\frac{t}{t_0}\right)^{2/3}. \tag{1.14}$$

Using (1.3), the relation between cosmic time and redshift can be obtained as $t = t_0(1+z_{eq})^{1/2}(1+z)^{-2}$ for the radiation era and $t = t_0(1+z)^{-3/2}$ for the matter era, where z_{eq} is the redshift at which matter-radiation equality occurs. Note that the scale factor is normalized such that $a(t_0) = 1$, and thus, $a' = (1+z_{eq})^{-1/4}$. The distance between an observer on Earth and a source at redshift z in the radiation and matter eras can be calculated from (1.9) as

$$r(z) \approx 3t_0, \quad z > z_{eq}, \tag{1.15}$$

$$r(z) = 3t_0[1-(1+z)^{-1/2}], \quad z < z_{eq}, \tag{1.16}$$

and the physical volume in the interval $(z, z+dz)$ is

$$dV(z) = 72\pi t_0^3(1+z_{eq})^{1/2}(1+z)^{-5}dz, \quad z > z_{eq}, \tag{1.17}$$

$$dV(z) = 54\pi t_0^3[(1+z)^{1/2}-1]^2(1+z)^{-11/2}dz, \quad z < z_{eq}. \tag{1.18}$$

When the vacuum energy is the dominant component of the energy density in the universe, the solution for the scale factor is $a(t) \propto e^{(\Lambda/3)^{1/2}t}$, where $\Lambda = 8\pi G\rho_\Lambda$ is the cosmological constant. A $\Lambda > 0$ solution exists for any spatial curvature and it is known as the de Sitter space (dS) [42]. On the other hand, when $\Lambda < 0$, there is only a solution with negative spatial curvature and the scale factor is $a(t) \propto sin[(\Lambda/3)^{1/2}t]$. This solution is known as the anti de Sitter space (AdS) [42].

Now, some of the most important problems in the standard model of cosmology and a profound solution to them (inflation) will be discussed briefly. According to the most recent data the total density parameter $\Omega = 1$ to a good accuracy [36]. Defining conformal time as $d\tau = dt/a(t)$ and using (1.7) and (1.12), the time evolution of Ω can be obtained as

$$\frac{d\Omega}{d\tau} = \frac{1}{a}\frac{da}{d\tau}\Omega(\Omega - 1). \tag{1.19}$$

In an expanding universe the scale factor always increases with time, i.e., $da/d\tau > 0$. Hence, Eq. (1.19) implies that when $\Omega < 1$, $d\Omega/d\tau < 1$, namely, the density parameter decreases and we are left with a curvature dominated universe. When $\Omega > 1$, on the other hand, $d\Omega/d\tau > 1$, and thus, the density parameter becomes larger and larger. This simple argument shows that only when the density parameter is finely tuned at about $\Omega = 1$, the universe stays flat. This is known as the *flatness problem* in cosmology.

One of the most important evidence that supports the big bang theory was the discovery of the cosmic microwave background (CMB) in 1964 by Arno Penzias and Robert Wilson [43]. The CMB has a blackbody spectrum with temperature $T_{CMB} = 2.7$K and it is isotropic to one part in 10^5 [36]. The

anisotropy in the CMB –the imprints of the density fluctuations in the early universe– [44] and the blackbody spectrum [45] were first confirmed by the COBE satellite. Another important conclusion one can draw from the CMB measurements is that causally disconnected points in the sky have nearly the same temperature. A causally connected patch of the sky at the surface of last scattering only subtends an angle of an order 1^o whereas the temperature of the CMB is the same in all directions. The puzzle is how these causally unrelated patches come to a thermal equilibrium. This is known as the *horizon problem* in cosmology.

Grand unified theories (GUTs) is the generic name for the gauge theories that unifies the electroweak and the strong interactions. GUTs have a larger simple symmetry group G that breaks into the standard model symmetry group $SU(3)_c \times SU(2)_L \times U(1)_Y$ as the universe cools down. As the larger symmetries are broken down to smaller symmetry groups, topological defects may arise. Monopoles can exist if the vacuum manifold has a nontrivial second homotopy group. In the case of breaking of G into $SU(3) \times U(1)$, the second homotopy group $\pi_2(G/SU(3) \times U(1)) \cong \mathbb{Z}$. Hence, the existence of monopoles is guaranteed in GUTs independent of the symmetry group [5]. As a relic of the GUTs, monopoles can be very heavy, i.e., $m_M \sim m_{GUT} \sim 10^{16}$ GeV, and the universe rapidly becomes monopole dominated since they scale as matter, $\rho_M \propto a^{-3}$. If this was the case, we would have about one monopole per nucleon, which is in total disagreement with what is observed [1]. This is known as the *monopole problem*.

All these problems, namely, the flatness, horizon and monopole problems can be avoided with an early period of exponentially fast expansion of the

universe, i.e., the so called inflation [46, 47, 48]. Density fluctuations that are seen as anisotropies in the CMB can also be explained well within the inflationary paradigm in terms of quantum fluctuations of the inflaton field that later serve as the seeds for the structure formation in the universe [49]. All the inhomogeneities and topological defects formed before inflation are swept away. In other words, inflation erases the memory of the universe and gives it a fresh start.

In a nutshell, inflation is caused by a scalar field slowly rolling down its potential, thus the energy density stays almost constant, hence the exponential growth of the scale factor. As the inflaton oscillates back and forth about the minimum of the potential, the inflaton potential energy is converted into thermal radiation and particles in this stage, which is known as reheating. This process heats up the universe to high enough temperatures so that baryogenesis –the mechanism to create baryon-antibaryon asymmetry–, and then, nucleosynthesis could occur [50].

After reheating, the universe is filled with hot and dense plasma of ultrarelativistic particles, namely, quarks, leptons, neutrinos, gauge bosons and their anti-particles. Thanks to the decrease in the effective strength of the electroweak and strong interactions at high energies, the equation of state can be approximated as $p = \rho/3$ and by using Bose-Einstein and Fermi-Dirac distributions, the energy density $\rho(T)$ and entropy density $s(T)$ can be obtained as a function of temperature for the ultrarelativistic particles as [50]:

$$\rho(T) = \frac{\pi^2}{30}\mathcal{N}(T)T^4, \tag{1.20}$$

$$s(T) = \frac{2\pi^2}{45}\mathcal{N}(T)T^3, \tag{1.21}$$

where $N(T)$ is the effective number of degrees of freedom given by

$$N(T) = N_B(T) + \frac{7}{8} N_F(T), \tag{1.22}$$

for the bosonic and the fermionic species available at temperature T. Using (1.5) and (1.20), a useful relation between time and temperature can be obtained as

$$t = \frac{1}{4\pi} \left(\frac{45}{\pi \mathcal{N}(T)} \right)^{1/2} \frac{m_p^2}{T^2}, \tag{1.23}$$

which can be calculated as $t/sec \sim (T/MeV)^2$ taking $N(T) \sim 100$.

The following main events occurred during the thermal history of the universe: Intermediate stages of symmetry breaking could have occurred after the reheating which leads to formation of topological defects including cosmic strings [1]. At about 10^2 GeV, electroweak symmetry breaking occurs that breaks the Standard Model (SM) symmetry group $SU(3)_c \times SU(2)_L \times U(1)_Y$ down to $SU(3)_c \times U(1)_{em}$ via Higgs mechanism. QCD phase transition occurs at $T \sim 10^2$ MeV, where chiral invariance in strong interactions is broken and free quarks are confined to form baryons and mesons. Nucleosynthesis begins at $T \sim 0.8$ MeV when the neutron-proton ratio freezes out. Then, most of the neutrons form bound state with protons via interaction $p + n \rightarrow D + \gamma$ at $T \sim 0.1$ MeV. Then, in a series of interactions, ^{3}He, ^{4}He and ^{7}Li nuclei are formed. The primordial abundances of these nuclei can be calculated by using the standard model of cosmology as $Y_{^4He} \sim 0.25$, $Y_D \sim 3 \times 10^{-5}, Y_{^3He} \sim 2 \times 10^{-5}, Y_{^7Li} \sim 10^{-9}$. The observed value of the primordial ^{4}He abundance $Y_{^4He} = 0.248$ agrees well with the estimates of the hot big bang theory with nucleon to photon ratio of $\eta = 5.81 \times 10^{-10}$ [51].

Before nucleosynthesis, there was a small excess of matter over antimatter.

This can be achieved via non-equilbrium processes, where baryon number, C and CP are violated so that pair annihilations do not occur efficiently, hence, the baryon asymmetry is established [52].

As the universe expands, the matter density catches up with the radiation density and eventually becomes dominant when $\Omega_m(z_{eq}) = \Omega_r(z_{eq})$. This occurs at redshift $z_{eq} = 3200$ [36].

As the universe reaches to the temperature below the hydrogen reionization threshold 13.1 eV, electrons and protons form neutral hydrogen atoms. This process is called recombination. At this stage, there is a sudden decrease in the electron to photon ratio as a result of which the universe becomes transparent to photons. This stage of the thermal history of the universe is also called decoupling. We observe the relic radiation propagating to us from the decoupling time as the CMB today. The decoupling occurs at redshift $z_{dec} = 1090$ [36].

This section will be closed with the current parameters of cosmology. According to WMAP 7-year-data combined with astrophysical data, $h = 0.7$, the age of the universe $t_0 = 13.8$ Gyr, and the density parameter for baryons $\Omega_b = 0.0458$, cold dark matter $\Omega_c = 0.229$, radiation $\Omega_r = 9 \times 10^{-5}$ and dark energy $\Omega_\Lambda = 0.725$ [36]. Therefore, the energy density in the universe is mostly composed of dark energy that causes an accelerated expansion of the universe today and dark matter that only interacts gravitationally. The equation of state of the dark energy component is $\omega \approx -1$, which is in favor of the cosmological constant. Besides, inflationary paradigm agrees well with the observed CMB temperature anisotropies [36].

In the next section, various properties of cosmic (super)strings will be

discussed.

1.2 Cosmic strings

1.2.1 Gauge theories and spontaneous symmetry breaking

Lagrangian[2] of a field theory respects the symmetries of that theory. However, in some cases the vacuum state does not respect the symmetry of the theory in which case the symmetry is said to be spontaneously broken. A simple example in relativistic field theory was the self interacting complex scalar field with the potential

$$V(\phi) = \frac{1}{4}\lambda(\phi^*\phi - \eta^2)^2, \tag{1.24}$$

which is called the Goldstone model [53]. This model is invariant under global phase transformations, namely $\phi(x) \rightarrow e^{i\alpha}\phi(x)$, but the minima of the potential have a non-zero expectation value $\eta e^{i\theta}$ that transforms as $\eta e^{i(\theta+\alpha)}$. Therefore, the vacuum does not remain invariant under the global phase transformations, hence the symmetry is spontaneously broken. The low energy states can be expressed as

$$\phi(x) = \left(\eta + \frac{1}{\sqrt{2}}\varphi(x)\right) e^{iv(x)}, \tag{1.25}$$

where $\varphi(x)$ corresponds to the radial excitations about the minima whereas $v(x)$ corresponds to the motion around the circle of minima [1]. Ignoring the

[2]The term Lagrangian will be used instead of Lagrangian density for brevity in what follows.

interaction terms the Lagrangian can be written in terms of these fields as

$$\mathcal{L} \sim \frac{1}{2}(\partial_\mu \varphi)^2 + \eta^2(\partial_\mu v)^2 - \frac{1}{2}\lambda\eta^2\varphi^2. \tag{1.26}$$

Note that in addition to the massive field φ, there is a massless field v known as the Goldstone boson. According to the Goldstone theorem, the Goldstone modes are inevitable in theories with spontaneously broken global symmetries. The problem with massless scalar fields is that they create infinite range forces like gravity, hence ruled out by non-existance of such forces in nature. On the other hand, when the theory has a local gauge symmetry, i.e., the symmetry transformations are spacetime dependent, then the degree of freedom carried by the Goldstone mode is absorbed into the vector boson. In other words, the spontaneous breaking of a local gauge symmetry generates a mass for the massless vector gauge bosons [54, 55, 56]. The simplest model with local gauge symmetry is the Abelian Higgs model given by the Lagrangian [54]

$$\mathcal{L} = D^*_\mu \phi^* D^\mu \phi - \frac{1}{4}\lambda(\phi^*\phi - \eta^2)^2 - \frac{1}{4}F_{\mu\nu}F^{\mu\nu}, \tag{1.27}$$

where $D_\mu = \partial_\mu - ieA_\mu$, A_μ is the gauge vector boson, e is the gauge coupling constant and $F_{\mu\nu} = \partial_\mu A_\nu - \partial_\nu A_\mu$ is the field strength tensor. This theory is invariant under the local phase transformations, i.e., it has local U(1) symmetry, and the fields transform as $\phi(x) \to e^{i\alpha(x)}\phi(x)$ and $A_\mu(x) \to A_\mu(x) + e^{-1}\partial_\mu\alpha(x)$. Substituting the low energy states as in Eq. (1.25) and ignoring the interaction terms, we arrive at the effective Lagrangian

$$\mathcal{L} \sim \partial_\mu\varphi^*\partial^\mu\varphi - \frac{1}{2}\lambda\eta^2\varphi^2 - \frac{1}{4}F_{\mu\nu}F^{\mu\nu} + e^2\eta^2 A_\mu A^\mu. \tag{1.28}$$

Note that the Goldstone mode is absent in this case; its degree of freedom is absorbed into the vector gauge boson, hence the mass term for A_μ. Generalization of this model to non-abelian gauge groups, in particular to SU(2)

[57], opened up a new way to understand fundamental interactions of particle physics. One of the most successful theories in particle physics is the electroweak theory of Glashow-Weinberg-Salam [58, 59, 60], where $SU(2)_L \times U(1)_Y$ gauge group is broken via Higgs mechanism to $U(1)_{em}$. The prediction of this theory was three massive vector bosons $W^{\pm}$, Z^0 that are responsible for the weak interactions. Weinberg predicted their masses from the gauge couplings as $m_W > 40$ GeV, $m_Z > 80$ GeV [59]. In 1983, the electroweak theory was confirmed with the discovery of $W^{\pm}$, Z^0 bosons at CERN [61, 62] with the masses close to what Weinberg predicted. The Higgs boson still awaits to be discovered at the LHC at CERN as of today.

The developments in particle physics such as the electroweak theory and quantum chromodynamics made physicist wonder about larger gauge groups, where strong and electroweak interactions are unified. Such theories are generically called grand unified theories (GUTs). The first GUT was based on the gauge group SU(5) [63], which had some problems, such as too small lifetime for protons. Later, several other models have been proposed all of which have the problem that the three gauge couplings do not unify at a single energy unless the theory is supersymmetric.

Supersymmetry was invented in order to combine the internal symmetries with the spacetime symmetries. In 1967, Coleman and Mandula showed that it is not possible to combine the internal symmetries of the S matrix with the spacatime symmetries non-tirivially in terms of Lie groups [64]. This no-go theorem basically tells the following: Assume that the S matrix exists and non-trivial, the vacuum is non-degenerate and there are finite number of particles whose mass is less than a given value. Under these assumptions, a Lie

group which combines the internal symmetry group with the Poincare group leads to an S matrix which is zero for all processes [65]. Coleman-Mandula theorem relates the transformations between bosons and bosons or fermions and fermions. Therefore, these transformations are generated either by operators satisfying commutators for bosons or operators satisfying anticommutators for fermions. Supersymmetry has a $\mathbb{Z}_2$-graded Lie algebra which relates bosons to fermions and vice versa in a given theory. Thus, the obvious prediction of supersymmetry is the existence of superpartners for every particle in the standard model. Since we do not observe such particles in nature, supersymmetry must have been broken at some high energy. TeV scale supersymmetry is phenomenologically preferred since it solves the gauge hierarchy problem. The LHC has also been searching for supersymmetric particles as of today. The running of gauge coupling constants for the minimal supersymmetric standard model (MSSM) by using the renormalization group techniques showed that the coupling constants actually do unify at 10^{16} GeV [67].

Supersymmetry is also required for consistency in string theory –a framework, where all the interactions of nature are explained in terms of the relativistic quantum theory of one dimensional objects, namely open and closed strings. There are five distinct supersymmetric string theories which are related to one another and to 11D supergravity via dualities [68].

In the next sections, cosmological phase transitions in terms of breaking of larger symmetry groups down to $SU(3)_c \times U(1)$ and formation of topological defects as the relics of these processes will be discussed.

1.2.2 Phase transitions in cosmology and topological defects

The universe goes through phase transitions as it cools down. As the symmetries of gauge theories with larger gauge groups are spontaneously broken, topological defects can appear as the residues of the false vacuum at the corresponding energies. After the success of the gauge theories with symmetry breaking, it was shown that the gauge symmetries can be restored at high temperatures [69, 70] as in the case of melting of ice –as the ice melts the lattice structure disappears, hence the rotational symmetry is restored above the melting temperature.

According to the standard model of cosmology, the universe was a lot hotter and denser in the earlier epochs, hence larger symmetry groups could be broken as it cooled down leaving the topological defects as relics. When the order parameter –a parameter characterizing the order of the phases before and after the phase transition– changes continuously from zero in the symmetric phase to a non-zero value in the broken phase, the process is called the second order phase transition [50]. In a second order phase transition, two phases do not coexist. For instance, the spontaneous breaking of a gauge symmetry via Higgs mechanism is a second order phase transition, where the order parameter ϕ changes continuously from zero to its final value $< \phi >= \eta$. On the other hand, if different phases coexist, then the symmetric phase develops a metastable state which is subject to decay to the absolute minima via bubble formation, similar to formation of bubbles in boiling water. The so called old inflation scenario is an example of a first order phase transition, where the

order parameter changes discontinuously via quantum tunneling from a local minimum to the absolute minimum [46].

The first topological defect solution in the context of gauge theories was the vortex solution in the Abelian Higgs model by Nielsen and Olesen [71]. In the radial gauge $A_\rho = 0$, the cylindrically symmetric ansatz for the gauge field of the model (1.27) can be written as [2]

$$\phi = \frac{\eta}{\sqrt{2}} f(e\eta\rho) e^{in\varphi}, \quad A_\theta = \frac{n}{e\rho} a(e\eta\rho), \tag{1.29}$$

where ρ and θ are the radial and polar coordinates in the cylindrical coordinate system, respectively, $n \in \mathbb{Z}$ is the winding number, f and a are the solutions of the equations of motion, which cannot be expressed in terms of the elementary functions, but the asymptotic behaviors can be obtained as:

$$f \sim f_0 \xi^{|n|}, \quad a \sim a_0 \xi^2 - \frac{|n| f_0^2}{4(|n|+1)} \xi^{2|n|+2}, \quad \xi \to 0, \tag{1.30}$$

$$f \sim 1 - f_1 \xi^{-1/2} e^{-\sqrt{\beta}\xi}, \quad a \sim 1 - a_1 \xi^{1/2} e^{-\xi}, \quad \xi \to \infty, \tag{1.31}$$

where $\beta = \lambda/e^2$ and $\xi = e\eta\rho$. When $\beta > 4$, $f(\infty)$ is given by $f \sim 1 - f_1 \xi^{-1} e^{-2\xi}$. The asymptotic behavior of the vortex solution shows that it is regular at the origin, i.e., there is no singularity, and the fields approach to their absolute vacuum value η at larger distances. The vortex contains a tube of magnetic flux $2\pi n/e$. When $\beta < 1$, this solution is stable for all winding numbers n. When $\beta > 1$, it is only stable for $n = 1$. The tension of the vortex, which is also equal to the energy per unit length, can be calculated from

$$\mu = \int d\varphi d\rho \rho \mathcal{E}(\rho) \sim \pi \eta^2 \epsilon(\beta), \tag{1.32}$$

where $\mathcal{E}$ is the energy density of the vortex and ϵ is a slowly varying parameter of order one [2]. At the critical coupling, i.e., $\beta = 1$, $\epsilon = 1$ [72]. Therefore, in

general it is safe to assume that the string tension is $\mu \sim \eta^2$.

Topological structure of the vacuum manifold determines whether domain wall, vortex or monopole solutions exist in a given theory. In the Nielsen-Olesen vortex solution discussed above, the vacuum manifold is not simply connected, i.e., it contains closed curves which cannot be shrunk to zero continuously. It can be easily seen from the potential term in Eq. (1.27) that the vacuum is not a single point, but a circle of minima $\phi \sim \eta e^{in\theta}$. Technically speaking, the fundamental homotopy group of this manifold is non-trivial, i.e., $\pi_1(U(1)) = \mathbb{Z}$ [1].

The classification of the topological defects according to the homotopy groups of their vacuum manifolds was suggested by Kibble [73]. Homotopy groups classify the mapping from an n-sphere into the manifold, hence they are used to understand the topological properties of manifolds.. If the vacuum manifold $\mathcal{M}$ has disconnected components, domain walls can form. This occurs when the zeroth order homotopy group $\pi_0(\mathcal{M})$ is non-trivial. They appear in theories with broken discrete symmetries [6, 7], such as the breaking of the reflection symmetry, $\phi \to -\phi$, in a model with a double-well potential $V(\phi) = (\lambda/4)(\phi^2 - \eta)^2$, where ϕ is a real scalar field. If $\mathcal{M}$ is not simply connected as explained above for the Nielsen-Olesen vortex, i.e., the fundamental homotopy group $\pi_1(\mathcal{M}) \neq I$, then string solutions can exist. Thus, whenever a U(1) symmetry is broken, there is a string solution since $\pi_1(U(1)) = \mathbb{Z}$. If there are unshrinkable surfaces in $\mathcal{M}$, i.e., $\pi_2(\mathcal{M}) \neq I$, then monopole solutions exist.

1.2.3 Kibble mechanism and cosmic string evolution

As the universe cools down below the temperature at which spontaneous symmetry breaking occurs, topological defects can form in the universe via so called Kibble mechanism [73]. As an example let us consider the Abelian Higgs model given by Eq. (1.27). The Higgs field acquires a nonzero expectation value with an arbitrary phase $<\phi>\sim \eta e^{i\theta}$ after the symmetry breaking. As the symmetry breaking occurs in different regions of the universe that are causally disconnected from each other, the phase of the Higgs field takes an arbitrary value in each region, i.e., different regions of the universe randomly falls into minima with different phases. In two dimensions, core of a string can be visualized as a point around which the phase of the Higgs field changes continuously from 0 to 2π. Closed curves cannot be shrunk to zero around such points, hence the non-trivial fundamental homotopy group of the vacuum manifold. Considering this picture in three dimensions, we can identify the line along the extension of this point to the third dimension as a cosmic string. Cosmic string networks form with a characteristic scale ξ whose upper bound is the causal horizon, i.e., $\xi \lesssim H^{-1} \sim t$. Then, the energy density of the string network can be estimated as $\rho \sim \mu/\xi^2$.

When the cosmic string network forms, the universe is still very dense and hot, thus, the motion of the strings is heavily damped. The damped epoch lasts until time $t_d \sim (G\mu)^{-2} t_p$ [1] after which strings start moving freely. Since the thickness of a string is much less than its radius of curvature, its motion can be described by the Nambu-Goto action

$$S = -\mu \int d^2\sigma \sqrt{-\gamma}, \tag{1.33}$$

where γ is the determinant of the worldsheet metric $\gamma_{ab} = g_{\mu\nu} X^{\mu}_{,a} X^{\nu}_{,b}$, $X^{\mu}(\sigma^{a})$ is the string worldsheet –two dimensional surface characterizing the history of a string. This description of string motion is valid for strings that do not intersect with themselves or other strings. However, strings can interact in three ways. They can pass through each other, reconnect or get entangled. Field theory simulations of Abelian Higgs model show that strings intercommute, i.e., exchange partners with probability $p \approx 1$ [74, 75, 76]. String solutions with the parameter $\lambda < e^2$ are stable for large winding numbers and these can form bound states [77]. Furthermore, strings can form bound states in models, where vacuum manifold has a non-abelian fundamental homotopy group [78]. Reconnection of cosmic F- and D-strings is a quantum mechanical process, thus the reconnection probability can be much smaller than unity, i.e., $10^{-3} < p < 1$ [79]. They can also form bound states called FD string networks [80]. We will discuss cosmic F-, D-strings in the following section in more details.

Both theoretical analyses [81] and simulations [82, 83, 84] show that the string network reaches a scaling regime. It may first seem problematic that if the string network scales with the horizon, the energy density of the strings will dominate the universe since strings will be stretched and the density goes as $\rho \propto 1/t^2$. However, loops are formed via intercommuting of a string with itself or with other strings. Loops radiate gravitational waves, hence, some energy is removed from the network of strings. The typical size of a loop is determined by the scaling parameter $\beta = L/t$, where L is the invariant length of a loop. According to the largest simulations performed up to date, the value of the scaling parameter is $\beta \sim 0.1$ in the radiation era, and $\beta \sim 0.15$

in the matter era [84]. There is still a debate about whether most of the energy goes into these large loops with $\beta \sim 0.1$ or smaller loops that have lifetimes smaller than Hubble time. Analytical studies suggest that there are two populations of loops: Scaling large loops of size of order horizon scale and non-scaling small loops that have gravitational back reaction scale $(\Gamma G\mu)^{\nu}t$ with $\nu = 1.5, 1.2$ for matter and radiation eras, respectively [85]. On the other hand, the most recent and the largest simulation shows that the non-scaling small loop population is transient and the scaling large loops eventually dominate [84].

1.2.4 Superconducting strings

Cosmic strings become superconducting when a local gauge invariance is spontaneously broken within their core. This can be achieved via a scalar field [86] or a charged vector field in a non-abelian theory [87]. The simplest model consists of two gauge and two scalar fields with $\bar{U}(1) \times U(1)$ symmetry and has a Lagrangian [86]

$$\mathcal{L} = |\bar{D}_\mu \phi|^2 + |D_\mu \chi|^2 - V(\phi, \chi) - \frac{1}{4}\bar{F}_{\mu\nu}\bar{F}^{\mu\nu} - \frac{1}{4}F_{\mu\nu}F^{\mu\nu}, \tag{1.34}$$

where $\bar{D}_\mu = \partial_\mu - ig\bar{A}_\mu$, $D_\mu = \partial_\mu - ieA_\mu$ and

$$V(\phi, \chi) = \frac{1}{4}\lambda_\phi(|\phi|^2 - \eta_\phi^2) + \frac{1}{4}\lambda_\chi(|\chi|^2 - \eta_\chi^2) + \gamma|\phi|^2|\chi|^2. \tag{1.35}$$

Superconductivity is achieved when γ is larger than the self couplings λ_ϕ, λ_χ and, $m_\chi^2 = \gamma\eta_\phi^2 - \lambda_\chi\eta_\chi^2 > 0$. $\bar{U}(1)$ is broken when $\lambda_\phi\eta_\phi^4 > \lambda_\chi\eta_\chi^4$ whereas $U(1)$ is not broken. In this case, the vacuum with $|\phi| = \eta_\phi$, $|\chi| = 0$ becomes stable. However, for a large region in the parameter space, bound states exist as scalar condensates in the core of the string, where $|\chi| \neq 0$ [88, 89, 90].

Superconducting strings develop currents as they oscillate and travel through the regions of space that has magnetic fields. The current has a value of order $J \sim e^2BL$, where B is the magnitude of the magnetic field [1]. The current inside the string is saturated when it reaches a critical value $J_c \sim i_c e\eta$, where $0 < i_c < 1$ is a model dependent parameter. Particles are ejected from the portions of the strings, where the critical current is reached. This occurs most efficiently around the cusps, where the current is boosted to extremely large values, hence the emission of electromagnetic [20, 21, 22] and neutrino bursts [11]. The latter effect has unique signatures, such as multiple hits from the same burst that can be detected at the planned neutrino detector JEM-EUSO. This model will be discussed in detail in Chapter 4.

Similar observable effects can be expected for cosmic strings with bosonic condensates [10]. In particular, standard model Higgs condensates can form on cosmic strings and can emit ultra high energy cosmic rays from cusps [10].

1.2.5 Cosmic F- and D-strings

The possibility that superstrings might have cosmic sizes was first discussed by Witten [91]. Witten argued that the strings of superstring theory have tension close to Planck scale, $G\mu \gtrsim 10^{-3}$, which would produce very large inhomogeneities in the CMB that is in conflict with the observations. Besides this scale is above the upper bound on the inflaton vacuum energy, thus, they would not have been produced after inflation and any strings produced before inflation would be diluted away. In Type-I theory, macroscopic strings suffer instability against breaking into smaller strings. Furthermore, macroscopic heterotic strings appear as the boundaries of axion domain walls, whose

strong gravitational forces make the strings collapse [92]. However, recent developments in superstring theory, namely, the discovery of non-perturbative objects such as D-branes and the idea of flux compatification, make it possible to have stable cosmic superstrings with smaller tensions. The tension of superstrings can be well below Planck scale due to gravitational redshift effect of the warped geometry or large extra dimensions [80].

Brane inflation was suggested as an inflation mechanism within the framework of Type-IIB string theory [93]. Later, it was shown that cosmic superstrings can form when the brane inflation ends [94]. In the brane inflation scenario, the role of the inflaton is played by the radial modulus characterizing the distance between a D3-brane and an anti D3-brane. The potential for the radial modulus is similar to that of the hybrid inflation model [95]. As the separation between the branes gets below a certain value, the radial modulus becomes tachyonic like in hybrid inflation, i.e., its mass squared term becomes negative. Each brane has a U(1) gauge field confined on its worldvolume, one of which experiences a spontaneous symmetry breaking via coupling to the tachyon field. This leads to formation of D-strings via Kibble mechanism. When the brane and anti-brane annihilate, the other U(1) is confined as flux tubes which are identified as F-strings.

Unlike ordinary gauge theory strings, cosmic F- and D-strings do not always reconnect. Reconnection is a quantum mechanical process and depends primarily on the string coupling constant $g_s < 1$. It can be estimated as $p \sim g_s^2$, hence smaller reconnection probability. With a smaller reconnection probability, it takes several attempts for strings to reconnect. Therefore, the density of strings is expected to be larger than ordinary strings with $p = 1$.

The dependence of the density of strings on p can be estimated as $\rho \propto p^{-1}$ based on the simple arguments in Refs. [24, 96]. Reconnection probability has been estimated as $10^{-3} \lesssim p \lesssim 1$ for F-strings and $10^{-1} \lesssim p \lesssim 1$ for D-strings [79]. F- and D-strings can also form bound states provided that they live in the same potential well in the bulk space. The tension of the FD-network is determined by the number of F- and D-strings involved in the junctions [80]. Reconnection probability might be useful to distinguish between the ordinary gauge theory strings and F-, D-strings since the latter will have a larger density, and thus, they will have stronger effects than ordinary strings.

1.2.6 Observable effects of cosmic strings

Cosmic (super)strings can be a significant source of gravitational waves. The stochastic background of gravitational waves coming from cosmic string loops at different cosmic epochs disturbs the timing of the pulses from milisecond pulsars which otherwise act as very accurate clocks. The current upper bound on the string tension from pulsar timing is $G\mu \lesssim 1.5 \times 10^{-8}$ [97]. This is the most stringent upper bound on the string tension so far.

In addition to the stochastic background, gravitational wave bursts can be produced from cusps. These bursts should be detectable by LIGO and LISA interferometers for string tensions as small as $G\mu \sim 10^{-14}$ [23].

Spacetime around a straight cosmic string is locally flat, i.e., particles near a cosmic string do not experience gravitational attraction since tension of the string is equal to its energy density in magnitude, hence, the attractive force due to the energy density is cancelled exactly by the repulsive force due to the tension of the string. However, globally the spacetime is conic with a deficit

angle $\delta = 8\pi G\mu$ [7]. If an astrophysical object happens to be behind a cosmic string, then a double image of the object is created with an angular separation of order δ. This is true for a straight string, but some distortion of the images could occur because of wiggles on the strings. The recent upper limit due to this effect is given as $G\mu < 2.3 \times 10^{-6}$ based on a survey that compares the optical images of close pairs of similar objects [12].

Cosmic strings can also generate scale invariant density perturbations which was considered to be the source of the primordial density fluctuations [98]. The accurate measurements of the CMB by WMAP show that the cosmic string contribution to the total power is less than 10 % [14, 16, 15]. The acoustic peaks in the observed CMB power spectrum are explained well within the inflationary paradigm whereas cosmic strings can only produce a single peak from which an upper bound on the string tension is obtained by using WMAP data as $G\mu \lesssim 2.1 \times 10^{-7}$ [17].

Cosmic strings can be sources of temperature anisotropies in the CMB – known as the Kaiser-Stebbins effect [13]. When a cosmic string passes through the uniform background of photons with speed v, the photons ahead of the strings redshift whereas the ones behind it blueshift due to the conical geometry of the spacetime around it. This effect can show itself as a discontinuous change in the temperature of the background as $\delta T/T \sim 8\pi G\mu v$, which might be detected by the Planck satellite that is collecting data now.

Inflation predicts scalar and tensor fluctuations, on the other hand, cosmic strings mostly produce vector perturbations except for the very small scales. This unique property can serve as a way of detecting cosmic strings in the B-mode polarization of the CMB [18] which will also be detectable by the

Planck satellite.

Since cosmic strings have the energy densities of up to order of GUT or string theory scales, they could also be responsible for the highest energy events in the universe, such as gamma ray bursts and UHE cosmic rays. Several mechanisms have been suggested for UHE particle production from cosmic strings. Emission of particles from a collapse of a loop into a double line [99, 100] produce very small fluxes since the probability of the collapse is very small [101]. As a cosmic string loop loses its energy via gravitational and particle radiation, it shrinks and eventually annihilate into UHE particles. It turns out that this mechanism also produces a few particles per loop whose flux is too small to be observable [102]. As a cosmic string loop oscillates, it might self intersect and split into smaller loops. If this process is efficient enough, the resulting small loops can decay into UHE particles in turn [101]. However, this mechanism is not supported by the cosmic string simulations, namely such small loops constitute only a very small fraction of the total energy density of the network [84]. Small portion of a cosmic string can be annihilated when a string doubles on itself about the very tip a cusp. This cusp annihilation mechanism also does not turn out to yield observable UHE particle fluxes [103, 104, 105].

Good news is that there are other mechanisms, where observable UHE cosmic ray fluxes can be obtained which constitute a large portion of this dissertation. It has been suggested that radiation from cusps of superconducting cosmic strings could explain the highest energy gamma ray bursts in the universe [19, 20, 21]. Vachaspati also suggested that superconducting cosmic string cusps could produce electomagnetic bursts and argued that an

observed radioburst in the extragalactic region of the space could be explained by this mechanism [22]. Higgs condensates can form on cosmic strings and large number of Higgs particles can be produced from cusps, which leads to UHE cosmic rays [10]. Superconducting cosmic strings can also produce UHE neutrino bursts from cusps that can be observed at JEM-EUSO. This model has a unique signature, such as multiple hits coming from the same direction without a time lapse [11], and thus, it can be interpreted as a clear signal that can be accounted for cosmic strings. This model will be discussed in detail in Chapter 4. There is yet another mechanism to produce UHE cosmic rays, in particular neutrinos, from cosmic string cusps which does not require superconductivity. This model is based on the existence of relatively light scalar particles called moduli –scalar particles that are predicted in supersymmetric field theories including superstring theory. Moduli are often assumed to have gravitational strength couplings, in which case the resulting particle flux is too small. However, with the recent developments in string theory, namely, the models with warped and large extra dimensions, there exist moduli with stronger coupling to matter, which can lead to observable UHE cosmic ray fluxes. The effect of such moduli in the early universe cosmology [28] and their observable effects will be discussed in detail in Chapter 2 and Chapter 3, respectively. Now, we will turn our attention to some more detailed discussion of cosmic rays.

1.3 Cosmic rays

Cosmic rays are particles that can have solar, galactic or extragalactic origins, namely they can be produced by stars, active galactic nuclei (AGN) and topological defects. Primary cosmic ray particles can be heavy nuclei, protons, electrons, neutrinos and gamma rays, where protons constitute about 90% of them. As they enter the earth's atmosphere, they interact with the nuclei in the air molecules and give rise to secondary particles, mostly muons, which in turn decay into electrons, positrons and neutrinos, hence they are detected via interaction of these secondary particles at the detectors on earth. Cosmic rays span a wide energy range from a few MeV all the way up to 10^{11} GeV. The dependence of the flux on energy can be seen in Fig. 1.1 The flux in units of number of particles per (cm^2 sec GeV) can be fit as $I(E) \propto E^{-n}$. For the energy range between 100 GeV and 10^6 GeV, $n = -1.7$. At about $E \sim 10^6$ GeV, there is a knee, after which the index n ranges from -2 to -2.2. Eventually, there is a steepening to $n = -2.7$. The knee is considered to occur about the maximum energy that supernovae can accelerate cosmic rays. There is a dip in the spectrum which is caused by pair production from protons interacting with the CMB photons. There is also a cutoff at the high energy end of the spectrum due to photo-pion production from protons interacting with the CMB.

There are several energy loss mechanisms for cosmic rays. Due to the expansion of the universe, the energy of an ultrarelativistic particle produced at redshift z decreases as $E \propto 1/(1+z)$. Besides, charged particles interacting with the CMB photons produce electron-positron pairs and pions. Heavy

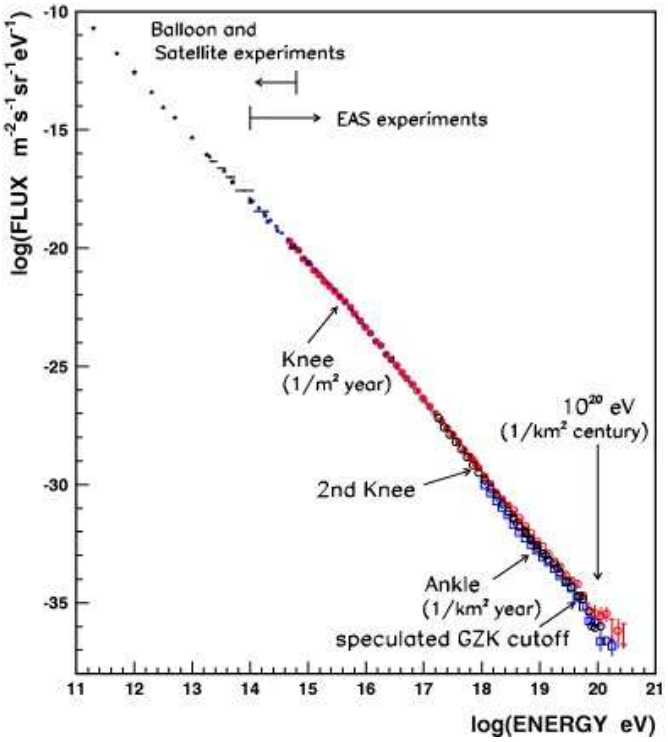

Figure 1.1: The energy spectrum of cosmic rays. The spectrum can be expressed by a power law from 10^2 GeV to 10^{11} GeV with only small changes of slope around 10^6 GeV (the first knee), 10^9 GeV (the second knee) and 10^{11}GeV (the ankle) (The figure is taken from [106]).

nuclei interacting with photons disintegrate into smaller nuclei. Protons lose energy via pair production effect above energies $m_e^2/E_{CMB} \sim 10^6$ GeV which is considered to be the reason for the dip in the spectrum. They also lose energy via photo-pion production above energies $m_\pi m_{proton}/E_{CMB} \sim 10^{11}$ GeV, which shows itself as a cutoff in the spectrum. The latter effect was first studied by Greisen [107], Zatsepin and Kuz'min [108] and is known as the GZK process. Due to this effect, protons with energies above 10^{11} GeV are strongly suppressed, hence not expected to be observed. The most recent data from HiRes and AUGER experiments confirms the cutoff at $E \sim 6 \times 10^{10}$ GeV [109, 110].

1.3.1 Ultra high energy neutrinos

UHE neutrinos lose energy as they interact with the cosmic neutrino background. This leads to an effective horizon for neutrinos beyond which they are absorbed due to $\nu\bar{\nu}$ interactions. The neutrino horizon is given by $z_\nu \sim 7.9 \times 10^4 E_3^{-1/3}$ in the radiation dominated era and $z_\nu \sim 220 E_{11}^{-2/5}$ in the matter era, where $E_3 \equiv E/(10^3 \text{ GeV})$ and E is the neutrino energy [111]. If neutrinos are produced at large redshifts, they could produce MeV photons in electromagnetic cascades, which in turn produce D and ^{4}He. Therefore, primordial element abundances restrict the flux of neutrinos at large redshifts. When neutrinos are produced from the decay of pions and kaons, they are always accompanied by high energy photons, electrons and positrons. As the primary photons and electrons interact with the CMB photons, a cascade photon background is produced, hence restricted by diffuse gamma ray background [112, 113]. This is one of the most important restriction on the models that will be discussed in Chapter 3 and 4, where UHE neutrinos are produced from hadronic cascades, i.e., via decays of pions and kaons.

1.3.1.1 The cascade bound

The neutrino fluxes are limited from above. The most general upper bound for UHE neutrinos, valid for both cosmogenic neutrinos –neutrinos produced via decays of photo-pions originated from interaction of protons with the CMB photons– and neutrinos from top-down models, is given by the cascade upper limit, first considered in [114, 115]. The production of neutrinos in these scenarios is accompanied by production of high energy photons and electrons.

Colliding with low-energy target photons, a primary photon or electron produces an electromagnetic cascade due to the reactions $\gamma + \gamma_{\rm target} \to e^+ + e^-$, $e + \gamma_{\rm target} \to e' + \gamma'$, etc. The cascade spectrum is very close to the EGRET and FERMI-LAT observations in the range 3 MeV - 100 GeV [112, 113]. The observed energy density in this range is $\omega_{\rm Fermi} \approx 5.8 \times 10^{-7}$ eV/cm^3. It provides the upper limit for the cascade energy density. The upper limit on UHE neutrino flux $J_\nu(> E)$ (sum of all flavors) is given by the following chain of inequalities

$$\omega_{\rm cas} > 4\pi \int_E^\infty E' J_\nu(E') dE' > 4\pi E \int_E^\infty J_\nu(E') dE' \equiv 4\pi E^2 J_\nu(> E)\,. \quad (1.36)$$

In terms of the differential neutrino spectrum, Eq. (1.36) gives $J_\nu(E)$ as

$$E^2 J_\nu(E) < \frac{1}{4\pi}\omega_{\rm cas}, \quad \text{with } \omega_{\rm cas} < \omega_{\rm Fermi}. \quad (1.37)$$

Eq. (1.37) gives a rigorous upper limit on the neutrino flux. It is valid for neutrinos produced by HE protons, by topological defects, by annihilation and decays of superheavy particles, i.e., in all cases when neutrinos are produced through decay of pions and kaons. It holds for an arbitrary neutrino injection spectrum decreasing with energy. If one assumes some specific shape of neutrino spectrum, the cascade limit becomes stronger. For a generation spectrum proportional to E^{-2}, which is often assumed in model calculations, one obtains a stronger upper limit. Given for one neutrino flavor it reads [116]

$$E^2 J_i(E) \leq \frac{1}{3}\frac{1}{4\pi}\frac{\omega_{\rm cas}}{\ln(E_{\rm max}/E_{\rm min})}, \quad (1.38)$$

where $E_{\rm max}$ and $E_{\rm min}$ give the range of neutrino energies to which the E^{-2} spectrum extends, and $i = \nu_\mu + \bar\nu_\mu$, or $i = \nu_e + \bar\nu_e$, or $i = \nu_\tau + \bar\nu_\tau$. This upper

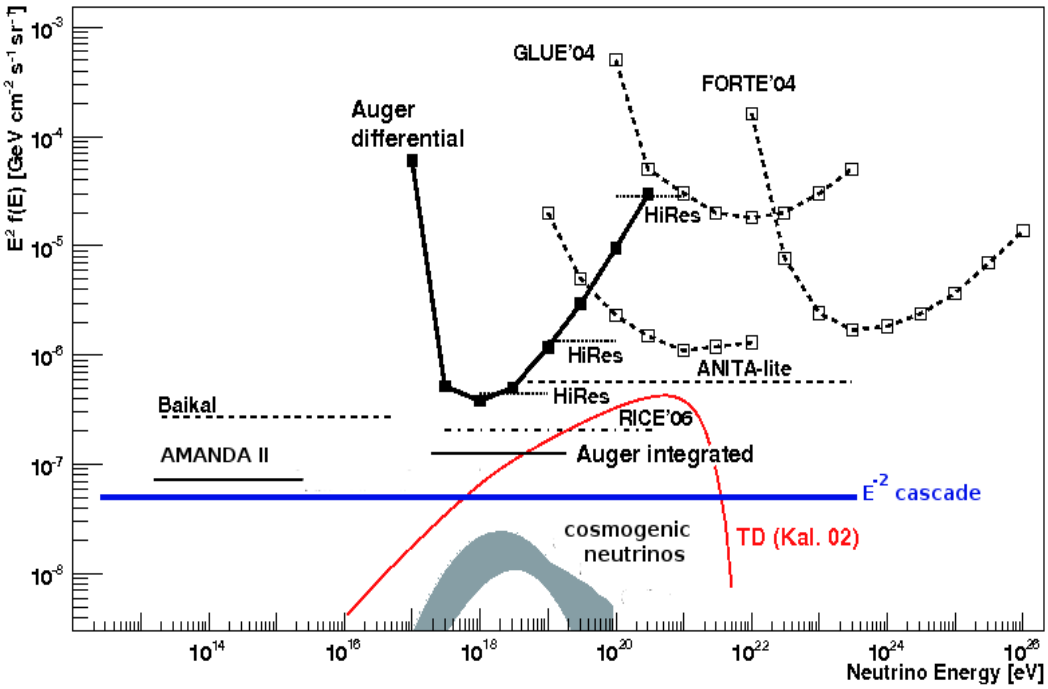

Figure 1.2: The experimental upper limits on UHE neutrino fluxes in comparison with the electromagnetic cascade upper limit in assumption of E^{-2} generation spectrum (labeled "E^{-2} cascade") and with predictions for cosmogenic neutrinos. Neutrino fluxes are given for one neutrino flavor $\nu_i + \bar{\nu}_i$.

limit is shown in Fig. 1.2. One can see that the observations almost reach the cascade upper limit and thus almost enter the region of allowed fluxes.

The most interesting energy range in Fig. 1.2 corresponds to $E_\nu > 10^{21}$ eV, where astrophysical acceleration mechanisms cannot provide protons with sufficient energy for production of these neutrinos. At present the region of $E_\nu > 10^{21}$ eV, and especially $E_\nu \gg 10^{21}$ eV is considered as a signature of top-down models, which provide these energies quite naturally.

1.3.1.2 UHE neutrino sources

Ultra high energy cosmic ray (UHECR) particles interacting with the CMB photons produce cosmogenic neutrinos. Besides, there may be neutrinos pro-

duced in decays or annihilation of superheavy particles. Cosmogenic neutrinos were first discussed in [117], soon after the prediction of the GZK cutoff [107, 108]. There, it was shown that UHE neutrino fluxes much higher than the observed UHECR flux can be produced by protons interacting with CMB photons at large redshifts. The predicted flux depends on the cosmological evolution of the sources of UHE protons and on the assumed acceleration mechanisms. Recent calculations of cosmogenic neutrino fluxes [118, 119] are normalized to the observed UHECR flux, with different assumptions about the sources.

The energies of cosmogenic neutrinos are limited by the maximum energy of acceleration, $E_{\rm acc}^{\rm max}$. To provide neutrinos with energies above 1×10^{20} eV, the energies of accelerated protons must exceed 2×10^{21} eV. For non-relativistic shocks, the maximum energy of acceleration $E_p^{\rm max}$ can optimistically reach 1×10^{21} eV. For relativistic shocks this energy can be somewhat higher. Production of cosmogenic neutrinos with still higher energies depends on less developed ideas, such as acceleration in strong electromagnetic waves, exotic plasma mechanisms of acceleration and unipolar induction.

The top-down scenarios, on the other hand, naturally provide neutrinos with energies higher and much higher than 1×10^{20} eV [120]. The mechanism common to many models assumes the existence of superheavy particles with very large masses up to the GUT scale $\sim 10^{16}$ GeV. Such particles can be produced by topological defects (TD)s. They then rapidly decay and produce a parton cascade, which is terminated by production of pions and other hadrons. Neutrinos are produced in hadron decays.

The production of unstable superheavy particles –the constituent fields

of TD– is a very common feature of the TD [9]. However, the dynamics of TD is highly nonlinear and complicated, the distance between TDs is model-dependent, and the calculation of UHE particle fluxes requires special consideration for different types of TD [8].

Apart from TDs, superheavy particles can naturally be produced by thermal processes [121, 122] and by time-varying gravitational fields [123, 124] shortly after the end of inflation. These particles can survive until present and produce neutrinos in their decays. Protected by symmetry, e.g. discrete gauge symmetry, in particular R-parity in supersymmetric theories, these particles can have very long lifetimes exceeding the age of the universe. The resulting neutrino flux may exceed the observed flux of UHECR. However, like any other form of cold dark matter (CDM), superheavy particles accumulate in the Milky Way halo and produce a large flux of UHE photons. The non-observation of these photons puts an upper limit on the neutrino flux from intergalactic space.

Some of the greatest discoveries in the field of high energy physics were thanks to studying cosmic rays, which include discovery of positron in 1932 [125], muon in 1936 [126, 127] and pion in 1947 [128]. Besides, the discovery of heavier mesons and baryons in cosmic ray experiments eventually led to the theory of strong interactions. Later, the experimental particle physics was taken over by accelerator experiments, where particles can be produced in a controlled way and their properties can be measured more accurately. As of today, the highest energies that can be reached at a particle accelerator is 14 TeV at the large hadron collider (LHC) at CERN. On the other hand, one needs to go beyond these energies to understand the physics of the early

universe, namely GUTs or superstring theory. Any piece of information from the early universe could serve as useful hints in this respect, hence the important role of UHE cosmic rays. One area of research, where fundamental physics and cosmic rays meet is the topological defects, in particular cosmic strings. Therefore, cosmic ray physics might be awaiting some new exciting discoveries.

As it was mentioned in the previous sections cosmic strings can produce observable UHE cosmic ray fluxes. Neutrinos are of particular interest to us since they can travel large cosmic distances without being absorbed or scattered much. The source of the neutrinos can be identified more accurately since they do not deflect in cosmic magnetic fields as protons do. We will estimate UHE neutrino fluxes originated from the cusps of cosmic string loops and the detectability conditions at the planned space based neutrino detector JEM-EUSO [129], which is the subject of Chapter 3 and 4.

Before closing this chapter, let us summarize the basic properties of the neutrino detector JEM-EUSO. JEM-EUSO will detect the extensive air showers (EAS) from the surface of the earth –UHE neutrinos produce EAS as they enter Earth's atmosphere. 90% of the energy is radiated as isotropic fluorescent light that can be detected by the optical telescope of the JEM-EUSO detector in space. JEM-EUSO has an optical telescope with a diameter of 2.5 m and it will observe an area of order 10^5 km^2 with a threshold energy 6×10^{10} GeV. It is planned to operate in 2012 [129].

Now in Chapter 2, we will turn our attention to the cosmological constraints on the abundance of moduli produced by the small loops of cosmic strings in the early universe.

Chapter 2

Cosmological Constraints

2.1 Introduction

String theory requires the presence of scalar fields called moduli such as complex structure and Kahler moduli which parametrize the volume and the shape of a six dimensional manifold representing the extra dimensions in string theory. There is also the modulus called dilaton whose expectation value determines the strength of the string coupling constant. Moduli are originally massless and their values are presumably fixed by the dynamics of the theory so that in the effective theory they become massive scalar fields. The idea of flux compactification made it possible to fix moduli by turning on some fluxes in the internal manifold [130]. The possibility of having a large number of values for different fluxes leads to the picture of string theory landscape where there exist 10^{500} different vacua [131]. In this large landscape of vacua, there are attractive models where some of the long standing problems are revisited such as the hierarchy [130, 32], the possibility of having a de Sitter vacuum

in string theory [132], brane inflation as the origin of inflation [93, 133] and cosmic superstrings [94, 134, 80, 3].

Moduli can be produced by the oscillating loops of cosmic strings[1]. Such moduli can have effects on big bang nucleosynthesis (BBN) and can also contribute to dark matter and diffuse gamma ray background. These effects for the gravitationally coupled moduli have been studied in detail [25, 27, 26]. Moduli are often expected to have Planck mass suppressed couplings. However, it was recently argued that some moduli couple to matter more strongly than the Planck mass suppressed coupling in warped and large volume flux compactification scenarios [34, 35, 33]. Refs. [34, 35] argue that the dilaton is localized in the IR region of a throat for a large warping, i.e., they are localized on the brane where all standard model fields live on. The dilaton mass is suppressed by the warp factor and coupling to matter is stronger than the Planck mass suppressed coupling. Localization of wavefunctions and stronger couplings to matter are expected for other moduli as well [34, 35].

The Giddings-Kachru-Polchinski model [130] was the first string theory realization of producing large hierarchies from pure numbers, i.e., quanta of fluxes. It was argued that the RS model gives an effective description of the warped compactification scenario with a large warp factor where the bulk space is replaced by the UV brane and all the 4D physics except for gravity is localized on the IR brane located at the bottom of the throat [31]. In the original RS model, the radial modulus is not fixed and left as a free parameter. A mechanism for stabilizing this modulus was proposed by Goldberger

[1]Moduli can also be produced thermally if the reheating temperature is high enough. We will comment on that possibility in Section 2.5.

and Wise [30], who showed that this modulus has a TeV suppressed coupling rather than Planck mass suppressed and has a TeV scale mass if the hierarchy problem is solved. Brummer *et al.* further showed that the RS model with the radial modulus stabilized by the Goldberger-Wise mechanism is the effective description of the warped compactification scenario [31]. Therefore, moduli with strong coupling seem generic in the warped Type-IIB flux compactification scenario.

Another model where a strongly coupled modulus is present is the so called large volume compactification where volume becomes exponentially large [32]. It was shown in [33] that one of the Kahler moduli can have mass $m \sim 10^6$ GeV and coupling to matter suppressed by the string mass scale $m_s \sim 10^{11}$ GeV for a particular value of the volume which leads to TeV scale SUSY breaking. In this model, there is another Kahler modulus with $m \sim 1$ MeV and Planck mass suppressed coupling to matter, which suggests the presence of both strongly and weakly coupled moduli together.

In this chapter, we derive the constraints on strongly and weakly coupled moduli produced by oscillating loops of cosmic strings and show that they are significantly relaxed for large modulus coupling constants. Organization of this chapter is as follows: In Sec. 2.2, modulus radiation from cosmic string loops is summarized. In Sec. 2.3, modulus and loop lifetimes are estimated and the density of loops in the universe is given. In Sec. 2.4, we derive the abundance of moduli produced by strings and obtain the upper limits on both strongly and weakly coupled moduli abundances from diffuse gamma ray background [112], big bang nucleosynthesis [135, 136, 137], the dark matter density [36], and use the lower limit on scalar field mass from Cavendish-type experiments

[138]. The regions free from constraints are shown in Fig. 2.1 and Fig. 2.2 for the parameter space in terms of string tension $G\mu$ and modulus mass m for various values of modulus coupling constant α. Finally, in Sec. 2.5, thermal production of moduli is discussed.

2.2 Modulus radiation from strings

A modulus ϕ couples to matter via trace of its energy momentum tensor [25, 30, 33]

$$\mathcal{L}_{int} \sim \frac{\alpha}{m_p}\phi T^{\mu}_{\mu}, \tag{2.1}$$

where α is the modulus coupling constant, m_p is the Planck mass and T^{μ}_{μ} is the trace of the matter energy momentum tensor.

We consider oscillating loops of cosmic strings coupled to a modulus as a periodic source of moduli production. Modulus radiation from a loop of cosmic string occurs with the power [25]

$$P_m \sim 30\alpha^2 G\mu^2, \tag{2.2}$$

when the loop size $L \lesssim 4\pi/m$, where m is the modulus mass. This part of the spectrum corresponds to moduli produced from small oscillating loops and so it is relevant to the early universe. We will call this part of the spectrum as background moduli. The corresponding average particle emission rate is

$$\dot{N} \sim 13\frac{\alpha^2 G\mu^2}{\omega}, \tag{2.3}$$

where ω is the energy of a modulus in the rest frame of the loop. Moduli are mainly produced in the fundamental oscillation mode with $\omega = 4\pi/L$, where

L is the size of the loop [25]. Thus, the particle emission rate can be expressed as

$$\dot{N} \sim \frac{13}{4\pi}\alpha^2 G\mu^2 L. \tag{2.4}$$

When $L >> 4\pi/m$, the main contribution to the radiation spectrum comes from cusps and has a different power spectrum. Such moduli are produced in late epochs and have larger lifetimes due to large boost factors of the cusps. Possible observable effects of such moduli will be discussed in Chapter 3. Here, we will only consider the background moduli and their cosmological effects.

2.3 Lifetime and loop density

The rate of decay of a modulus into the standard model (SM) gauge bosons can be estimated as

$$\Gamma \sim n_{SM}\left(\frac{\alpha}{m_p}\right)^2 m^3, \tag{2.5}$$

where $n_{SM} = 12$ is the total number of spin degrees of freedom for all SM gauge bosons, and m is the modulus mass and we assume interaction of the form [33]

$$\mathcal{L}_{int} \sim \frac{\alpha}{m_p}\phi F_{\mu\nu}F^{\mu\nu}. \tag{2.6}$$

The mean lifetime of such a modulus in its rest frame can be estimated as the inverse of the decay rate as

$$\tau \sim 8.1 \times 10^{12}\alpha^{-2} m_{GeV}^{-3}\, s, \tag{2.7}$$

where $m_{GeV} \equiv m/(1\text{ GeV})$.

An oscillating loop of cosmic string also produces gravitational radiation

with the power [1]

$$P_g \sim 50 G\mu^2. \tag{2.8}$$

The main energy loss mechanism for a loop of cosmic string is the gravitational radiation provided that $P_g \gtrsim P_m$ which occurs when $\alpha \lesssim 1$. The $\alpha \sim 1$ case was worked out in Refs. [25, 26, 27], where they found the upper bound on string tension as strong as $G\mu \lesssim 10^{-20}$ for a wide range of m. On the other hand, when moduli are strongly coupled to matter, i.e., $\alpha >> 1$, modulus radiation becomes the dominant energy loss mechanism for the loops, hence this leads to significant modifications of the constraints obtained in [25, 26, 27].

When the modulus radiation dominates, lifetime of a loop is given by

$$\tau_L \sim \frac{\mu L}{P_m} \sim \frac{L}{30\alpha^2 G\mu}. \tag{2.9}$$

The constraints we will obtain in the next section depend upon the length of the loops formed from the cosmic string network. There is still no consensus on the evolution of string network; Analytical works [81, 139, 140] and different simulations [141, 142, 82, 83, 84] yield different answers. However, the biggest recent simulations [84] suggest that a loop formed at cosmic time t has a typical length

$$L \sim \beta t, \tag{2.10}$$

with $\beta \sim 0.1$.

The loops of interest to us are the ones formed in the radiation dominated era whose number density is given by [1]

$$n(L,t) \sim \zeta \beta^{1/2} (tL)^{-3/2}, \tag{2.11}$$

where $\zeta \sim 16$, $30\alpha^2 G\mu t \lesssim L \lesssim \beta t$.

Loops cannot produce moduli efficiently at times $t \lesssim t_d \sim t_p/(G\mu)^2$, where t_p is the Planck time, since they lose most of their energy due to plasma friction [1]. Therefore, we consider later times where the loops reach a scaling solution and the modulus radiation becomes the main energy loss mechanism.

The particle emission rate (2.4) is valid for the loops of size $L \lesssim 4\pi/m$, which exist only at $t \lesssim t_m$, and t_m can be obtained from (2.9) as

$$t_m \sim \frac{4\pi}{30}\alpha^{-2}(G\mu)^{-1}m^{-1}. \tag{2.12}$$

Thus, we will be interested in moduli produced in the time interval

$$t_d \lesssim t \lesssim t_m. \tag{2.13}$$

This implies $t_m \gtrsim t_d$, which can be expressed as

$$G\mu \gtrsim \frac{30}{4\pi}\alpha^2\frac{m}{m_p} \sim 2\times 10^{-19}\alpha^2 m_{GeV}. \tag{2.14}$$

We represent this condition on the parameter space plots given in the next section as a dashed line below which no moduli are produced. Thus, the corresponding region is free from the constraints[2].

2.4 Cosmological constraints on moduli

2.4.1 Abundance

Modulus abundance is given by $Y(t) = n_m(t)/s(t)$ where $n_m(t)$ is the modulus number density and $s(t)$ is the entropy density given by

$$s(t) = 0.0725\mathcal{N}^{1/4}\left(\frac{m_p}{t}\right)^{3/2}, \tag{2.15}$$

[2]Plasma friction may or may not affect cosmic F- and D-strings depending on whether they interact with ordinary matter or not. However, thermally produced bulk field background, such as moduli, might have a similar effect on cosmic F- and D-strings. If they are not affected by friction, the condition (2.14) is removed for these types of cosmic strings.

where $\mathcal{N} \sim 100$ is the total number of spin degrees of freedom in the radiation dominated era at early times t.

The total number of moduli produced by a single loop until cosmic time $t < \tau_L$ can be obtained from (2.4) as

$$N \sim \dot{N}t \sim \frac{13}{4\pi}\alpha^2 G\mu^2 Lt. \tag{2.16}$$

By using (2.11) and (2.16), the number density of moduli in the universe produced by the loops of size L can be found as

$$n_m(t) \sim Nn(L,t) \sim \frac{13}{4\pi}\zeta\beta^{1/2}(Lt)^{-1/2}\alpha^2 G\mu^2. \tag{2.17}$$

Thus, the modulus abundance can be estimated as

$$Y \sim 4.5\zeta\beta^{1/2}L^{-1/2}tm_p^{-3/2}\alpha^2 G\mu^2, \tag{2.18}$$

Note that the smallest loops of size $L_{min} \sim 30\alpha^2 G\mu t$ dominate the abundance. After substituting $L = L_{\min}$ in (2.18), it can be seen from (2.13) that $t = t_m$ gives the most dominant contribution to the abundance. Using these facts, we obtain

$$Y \sim 2.7(G\mu)\left(\frac{m_p}{m}\right)^{1/2} \sim 9.4 \times 10^9 (G\mu) m_{GeV}^{-1/2}. \tag{2.19}$$

Note that the dependence on $G\mu$ in equation (2.19) is different from that found in [25], since there it was assumed that $\beta \sim 50G\mu$. Although $\beta \sim 0.1$ seems to lead to more stringent constraints on string tension $G\mu$, we will see that the constraints are relaxed when the coupling constant α becomes large enough.

2.4.2 Constraints on strongly coupled moduli

Short distance tests of Newton's Law of gravity in Cavendish-type experiments give a lower bound on the modulus mass as $m > 10^{-3}$ eV, i.e., $m_{GeV} > 10^{-12}$

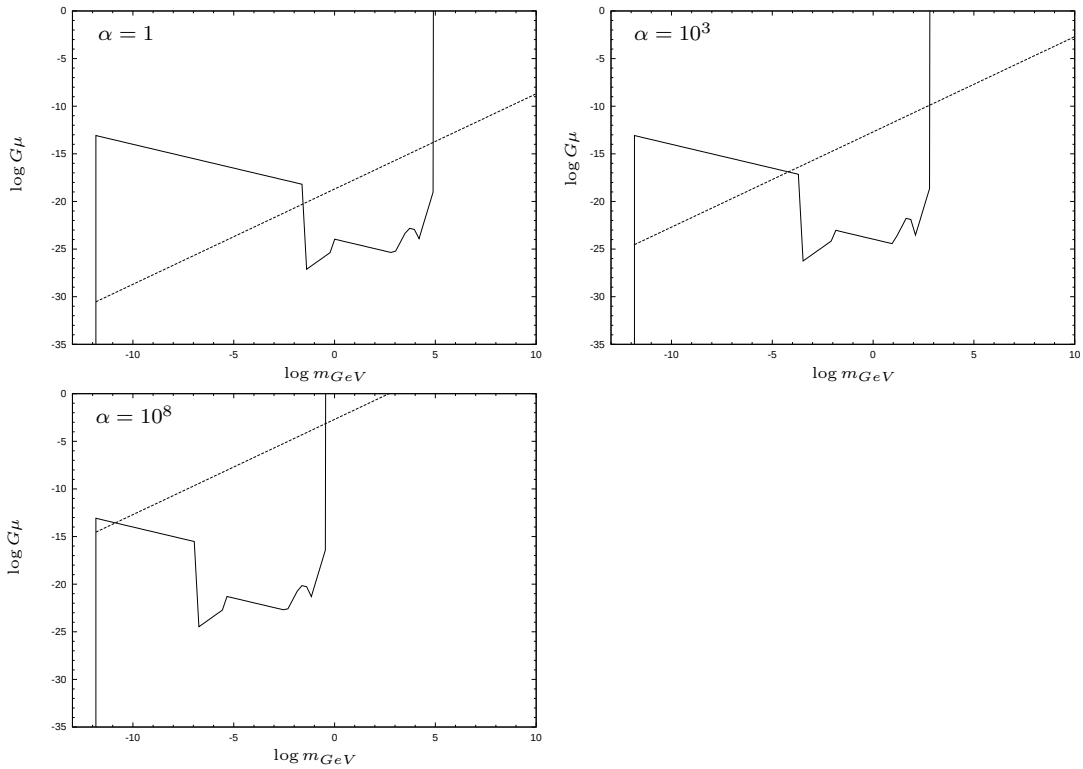

Figure 2.1: $\log G\mu$ vs. $\log m_{GeV}$ for strongly coupled moduli. The region above the solid line is forbidden by the cosmological constraints. The region below the dashed line is free from the constraints for the loops affected by plasma friction since such moduli are never produced because of friction domination. Note that if F- and D-strings do not interact with ordinary matter like solitonic cosmic strings do, the friction domination does not apply, and thus one should ignore the dashed line in that case.

[138].

If moduli are long-lived, i.e., $\tau \gtrsim t_0$, they contribute to the dark matter in the universe. Here, $t_0 \sim 4.3 \times 10^{17} s$ is the age of the universe. Thus, we have the upper bound $\Omega_m h^2 < 0.13$ [36] or in terms of abundance $Y < 9.6 \times 10^{-10} m_{GeV}^{-1}$.

If moduli are long-lived, they also contribute to the diffuse gamma ray background [111]. When $\tau \gtrsim t_0$, the energy density of moduli that decayed

into photons until the present time can be estimated as

$$\rho_m \sim Y s(t_0) m \frac{t_0}{\tau} \sim 2.2 \times 10^{17} Y m_{GeV}^4 \alpha^2 \; eV \, cm^{-3}, \tag{2.20}$$

where t_0/τ is the fraction of the decayed moduli and $s(t_0) = s(t_{eq})(t_{eq}/t_0)^2 \sim 2.9 \times 10^{-38}$ GeV^3. According to EGRET data, an approximate upper bound on the diffuse gamma ray density for the photons of energy $>$ MeV is $\rho_\gamma \sim 2.0 \times 10^{-6}$ eV cm^{-3} [112]. Using this upper bound, we can estimate the limit on the abundance from the constraint $\rho_m \lesssim \rho_\gamma$ as $Y \lesssim 9.1 \times 10^{-24} \alpha^{-2} m_{GeV}^{-4}$.

When $t_{dec} \sim 10^{13} \, s \lesssim \tau \lesssim t_0$, the most stringent constraint comes from the diffuse gamma ray background [111]. Assuming all the moduli decay by the time τ, the energy density can be estimated as

$$\rho_m \sim Y s(\tau) m \sim 1.1 \times 10^{22} Y \alpha^4 m_{GeV}^7 \; eV \, cm^{-3}, \tag{2.21}$$

where $s(\tau) = s(t_{eq})(t_{eq}/\tau)^2 \sim 8.2 \times 10^{-29} \alpha^4 m_{GeV}^6$ GeV^3. Redshifting the photon energy density to time $t = \tau$, we find

$$\rho_\gamma(\tau) \sim \rho_\gamma \left(\frac{t_0}{\tau} \right)^{8/3} \sim 1.0 \times 10^7 \alpha^{16/3} m_{GeV}^8 \, eV \, cm^{-3}, \tag{2.22}$$

which gives and upper bound on the modulus abundance as $Y \lesssim 9.1 \times 10^{-16} \, \alpha^{4/3} m_{GeV}$.

If the modulus lifetime is shorter than t_{dec}, they can have effects on primordial element abundances [135, 136, 137]. When such moduli decay electromagnetically, they dissolve the light elements created during nucleosynthesis. Besides, modulus-gluon coupling leads to hadron production which can also change the primordial light element abundances. We made a piecewise power law approximation to the results of [135, 136, 137], where the upper bounds

τ_s	Y
$10^4 \lesssim \tau_s \lesssim 10^{13}$	$10^{-14} m_{GeV}^{-1}$
$10^2 \lesssim \tau_s \lesssim 10^4$	$10^{-8} \tau_s^{-3/2} m_{GeV}^{-1}$
$10 \lesssim \tau_s \lesssim 10^2$	$10^{-11} m_{GeV}^{-1}$
$10^{-2} \lesssim \tau_s \lesssim 10$	$10^{-11} \tau_s^{-5/2} m_{GeV}^{-1}$

Table 2.1: BBN constraints on the strongly coupled modulus abundance. This table shows the approximate upper bounds on the strongly coupled modulus abundance as a function of modulus lifetime and modulus mass. Note that $\tau_s \equiv \tau/sec$.

on the abundance of long lived particles on BBN are given as a function of their lifetime. We summarized the upper bounds in Table 2.1.

Using the bounds obtained from Cavendish-type experiments, diffuse gamma ray background, BBN and dark matter constraints, we obtain the limits on string tension $G\mu$, modulus mass m and modulus coupling constant α. Using all these constraints, we obtained Fig. 2.1 for the parameter space of $G\mu$ vs. m_{GeV} for various values of α. The analytic forms of the constraints in all parameter ranges are given in Table 2.2. As it can be seen from Fig. 2.1, the constraints become weaker as α increases. The condition (2.14) shifts towards the upper end of the parameter space which leads to the region free from the constraints below the dashed line where no moduli are produced from cosmic strings.

2.4.3 Constraints on weakly coupled moduli

In the previous section, we analyzed the cosmological constraints on strongly coupled moduli. In this section, we will assume that there is at least one strongly coupled modulus and one weakly coupled modulus (coupling sup-

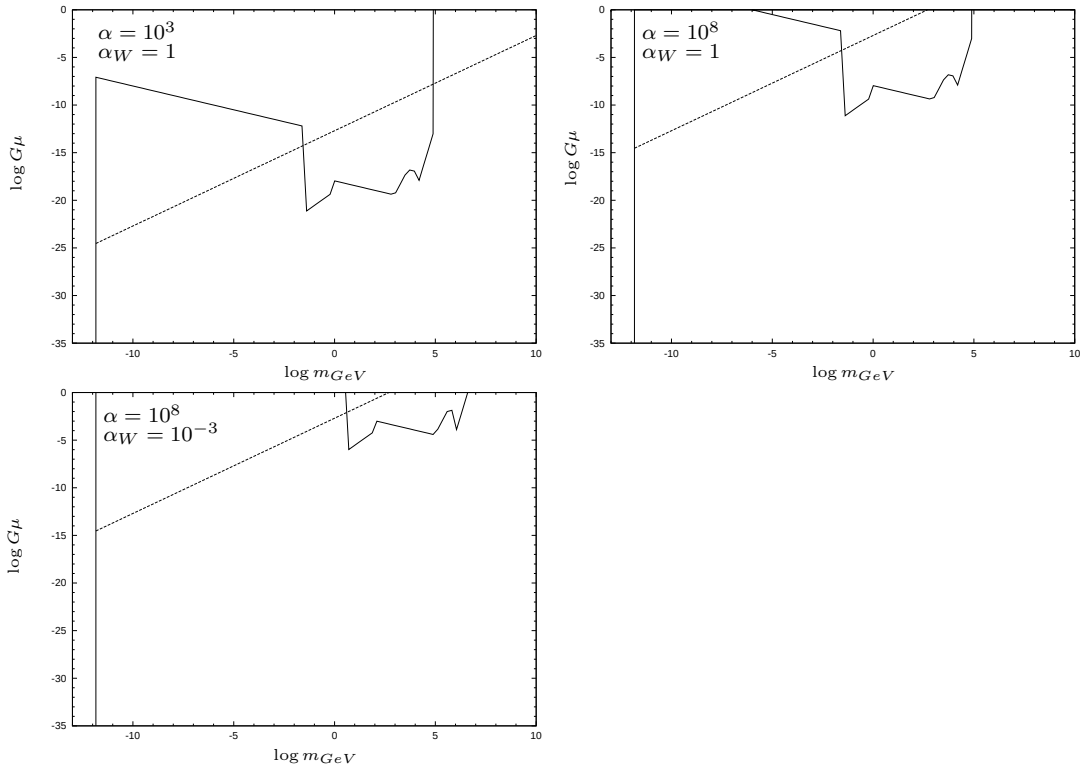

Figure 2.2: $\log G\mu$ vs. $\log m_{GeV}$ for weakly coupled moduli when $m_{weak} \gtrsim m_{strong}$. The region above the solid line is forbidden by the cosmological constraints. The region below the dashed line is free from the constraints for the loops affected by plasma friction since such moduli are never produced because of friction domination. Note that if F- and D-strings do not interact with ordinary matter like solitonic cosmic strings do, then the friction domination does not apply, and thus one should ignore the dashed line in that case.

m_{GeV}	$G\mu$
$10^{-12} \lesssim m_{GeV} \lesssim 3 \times 10^{-2}\alpha^{-2/3}$	$1.0 \times 10^{-19} m_{GeV}^{-1/2}$
$10^{-12} \lesssim m_{GeV} \lesssim 3 \times 10^{-2}\alpha^{-2/3}$	$9.7 \times 10^{-34}\alpha^{-2} m_{GeV}^{-7/2}$
$3 \times 10^{-2}\alpha^{-2/3} \lesssim m_{GeV} \lesssim 9.3 \times 10^{-1}\alpha^{-2/3}$	$9.1 \times 10^{-26}\alpha^{4/3} m_{GeV}^{3/2}$
$9.3 \times 10^{-1}\alpha^{-2/3} \lesssim m_{GeV} \lesssim 9.3 \times 10^{2}\alpha^{-2/3}$	$1.1 \times 10^{-24} m_{GeV}^{-1/2}$
$9.3 \times 10^{2}\alpha^{-2/3} \lesssim m_{GeV} \lesssim 4.3 \times 10^{3}\alpha^{-2/3}$	$4.6 \times 10^{-38}\alpha^{3} m_{GeV}^{4}$
$4.3 \times 10^{3}\alpha^{-2/3} \lesssim m_{GeV} \lesssim 9.3 \times 10^{3}\alpha^{-2/3}$	$1.1 \times 10^{-21} m_{GeV}^{-1/2}$
$9.3 \times 10^{3}\alpha^{-2/3} \lesssim m_{GeV} \lesssim 9.3 \times 10^{4}\alpha^{-2/3}$	$5.7 \times 10^{-54}\alpha^{5} m_{GeV}^{7}$

Table 2.2: Constraints on the string tension $G\mu$ for strongly coupled moduli. This table shows the upper bounds we obtain from Cavendish type experiments, diffuse gamma ray background, BBN and dark matter density constraints on $G\mu$ for strongly coupled moduli as a function of modulus mass m and modulus coupling constant α.

pressed by at least Planck mass) with coupling constants $\alpha >> 1$ and $\alpha_W \lesssim 1$, respectively. We will estimate the cosmological constraints on weakly coupled moduli similar to the previous section.

Note that the dominant energy loss mechanism for the loops is still via strongly coupled modulus radiation, thus the loop lifetime is given by (2.9) and the minimum size of the loops is $L_{min} \sim 30\alpha^2 G\mu t$. On the other hand, the modulus lifetime depends upon its coupling to matter and is given by

$$\tau_W \sim 8.1 \times 10^{12} \alpha_W^{-2} m_{GeV}^{-3}\, s. \tag{2.23}$$

The abundance of weakly coupled moduli can be calculated as

$$Y_W \sim 9.4 \times 10^{9} \alpha^{-2} \alpha_W^{2} (G\mu) m_{GeV}^{-1/2}. \tag{2.24}$$

which is valid for $m_{weak} \gtrsim m_{strong}$ where m_{weak} and m_{strong} are the masses of the strongly and the weakly coupled moduli, respectively. However, if $m_{weak} < m_{strong}$, although the strongly coupled moduli production terminates at $t_{m_{strong}}(\alpha)$ given by equation (2.12), weakly coupled moduli are still

produced and the process terminates at $t_{m_{weak}}(\alpha = 1)$. At this point, gravitational radiation starts dominating and the abundance becomes $Y_W \sim 5.6 \times 10^9 \alpha_W^2 (G\mu) m_{GeV}^{-1/2}$. Therefore, the constraints are the same as given on Fig. 2.1 for $\alpha = 1$ case when $m_{weak} < m_{strong}$ assuming $\alpha_W \sim 1$.

In the opposite regime, when $m_{weak} > m_{strong}$, by using (2.24) and all the constraints we discussed in the previous section, we obtained the parameter space in Fig. 2.2 for various values of α_W and α. Once again, the analytic forms of the constraints are given in Table 2.3. As can be seen from Fig. 2.2, the constraints become less important as α increases and α_W decreases since the abundance is suppressed by $\alpha^{-2}\alpha_W^2$. Besides, the condition (2.14) becomes stronger for larger α and there is a larger region in the parameter space below the dashed line free from the constraints.

m_{GeV}	$G\mu$
$10^{-12} \lesssim m_{GeV} \lesssim 3 \times 10^{-2} \alpha_W^{-2/3}$	$1.0 \times 10^{-19} \alpha^2 \alpha_W^{-2} m_{GeV}^{-1/2}$
$10^{-12} \lesssim m_{GeV} \lesssim 3 \times 10^{-2} \alpha_W^{-2/3}$	$9.7 \times 10^{-34} \alpha^2 \alpha_W^{-4} m_{GeV}^{-7/2}$
$3 \times 10^{-2} \alpha_W^{-2/3} \lesssim m_{GeV} \lesssim 9.3 \times 10^{-1} \alpha_W^{-2/3}$	$9.1 \times 10^{-26} \alpha^2 \alpha_W^{-2/3} m_{GeV}^{3/2}$
$9.3 \times 10^{-1} \alpha_W^{-2/3} \lesssim m_{GeV} \lesssim 9.3 \times 10^{2} \alpha_W^{-2/3}$	$1.1 \times 10^{-24} \alpha^2 \alpha_W^{-2} m_{GeV}^{-1/2}$
$9.3 \times 10^{2} \alpha_W^{-2/3} \lesssim m_{GeV} \lesssim 4.3 \times 10^{3} \alpha_W^{-2/3}$	$4.6 \times 10^{-38} \alpha^2 \alpha_W m_{GeV}^{4}$
$4.3 \times 10^{3} \alpha_W^{-2/3} \lesssim m_{GeV} \lesssim 9.3 \times 10^{3} \alpha_W^{-2/3}$	$1.1 \times 10^{-21} \alpha^2 \alpha_W^{-2} m_{GeV}^{-1/2}$
$9.3 \times 10^{3} \alpha_W^{-2/3} \lesssim m_{GeV} \lesssim 9.3 \times 10^{4} \alpha_W^{-2/3}$	$5.7 \times 10^{-54} \alpha^2 \alpha_W^{3} m_{GeV}^{7}$

Table 2.3: Constraints on the string tension $G\mu$ for weakly coupled moduli. This table shows the upper bounds we obtain from Cavendish-type experiments, diffuse gamma ray background, BBN and dark matter density constraints on $G\mu$ for weakly coupled moduli when $m_{weak} \gtrsim m_{strong}$ as a function of modulus mass m and moduli coupling constants α and α_W. When $m_{weak} < m_{strong}$, one should set $\alpha = 1$ in the above table.

2.5 Thermally produced moduli background

So far we have discussed the production of moduli from cosmic strings. Moduli can also be produced thermally if the reheating temperature is high enough. The photon-modulus interaction can be written as

$$\mathcal{L}_{int} \sim \frac{\alpha}{m_p}\phi F^{\mu\nu}F_{\mu\nu}. \tag{2.25}$$

Moduli should be in thermal equilibrium with photons for the thermal production to occur. The lowest order process which contributes to the interaction $\gamma\gamma \rightarrow \phi\phi$ is second order and the cross section can be estimated as

$$\sigma \sim \left(\frac{\alpha^2}{m_p^2}\right)^2 E^2, \tag{2.26}$$

where $E \sim T$ is the energy of photons at temperature T.

For substantial thermal production of moduli to occur, the rate of thermal modulus production should be greater than the expansion rate of the universe H, i.e.,

$$\Gamma_{th} \sim \sigma n_\gamma \gtrsim H, \tag{2.27}$$

where n_γ is the photon density at temperature T. Using (2.26), $n_\gamma \sim T^3$ and $H \sim T^2/m_p$ in (2.27), we obtain

$$T \gtrsim \alpha^{-4/3} m_p. \tag{2.28}$$

For instance, when $\alpha \sim 10^9$, (2.28) implies $T_{rh} \gtrsim 10^7$ GeV. Since reheating temperature is also model dependent, strongly coupled moduli may or may not be produced thermally. On the other hand, weakly coupled moduli cannot be produced since $T_{rh} \gtrsim m_p$ is required for $\alpha \lesssim 1$.

Assuming strongly coupled moduli are produced thermally and dominate the universe, we can estimate the temperature after their decay. The decay rate of moduli is

$$\Gamma_{dec} \sim \left(\frac{\alpha}{m_p}\right)^2 m^3, \tag{2.29}$$

and when $\Gamma_{dec} \sim H \sim T^2/m_p$, moduli will decay and reheat the universe to temperature T. Using that, we obtain

$$T \sim \alpha \left(\frac{m}{m_p}\right)^{1/2} m. \tag{2.30}$$

The weakest constraint one can consider is that T should be at least at the nucleosynthesis temperature ~ 1 MeV. Using $T \gtrsim 1$ MeV, we obtain the constraint

$$\alpha \gtrsim 10^6 m_{GeV}^{-3/2}. \tag{2.31}$$

2.6 Conclusions

We consider oscillating loops of cosmic strings as periodic sources of moduli production. When $\alpha \lesssim 1$, gravitational radiation is the dominant energy loss mechanism for the loops. The constraints for this case are identical to $\alpha = 1$ case for the strongly coupled moduli as we have shown on Fig. 2.1. Note that our results for $\alpha \sim 1$ are more stringent than that of [25, 27, 26]. This is mainly because of the fact that they assume $\beta \sim 50G\mu$ in their calculations whereas we use $\beta \sim 0.1$ from the recent simulations [82, 83, 84].

When a modulus is strongly coupled to matter, i.e., $\alpha \gtrsim 1$, modulus radiation is the dominant energy loss mechanism for the loops. Hence, loop lifetimes depend upon α. Besides, modulus lifetime shortens as α is increased

if the modulus mass is kept constant. These two effects make the cosmological constraints we obtained for the strongly coupled moduli less severe. Basically, for moduli to have effects on BBN, and to contribute to dark matter and diffuse gamma ray background, their lifetime should be long enough. As can seen from Fig. 2.1, this implies that strongly coupled moduli can have effects on cosmology only if their mass is small enough, since lighter moduli have longer lifetimes compared to the more massive ones.

In addition, loops cannot radiate moduli effectively in the friction dominated epoch since they lose their energy mostly via friction. The condition for friction domination (2.14) becomes stronger when α is larger. A larger region of the parameter space is allowed as α is increased since friction domination does not let moduli to be produced by cosmic strings in that region. This may not be the case for F- and D-strings since they may or may not interact with ordinary matter depending on where they are located in extra dimensions. However, if there is a thermally produced moduli background, a similar effect might occur for F- and D-strings which needs further investigation.

We consider warped and large volume compactifications as the two examples where at least one strongly coupled modulus is present. In the warped compactification scenario, there is some evidence for moduli localization in long throat regions which leads to stronger coupling to matter and smaller moduli masses [34, 35]. This suggests that warped compactification with a long throat can be effectively described by the RS model with its radion stabilized by Goldberger-Wise mechanism [31]. As it was argued some time ago by Goldberger and Wise, RS radion has TeV suppressed coupling to matter [30]. Interpolating our results for this particular case, we see that the RS

radions produced by cosmic strings are free from the cosmological constraints we considered in this work.

As a second example, we consider large volume compactification where a strongly coupled modulus is present. One of the Kahler moduli in this scenario has a mass $m \sim 10^6$ GeV and a string mass scale suppressed coupling where $m_s \sim 10^{11}$ GeV [33]. In our notation, this means that $\alpha \sim 10^8$, hence a strongly coupled modulus. As we can see from Fig. 2.1, this modulus is free from the cosmological constraints we considered.

In the large volume compactification scenario, there is another Kahler modulus with Planck mass suppressed coupling to matter, i.e., $\alpha \sim 1$. This suggests the possibility of having at least one strongly coupled and a weakly coupled modulus together. We also calculated the constraints on weakly coupled moduli and show our results in Fig. 2.1 with $\alpha = 1$ for $m_{weak} < m_{strong}$ case and in Fig. 2.2 for $m_{weak} \gtrsim m_{strong}$ case. In particular, the constraints on the weakly coupled Kahler modulus of the large volume scenario are the same as in the first plot of Fig. 2.1 ($\alpha = 1$), since $m_{weak} \sim 1$ MeV $< m_{strong} \sim 10^6$ GeV. Note that in this model, the maximum string tension can only be $G\mu \sim 10^{-16}$. If we take $\alpha_W \sim 1$ and $m_{weak} \sim 1$ MeV, the constraints on this weakly coupled modulus are not stringent. On the other hand, as can be seen from Fig. 2.2, constraints are quite weak for the $\alpha = 10^8$, $\alpha_W = 1$ case. If $\alpha_W << 1$, then weakly coupled moduli with $m_{weak} \gtrsim m_{strong}$ are free from constraints since their abundance is suppressed by $\alpha^{-2}\alpha_W^2$.

We also consider the possibility of producing moduli thermally. We found that if the universe has ever reached the temperature of order $T \sim \alpha^{-4/3} m_p$, then moduli can be produced thermally. If the hierarchy problem is solved

with warped geometry, the RS radion couples to matter with $\alpha \sim 10^{15}$ and (2.31) implies $m \gtrsim 10^{-6}$ GeV for the RS radion mass. Since it is expected that $m \sim 1$ TeV [30], the RS radion is free from both the cosmological constraints from cosmic strings and the thermally produced radion background constraint. For the strongly coupled Kahler modulus in the large volume scenario, the constraint (2.31) implies $m \gtrsim 10^{-2}$ GeV. Since $m \sim 10^{6}$ GeV in this model [33], it is also free from the thermally produced moduli background constraint. Finally, we also found that weakly coupled moduli cannot be produced thermally since $T \gtrsim m_p$ would be required for this to happen.

In this chapter, we assumed that the reconnection probability of strings is $p = 1$ which is true for the ordinary cosmic strings. However, for cosmic F- and D-strings $p < 1$ which leads to an enhancement of the string density in the universe [134, 80]. Therefore, the constraints are expected to be a little bit stronger for $p < 1$ case. However, this turns out to be an insignificant effect [27].

The main conclusion of this chapter is that when there is at least one type of strongly coupled modulus, both the cosmological and the thermally produced moduli background constraints on strongly and weakly coupled moduli become less severe and for sufficiently large values of α, they are free from the constraints considered in this chapter.

Chapter 3

Modulus radiation from cusps

3.1 Introduction

In this chapter, we will discuss modulus radiation from cosmic string cusps as a mechanism of cosmic ray production, which does not assume string superconductivity or Higgs condensates. It relies on the existence of moduli –relatively light, weakly coupled scalar fields, predicted in supersymmetric particle theories, including string theory. Moduli would be copiously radiated by oscillating loops of string at early cosmic times, when the loops are very small and their frequency of oscillation is greater than the modulus mass. The emitted moduli and their decay products can manifest themselves observationally in many different ways; this leads to stringent constraints on both the cosmic string tension and modulus mass as discussed in Chapter 2 [25, 26]. We showed in Chapter 2 that the constraints are relaxed significantly for strongly coupled moduli [28]. It turns out that the range of the parameters for strongly coupled moduli that give rise to observable neutrino fluxes are in the allowed range of

the constraints discussed in Chapter 2.

At later times, moduli can only be emitted from cusps, resulting in sharp bursts of high-energy moduli. Eventually moduli decay into standard model particles, and their decay products can be observed as cosmic rays. Of particular interest are neutrinos, which can travel over cosmological distances, so moduli decaying in a wide redshift interval from $z = 0$ to the neutrino horizon $z_\nu \sim 10^2$ can yield observable events.

In this chapter, we will treat the modulus mass and coupling constant and the string tension as free parameters. We will estimate the ultra-high energy (UHE) neutrino flux resulting from modulus decays and indicate some values of the parameters that can yield observable fluxes. This chapter is organized as follows. In Sec. 3.2, we review modulus emission from cosmic string cusps. In Sec. 3.3, we discuss modulus decay, UHE neutrino production in the resulting hadronic cascades, and subsequent neutrino propagation. In Sec. 3.4, we review the size distribution of cosmic string loops and calculate the rate of bursts and the diffuse flux of UHE neutrinos. We also discuss the upper bound on the neutrino flux, resulting from the diffuse gamma ray background observations. In Sec. 3.5, we give an illustrative example where our scenario can be implemented, namely the strongly coupled moduli in the large volume compactification model in string theory, and find the values of the string tension μ for which observable UHE neutrino fluxes can be obtained.

3.2 Modulus radiation from cosmic string cusps

The effective action for a modulus field ϕ interacting with a cosmic string of tension μ is given by [25, 30, 33]

$$S = -\int d^4x \left[\frac{1}{2}(\nabla\phi)^2 + \frac{1}{2}m^2\phi^2 + \frac{\sqrt{4\pi}\alpha}{m_p}\phi T^\nu_\nu\right] - \mu\int d^2\sigma\sqrt{-\gamma}, \qquad (3.1)$$

where γ is the determinant of the induced worldsheet metric $\gamma_{ab} = g_{\mu\nu}X^\mu_{,a}X^\nu_{,b}$, $X^\mu(\sigma,\tau)$ is the string worldsheet, T^ν_ν is the trace of the energy momentum tensor of the string, α is the modulus coupling constant, m is the modulus mass and m_p is the Planck mass. For $\alpha \sim 1$, the modulus coupling to matter is suppressed by the Planck scale. Here, we treat α as a free parameter and are mainly interested in $\alpha \gg 1$. Then, the mass scale characterizing the modulus interactions is $\sim m_p/\alpha \ll m_p$. Values as large as $\alpha \sim 10^{15}$ have been discussed in the literature [30].

The modulus field equation has the form

$$(\nabla^2 - m^2)\phi(x) = -\frac{\sqrt{4\pi}\alpha}{m_p}T^\nu_\nu(x), \qquad (3.2)$$

with

$$T^\nu_\nu(x) = -2\mu\int d\tau d\sigma\sqrt{-\gamma}\delta^4(x^\alpha - x^\alpha(\sigma,\tau)). \qquad (3.3)$$

The power spectrum of modulus radiation from an oscillating loop of string can be decomposed in Fourier modes as [25]

$$\frac{dP_n}{d\Omega} = \frac{G\alpha^2}{2\pi}\omega_n k|T(\mathbf{k},\omega_n)|^2, \qquad (3.4)$$

where G is the Newton's constant, $\omega_n = \sqrt{k^2+m^2} = 4\pi n/L$, L is the length of the loop,

$$T(\mathbf{k},\omega_n) = -\frac{4\mu}{L}\int d^4x\int d\sigma d\tau\sqrt{-\gamma}\delta^4(x^\alpha - x^\alpha(\sigma,\tau))e^{ik_\nu X^\nu(\sigma,\tau)}, \qquad (3.5)$$

and $k^\nu = (\omega_n, \mathbf{k})$.

We will be interested in the modulus emission from large loops of string, having length $L \gg m^{-1}$. In this case, the characteristic frequency of loop oscillation is $\omega \sim 1/L \ll m$, so modulus production is suppressed, except in the vicinity of cusps, where extremely high frequencies can be reached in a localized portion of the loop for a brief period of time. Lorentz factors greater than γ are reached in a fraction of the loop of invariant length $\Delta L \sim L/\gamma$.

In a flat background, i.e., $g_{\mu\nu} = \eta_{\mu\nu} = diag(-1, 1, 1, 1)$, the equation of motion for the string worldsheet $X^\mu(\sigma^a)$ is

$$\partial_a \left(\sqrt{-\gamma}\gamma^{ab} X^\mu_{,b}\right) = 0. \tag{3.6}$$

Using the conformal gauge and $\sigma^0 \equiv \tau$, $\sigma^1 \equiv \sigma$ one obtains

$$\ddot{X}^\mu - X''^\mu = 0, \tag{3.7}$$

and the gauge conditions are

$$\dot{\mathbf{X}} \cdot \mathbf{X}' = 0, \tag{3.8}$$

$$\dot{\mathbf{X}}^2 + \mathbf{X}'^2 = 1. \tag{3.9}$$

In this gauge, the worldsheet coordinate τ can be identified with the Minkowski time coordinate t. The solution for (3.7) can be written in terms of the right moving and the left moving waves as

$$\mathbf{X}(\sigma, \tau) = \frac{1}{2}\left[\mathbf{X}_+(\sigma_+) + \mathbf{X}_-(\sigma_-)\right], \tag{3.10}$$

where the lightcone coordinates are defined as $\sigma_+ \equiv \sigma + \tau$, $\sigma_- \equiv \sigma - \tau$. The corresponding gauge conditions are $\mathbf{X}'^{\,2}_+ = \mathbf{X}'^{\,2}_- = 1$, where primes denote derivatives with respect to the lightcone coordinates.

Using the lightcone coordinates, Eq. (3.5) can be written in the form

$$T(\mathbf{k},\omega_n) = -\frac{\mu}{L}\int_{-L}^{L} d\sigma_+ \int_{-L}^{L} d\sigma_- \left(1+\mathbf{X}'_+\cdot\mathbf{X}'_-\right) e^{\frac{i}{2}[(\omega_n\sigma_+ - \mathbf{k}\cdot\mathbf{X}_+)-(\omega_n\sigma_- + \mathbf{k}\cdot\mathbf{X}_-)]}. \tag{3.11}$$

Since we will be mainly interested in moduli bursts from cusps, we use the expansion of string worldsheet about a cusp, which we take to be at $\sigma_+ = \sigma_- = 0$. The functions in the integrand of (3.11) can be calculated from the expansions as

$$1+\mathbf{X}'_+\cdot\mathbf{X}'_- \approx -\frac{4\pi^2 s}{L^2}\sigma_+\sigma_-, \tag{3.12}$$

and

$$\mathbf{k}\cdot\mathbf{X}_\pm \approx k\left(\pm\sigma_\pm \mp \frac{2\pi^2}{3L^2}\sigma_\pm^3\right), \tag{3.13}$$

where s is an $O(1)$ parameter which depends on the loop trajectory and $\mathbf{k}$ is assumed to be in the direction of the string velocity at the cusp.

Eq. (3.11) can now be separated into two integrals as

$$T(\mathbf{k},\omega_n) = \frac{4\pi^2\mu\, s}{L^3} I_+ I_-, \tag{3.14}$$

where

$$I_\pm = \int_{-L}^{L} d\sigma_\pm\, \sigma_\pm\, e^{\pm i\left[\frac{\omega_n - k}{2}\sigma_\pm + \frac{\pi^2 k}{3L^2}\sigma_\pm^3\right]}. \tag{3.15}$$

After a change of variables, we obtain the integral

$$I_\pm(u) = \frac{L^2}{2\pi^2}\left(\frac{\omega_n}{k}-1\right)\int_{-\infty}^{\infty} dx\, x\, e^{\pm i\frac{3}{2}u\left[x+\frac{1}{3}x^3\right]}, \tag{3.16}$$

where

$$u \equiv \frac{Lk}{3\sqrt{2}\pi}\left(\frac{\omega_n}{k}-1\right)^{3/2}, \tag{3.17}$$

and we have approximated the upper and lower limits of integration as $\pm\infty$. The real part of the integral is zero since it is an odd function of x. The

imaginary part can be expressed in terms of the modified Bessel function,

$$I_{\pm}(u) = \pm i \frac{L^2}{2\pi^2} \left(\frac{\omega_n}{k} - 1 \right) \frac{2}{\sqrt{3}} K_{2/3}(u). \tag{3.18}$$

Then, (3.14) can be calculated as

$$T(\mathbf{k}, \omega_n) = \frac{4L\mu\, s}{3\pi^2} \left(\frac{\omega_n}{k} - 1 \right)^2 K_{2/3}^2(u), \tag{3.19}$$

and the power spectrum for the moduli radiation (3.4) from a cusp is

$$\frac{dP_n}{d\Omega} = \frac{8L^2\alpha^2 s^2 G\mu^2}{9\pi^5} \omega_n k \left(\frac{\omega_n}{k} - 1 \right)^4 K_{2/3}^4(u). \tag{3.20}$$

The asymptotic form of the power spectrum for $k >> m$ and $\omega_n \approx k$, i.e., $u << 1$, is[1]

$$\frac{dP_n}{d\Omega} \approx \tilde{\Gamma} \alpha^2 s^2 G\mu^2 n^{-2/3}. \tag{3.21}$$

where $\tilde{\Gamma} \sim 1$. This is the same as the power spectrum for gravitons, except that for gravitons there is no additional coupling constant α and the numerical coefficient is somewhat different.

The average rate of modulus radiation per solid angle is

$$\frac{d\dot{N}}{d\Omega} = \sum_n \frac{1}{\omega_n} \frac{dP_n}{d\Omega}. \tag{3.22}$$

The sum over n can be converted into an integral over k by using the relation $\omega_n = \frac{4\pi n}{L} = \sqrt{k^2 + m^2}$

$$\sum_n = \frac{L}{4\pi} \int \frac{k\, dk}{\sqrt{k^2 + m^2}}. \tag{3.23}$$

Here we only consider the modulus bursts which have very large Lorentz factors, thus we keep the leading order term in the limit $k >> m$. In this limit,

[1] When $u << 1$, $K_\nu(u) \approx \frac{\Gamma(\nu)}{2} \left(\frac{2}{u} \right)^\nu$.

(3.17) becomes $u \approx \frac{Lm^3}{12\pi k^2}$. By substituting (3.20) into (3.22), using (3.23) and also by making a change of variable $u \equiv \frac{Lm^3}{12\pi k^2}$, we obtain

$$d\dot{N} \sim \frac{\alpha^2 s^2 G\mu^2}{m} K^4_{2/3}(u) u^2 du d\Omega. \tag{3.24}$$

The function $K_{2/3}(u)$ dies out exponentially at $u \gtrsim 1$. Hence, the main contribution to the rate comes from the region $u \lesssim 1$ which corresponds to

$$k \gtrsim k_{min} = k_c \sim \frac{1}{4} m\sqrt{mL}. \tag{3.25}$$

For $k >> k_{min}$, Eq. (3.24) gives

$$d\dot{N} \sim \alpha^2 s^2 G\mu^2 L^{1/3} k^{-5/3} dk d\Omega. \tag{3.26}$$

From (3.26), the number of moduli emitted from a cusp in a single burst, into solid angle $d\Omega$, having momentum between $(k, k+dk)$ can be estimated as

$$dN \sim L d\dot{N} \sim \alpha^2 s^2 G\mu^2 L^{4/3} k^{-5/3} dk d\Omega. \tag{3.27}$$

Here, we assumed one cusp event per oscillation period of a loop.

Moduli are emitted into a narrow opening angle around the direction of the string velocity $\mathbf{v}$ at the cusp. The spectral expansion (3.26) has been calculated for moduli emitted in the direction of $\mathbf{v}$. For moduli emitted at a small angle θ relative to $\mathbf{v}$, Eq. (3.26) still applies, but now the spectrum is cut off at $k_{max} \sim 1/L\theta^3$. In other words, the opening angle for the emission of particles with momenta $\gtrsim k$ is

$$\theta_k \sim (kL)^{-1/3}. \tag{3.28}$$

Integration over Ω in (3.26) gives a factor $\sim \theta_k^2$,

$$d\dot{N} \sim \alpha^2 s^2 G\mu^2 L^{-1/3} k^{-7/3} dk. \tag{3.29}$$

Therefore, the number of moduli emitted in a single burst with momenta k in the interval dk (in the center of mass frame of the loop) is given by[2]

$$dN(k) \sim \alpha^2 G\mu^2 L^{2/3} k^{-7/3} dk. \tag{3.30}$$

This distribution applies for $k > k_c$, where

$$k_c \sim \frac{1}{4} m\sqrt{mL}. \tag{3.31}$$

At smaller k the distribution is strongly suppressed, $dN \approx 0$.

The dominant contribution to the modulus emission comes from the lower momentum cutoff $k_{min} \sim k_c$, so the total number of moduli per burst is

$$N \sim \frac{\alpha^2 G\mu^2}{m^2}. \tag{3.32}$$

The particles come from a portion of the loop that reaches Lorentz factors in excess of

$$\gamma_c \sim k_c/m \sim \frac{1}{4}\sqrt{mL}, \tag{3.33}$$

and are emitted into a narrow opening angle θ_c around the direction of the string velocity $\mathbf{v}$ at the cusp,

$$\theta_c \sim \gamma_c^{-1} \sim 4(mL)^{-1/2}. \tag{3.34}$$

The total power of modulus radiation can be similarly calculated as

$$P_m \sim \alpha^2 G\mu^2 L^{-1/3} k_c^{-1/3} \sim \frac{\alpha^2 G\mu^2}{\sqrt{mL}}. \tag{3.35}$$

The loops also radiate gravitational waves with the power

$$P_g \sim \Gamma G\mu^2, \tag{3.36}$$

[2]Our detailed analysis confirms the results of Refs. [10, 26].

where $\Gamma \approx 50$ [1]. $P_g \sim P_m$ when $L \sim L_*$ which is given by

$$L_* \sim \Gamma^{-2}\alpha^4 m^{-1}. \tag{3.37}$$

The lifetime of a loop which mainly radiates gravitationally is

$$\tau_g \sim \frac{\mu L}{P_g} \sim \frac{L}{\Gamma G\mu}, \tag{3.38}$$

which implies that the characteristic size of the smallest (and most numerous) loops surviving at time t is

$$L^g_{min} \sim \Gamma G\mu t. \tag{3.39}$$

On the other hand, modulus radiation dominates when $P_g \lesssim P_m$ and the loop lifetime is given by

$$\tau_m \sim \frac{\mu L}{P_m} \sim \frac{L^{3/2}m^{1/2}}{\alpha^2 G\mu}. \tag{3.40}$$

The corresponding minimum loop size is

$$L^m_{min} \sim \alpha^{4/3}(G\mu)^{2/3}m^{-1/3}t^{2/3}. \tag{3.41}$$

The transition between the two regimes occurs at

$$t_* \sim \frac{\alpha^4}{\Gamma^3 G\mu m}. \tag{3.42}$$

Therefore, the minimum loop length is given by (3.39) for $t \gtrsim t_*$ and by (3.41) for $t \lesssim t_*$. The redshift corresponding to t_* is given by[3]

$$z_* \sim \Gamma^2\alpha^{-8/3}(G\mu)^{2/3}(mt_0)^{2/3}, \tag{3.43}$$

[3]Throughout this chapter, we assume cosmology with $\Lambda = 0$ and $\Omega_m + \Omega_r = 1$ and use $H_0 = 72\,km/sMpc$, $t_0 = 4.3 \times 10^{17}\,s$, $t_{eq} = 2.4 \times 10^{12}\,s$, $1 + z_{eq} = 3200$, the scale factor in the matter and radiation dominated eras are $a_r(t) \propto t^{1/2}$ and $a_m(t) \propto t^{2/3}$. The corresponding time-redshift relations are respectively given by $(t/t_0) = (1+z_{eq})^{1/2}(1+z)^{-2}$ and $(t/t_0) = (1+z)^{-3/2}$.

where we have assumed that $1 < z_* < z_{eq}$. An expression for the case when $z_* > z_{eq}$ can be similarly obtained, but we will not need it in what follows. If Eq. (3.43) gives a value $z_* < 1$, this means that modulus radiation dominates at all redshifts.

Anticipating the parameter values for which detectable neutrino fluxes can be obtained, we define

$$m_5 = m/10^5 GeV, \quad \alpha_7 = \alpha/10^7, \quad \mu_{-20} = G\mu/10^{-20}. \tag{3.44}$$

Then Eq. (3.43) gives

$$z_* \sim 404 m_5^{2/3} \alpha_7^{-8/3} \mu_{-20}^{2/3}. \tag{3.45}$$

3.3 Particle propagation

3.3.1 Neutrino propagation

When a UHE neutrino interacts with a neutrino in the cosmic neutrino background, the possible channels are $\nu\bar{\nu} \to e^+e^-, \mu^+\mu^-, \tau^+\tau^-$ and $\bar{d}d, \bar{s}s, \bar{c}c, \bar{u}, u$ for three colors of each quark. The total cross section is

$$\sigma_\nu \sim \frac{N}{\pi} G_F^2 s, \tag{3.46}$$

where $N \sim 15$, $G_F = 1.17 \times 10^{-5}$ GeV^{-2}, $s(z) = 2Em_\nu(1+z)$, E is the neutrino energy at the present epoch and $m_\nu \sim 0.1 - 0.2$ eV is the neutrino mass. The cosmic neutrino background energy is $\epsilon_\nu = 3.15T(1+z) = 5.29 \times 10^{-4}(1+z)$ eV and number density is $n_\nu = 56(1+z)$ cm^{-3}. UHE neutrino absorption becomes effective when the absorption rate is greater than the Hubble parameter. This occurs when [111]

$$\int dt \sigma_\nu(z) n_\nu(z) = 1. \tag{3.47}$$

In a flat, matter dominated universe

$$dt = \frac{3}{2} t_0 (1+z)^{-5/2} dz. \tag{3.48}$$

Substituting (3.48) in (3.47), we obtain the neutrino horizon as

$$1 + z_\nu = 220 E_{11}^{-2/5}, \tag{3.49}$$

where $E_{11} \equiv E/10^{11}$ GeV.

3.3.2 Modulus decay

The mean lifetime of the modulus in its rest frame is

$$\tau_0 \sim 8.1 \times 10^{-17} m_5^{-3} \alpha_7^{-2}\, s. \tag{3.50}$$

from Eq. (2.7) in Chapter 2. The lifetimes of moduli emitted from cusps are boosted by large Lorentz factors. Modulus emitted with momentum k at redshift z and decaying at redshift z_d has a lifetime

$$\tau = \tau_0 \gamma(z, z_d), \tag{3.51}$$

where

$$\gamma(z, z_d) = \frac{k}{m} \frac{1+z_d}{1+z}. \tag{3.52}$$

In order for neutrinos to reach the Earth, they should be produced within the neutrino horizon at redshifts $z_d \lesssim z_\nu$. Moduli emitted from cusps at $z > z_\nu$ can therefore yield observable events only if they have large enough lifetime, allowing them to survive until they reach z_ν. This gives the condition

$$\tau(z) \sim \tau_0 \frac{k}{m} \frac{1+z_\nu}{1+z} \gtrsim t(z_\nu) \approx t_0 (1+z_\nu)^{-3/2}, \tag{3.53}$$

where in the last step we used the fact that in the energy range of interest $z_\nu \lesssim z_{eq}$.

This condition turns out to be difficult to satisfy. As we will see, in order to get a detectable neutrino flux, the modulus coupling α has to be rather large, $\alpha \gtrsim 10^6$. This makes the lifetime (3.50) very short. For relevant values of the parameters, only a fraction of the moduli, emitted from a small vicinity of the cusp, will have their lifetime boosted enough to reach z_ν. We have verified that the resulting neutrino flux is too low to be detected in this case.

In what follows we will consider only cusp events occurring at $z < z_\nu < z_{eq}$. There are no restrictions on the modulus lifetime in this case, except that it should be short enough for sufficient fraction of moduli to decay before they reach the Earth. This is always satisfied in the parameter range of interest.

The decay channel relevant for the neutrino production is the decay into gluons, via the modulus-gluon interaction of the form (2.6). As moduli decay into gluons, gluons produce a cascade of decays into quarks, which eventually are converted into hadrons. Most of these hadrons decay into neutrinos and pions, which in turn decay into neutrinos and leptons again. Thus, modulus-gluon coupling leads to copious neutrino production.

To simplify the analysis, we will assume a simple fragmentation function of the modulus into hadrons, $dN/dE \propto E^{-2}$, which is close to the form $E^{-1.92}$ obtained using Monte Carlo simulations and the DGLAP method [143]. Then the neutrino spectrum, at the present epoch, produced by the decay of a modulus with momentum k at epoch z is

$$\frac{dN_\nu}{dE} \equiv \xi_\nu(E,k) \approx \frac{b}{1+z}\frac{k}{E^2}, \tag{3.54}$$

where E is the neutrino energy,

$$b = [\ln(E_{max}/E_{min})]^{-1}, \tag{3.55}$$

and the energies E_{max} and E_{min} define the range over which the spectrum (3.54) applies. Assuming a two-jet decay of the modulus and rough equipartition of particle energies in pion decays $\pi^{\pm} \to e^{\pm}\nu\nu\nu$, we have

$$E_{max} \sim \frac{1}{8} k (1+z)^{-1}, \tag{3.56}$$

and

$$E_{min} \sim \frac{1}{8}\frac{k}{m} m_{\pi} (1+z)^{-1}, \tag{3.57}$$

where m_{π} is the pion mass in the last equation. This lower cutoff is due to the fact that the hadronic cascade terminates at energies $\sim m_{\pi}$. For the normalization of the spectrum, we will use $b \sim 0.1$ in our numerical estimates. Note that moduli are emitted with Lorentz factors $\gamma = k/m \gtrsim \gamma_c$, with most of them saturating the lower bound, $\gamma \sim \gamma_c$. Then, E_{min} can be found as

$$E_{min}(z < z_*) \sim 9.0 \times 10^{12} m_5^{1/2} \mu_{-20}^{1/2} (1+z)^{-7/4}\, GeV, \tag{3.58}$$

$$E_{min}(z > z_*) \sim 2.0 \times 10^{12} m_5^{1/3} \mu_{-20}^{1/3} \alpha_7^{2/3} (1+z)^{-3/2}\, GeV. \tag{3.59}$$

We will require the energy of the neutrinos to be greater than E_{min} to make sure the cascade produces neutrinos with the energies we are interested in.

3.4 Neutrino bursts from moduli

3.4.1 Loop distribution

The predicted flux of UHE neutrinos depends on the typical length of loops produced by the string network. The characteristic length of loops formed at

cosmic time t is given by the scaling relation [84]

$$L \sim \beta t \tag{3.60}$$

with $\beta \sim 0.1$.

The number density of loops with lengths in the interval from L to $L + dL$ can be expressed as $n(L,t)dL$. Of greatest interest to us are the loops that formed during the radiation era ($t < t_{eq}$) and still survive at $t > t_{eq}$. The density of such loops is given by

$$n(L,t)dL \sim p^{-1}\zeta(\beta t_{eq})^{1/2} t^{-2} L^{-5/2} dL, \tag{3.61}$$

where p is the string reconnection probability and $\zeta \sim 16$ is the parameter characterizing the density of infinite strings with $p = 1$, $\rho_\infty = \zeta\mu/t^2$.

The dependence of the loop density on p is somewhat uncertain and can only be determined by large-scale numerical simulations. Here we have adopted the p^{-1} dependence suggested by simple arguments in, e.g., [24, 96]. The reconnection probability is $p = 1$ for ordinary cosmic strings. Its value for F- and D-strings of superstring theory has been estimated as [79]

$$10^{-3} \lesssim p \lesssim 1. \tag{3.62}$$

The distribution (3.61) applies for L in the range from the minimum length L_{min} to $L_{max} \sim \beta t_{eq}$. The lower cutoff L_{min} depends on whether the energy dissipation of loops is dominated by gravitational or by modulus radiation. It is given by (3.39) for $z < z_*$ and by (3.41) for $z_* < z < z_{eq}$, with z_* from Eq. (3.43). For $z_* > z_{eq}$, the dominant energy loss is gravitational radiation and Eq. (3.39) for L_{min} applies in the entire range of interest.

The string motion is overdamped at early cosmic times, as a result of friction due to particle scattering on moving strings. The overdamped epoch ends at [1]

$$t_d \sim (G\mu)^{-2} t_p, \tag{3.63}$$

where t_p is the Planck time. In the above analysis we have assumed that loops of interest to us are formed at $t > t_d$. The corresponding condition is

$$L_{min}(t) \gtrsim \beta t_d. \tag{3.64}$$

This bound assumes that the strings have non-negligible interactions with the standard model particles, so it may not apply to F- or D-strings of superstring theory. In any case, we have verified that (3.64) is satisfied for parameter values that give a detectable flux of neutrinos.

3.4.2 The rate of bursts

The rate of cusp events that occur at redshift z in the interval $(z, z + dz)$ can be expressed as

$$d\dot{N}_c = \frac{n(L,z)\, dL}{L/2} \frac{dV(z)}{1+z}, \tag{3.65}$$

where the proper volume in the matter era is given by

$$dV(z) = 54\pi t_0^3 [(1+z)^{1/2} - 1]^2 (1+z)^{-11/2} dz, \tag{3.66}$$

and we have assumed one cusp event per loop oscillation period $L/2$. The rate of modulus bursts emitted into solid angle $\Omega \sim \pi\theta^2$ is given by

$$d\dot{N}_b \sim d\dot{N}_c \frac{\Omega}{4\pi} \sim \frac{1}{4} d\dot{N}_c (k_c L)^{-2/3}. \tag{3.67}$$

Here, $\theta \sim (k_c L)^{-1/3}$ and $k_c \sim \frac{1}{4} m\sqrt{mL}$ is the lower momentum cutoff.

The total rate of bursts that occur at redshift z in the interval $\Delta z \sim z$ and whose opening angle includes the Earth is given by

$$\dot{N}_b(z) \equiv (1+z) \int_{L_{min(z)}}^{\beta t(z)} dL \frac{d\dot{N}_b}{dz dL}. \tag{3.68}$$

This gives

$$\dot{N}_b(z) \sim 68\pi p^{-1} \zeta \, \beta^{1/2} \left(\frac{t_{eq}}{t_0}\right)^{1/2} (mt_0)^{-1} t_0^{5/2} \frac{[(1+z)^{1/2}-1]^2}{(1+z)^{5/2}} \int_{L_{min}}^{\beta t(z)} dL \, L^{-9/2}. \tag{3.69}$$

The integral over L is dominated by the lower limit L_{min}, thus the burst rate is given by

$$\dot{N}_b(z) \sim 1.2 \times 10^{-57} p^{-1} m_5^{-1} (L_{min}/t_0)^{-7/2} (1+z)^{-3/2} \; yr^{-1}, \tag{3.70}$$

where we have assumed $z \gg 1$ and used $\zeta \sim 16$, $\beta \sim 0.1$.

For $z \lesssim z_*$, we use $L_{min} \sim \Gamma G\mu t_0 (1+z)^{-3/2}$ with $\Gamma \sim 50$, which gives

$$\dot{N}_b(z < z_*) \sim 1.3 \times 10^{7} p^{-1} m_5^{-1} \mu_{-20}^{-7/2} (1+z)^{15/4} \; yr^{-1}. \tag{3.71}$$

If $z_* < z_\nu$, we also have to consider the regime $z_* \lesssim z \lesssim z_\nu$, with $L_{min} \sim \alpha^{4/3} (G\mu)^{2/3} (mt_0)^{-1/3} t_0 (1+z)^{-1}$. We then have

$$\dot{N}_b(z > z_*) \sim 4.8 \times 10^{11} p^{-1} m_5^{1/6} \mu_{-20}^{-7/3} \alpha_7^{-14/3} (1+z)^2 \; yr^{-1}. \tag{3.72}$$

3.4.3 Average neutrino flux

The average flux of neutrinos from bursts originating at redshifts $\sim z$ can be estimated as

$$J_\nu(E;z) = \frac{(1+z)}{4\pi} \int \frac{d\dot{N}_c}{dz} \frac{\Omega_k}{4\pi} \xi_\nu(E,k) \frac{dN(k)}{\Omega_k r^2(z)}, \tag{3.73}$$

where $dN(k)$ is the number of moduli with momentum k in the interval $(k, k+dk)$ emitted per burst, given by (3.30), $r(z) = 3t_0(1+z)^{-1/2}[(1+z)^{1/2}-1]$ is the proper distance in the matter era, and $\xi_\nu(E,k)$ is the neutrino spectrum from the decay of a modulus with momentum k, given by (3.54). The factor $\Omega_k/4\pi$ is the probability that a randomly oriented burst is directed to the observer, and $\Omega_k r^2(z)$ is the area of the irradiated spot at the observer's location. The integrations in (3.73) are over the loop length L and over momentum k. Both integrations are dominated by their lower bounds.

Substitution of (3.65) and (3.54) into (3.73) gives

$$E^2 J_\nu(E;z) \sim \frac{7}{4\pi} p^{-1}\zeta\beta^{1/2} b \left(\frac{t_{eq}}{t_0}\right)^{1/2} \frac{\alpha^2(G\mu)^2}{(mt_0)^{1/2}} (1+z)^{-5/2} (L_{min}/t_0)^{-2} m_p t_p^{-1} t_0^{-2}. \tag{3.74}$$

Once again, considering separately the regimes $z < z_*$ and $z > z_*$, we find

$$E^2 J_\nu(E; z < z_*) \sim 2.1 \times 10^{-10} p^{-1} m_5^{-1/2} \alpha_7^2 (1+z)^{1/2}\, GeV/(cm^2\, s\, sr), \tag{3.75}$$

and

$$E^2 J_\nu(E; z > z_*) \sim 7.5 \times 10^{-8} p^{-1} m_5^{1/6} \mu_{-20}^{2/3} \alpha_7^{-2/3} (1+z)^{-1/2}\, GeV/(cm^2\, s\, sr). \tag{3.76}$$

The total neutrino flux is obtained by integrating over z,

$$J_\nu(E) = \int_0^{z_\nu(E)} \frac{dz}{1+z} J_\nu(E,z). \tag{3.77}$$

To estimate $J_\nu(E)$, we note from Eq. (3.75) that for $z_* > z_\nu$ the differential flux $J_\nu(E,z)$ is a growing function of z all the way up to z_ν. Hence,

$$E^2 J_\nu(E) \approx 2E^2 J_\nu(E, z_\nu(E)) \sim 6.2 \times 10^{-9} p^{-1} m_5^{-1/2} \alpha_7^2 E_{11}^{-1/5}\, GeV/(cm^2\, s\, sr). \tag{3.78}$$

For $z_* < z_\nu$, the differential neutrino flux grows with the redshift at $z < z_*$ and decreases at $z_* < z < z_\nu$, so the total flux can be estimated as

$$E^2 J_\nu(E) \approx 2E^2 J_\nu(E, z_*) \sim 8.4 \times 10^{-9} p^{-1} m_5^{-1/6} \mu_{-20}^{1/3} \alpha_7^{2/3}\, GeV/(cm^2\, s\, sr). \tag{3.79}$$

It should be noted that the average flux in Eq. (3.77) can be in principle be different from the observed flux. The reason is that neutrinos come in bursts, and we should exclude the contribution of very rare bursts which are not likely to occur during the observation time, even though such bursts may carry large numbers of neutrinos. The rate of bursts increases with redshift, so the condition that bursts occur at a rate of least once in the observation time of a detector T gives a lower bound on the redshift,

$$z > z_b. \tag{3.80}$$

The observed neutrino flux can then be expressed as

$$J_\nu^{(obs)}(E) = \int_0^{z_\nu(E)} \frac{dz}{1+z} J_\nu(E, z)\theta(z - z_b). \tag{3.81}$$

With $T \sim 1$ yr, we find from Eqs.(3.71),(3.72)

$$(1 + z_b)(z < z_*) \sim 1.3 \times 10^{-2} p^{4/15} m_5^{4/15} \mu_{-20}^{14/15} (T/yr)^{-4/15}, \tag{3.82}$$

$$(1 + z_b)(z > z_*) \sim 1.4 \times 10^{-6} p^{1/2} m_5^{-1/12} \mu_{-20}^{7/6} \alpha_7^{7/3} (T/yr)^{-1/2}. \tag{3.83}$$

The flux sensitivity of the JEM-EUSO detector in its tilted mode can be fit with a power law as [129]

$$E^2 J_\nu(E)_{JEM} \approx 8 \times 10^{-9}\, E_{11}^{0.5}\, GeV/(cm^2\, s\, sr), \tag{3.84}$$

where this fit is valid for the energies above 1.6×10^{11} GeV. For observable events at JEM-EUSO, flux given by Eqs. (3.78) and (3.79) should be greater than the or equal to the limit given by (3.84).

3.4.4 Cascade upper bound

An upper bound on the neutrino flux comes from the diffuse gamma-ray background, since neutrino production via pion/kaon decays is accompanied by high energy electron and photon production. A high energy electron or photon interacts with low energy photons and produces an electromagnetic cascade. The energy density of the resulting gamma-ray background cannot exceed the value $\omega_{Fermi} = 5.8 \times 10^{-7}\, eV/cm^3$, measured by Fermi-LAT [113].

The energy density for the electromagnetic cascade radiation resulting from modulus decays can be expressed as

$$\omega_{cas} = \frac{1}{2}\int_0^{z_{cas}} \frac{dz}{(1+z)^4} \int_{L_{min}} dL n(L,z) \int_{k_c} dN(k) k \tag{3.85}$$

where $dN(k)$ is given by (3.30), $n(L,z)$ is given by (3.61) and k is the modulus energy in the rest frame of the loop. The upper limit of z-integration, $z_{cas} \sim 60$, is the epoch at which the high-energy edge of cascade radiation is absorbed. The integrals over k and L are dominated by their lower limits, namely, $L_{min}(z)$ and $k_c \sim m\sqrt{mL}/4$. After these integrations, we obtain

$$\omega_{cas} \sim \frac{9}{8} p^{-1} \zeta \beta^{1/2} \left(\frac{t_{eq}}{t_0}\right)^{1/2} \frac{\alpha^2 (G\mu)^2}{(m t_0)^{1/2}} \frac{m_p}{t_p\, t_0^2} \int_0^{z_{cas}} dz (1+z)^{-7/2} (L_{min}/t_0)^{-2}. \tag{3.86}$$

Using $L_{min}(z)$ from (3.39) and (3.41) and integrating over z, for $z_{cas} < z_*$ we have

$$\omega_{cas} \sim 6.3 \times 10^{-9} p^{-1} m_5^{-1/2} \alpha_7^2 (z_{cas}/60)^{1/2}\, eV/cm^3, \tag{3.87}$$

where the integral over z is dominated by $z \sim z_{cas}$, and for $z_* < z_{cas}$

$$\omega_{cas} \sim 1.6 \times 10^{-8} p^{-1} m_5^{-1/6} \mu_{-20}^{1/3} \alpha_7^{2/3}\, eV/cm^3, \tag{3.88}$$

where the integral is dominated by $z \sim z_*$. The condition

$$\omega_{cas} < \omega_{Fermi} \tag{3.89}$$

provides a constraint on the parameters of the model.

It should be noted that in our model the gamma radiation is produced in bursts, just like the UHE neutrinos. These bursts can be dispersed due to deflection of the cascade electrons and positrons in cosmic magnetic fields, resulting in a diffuse gamma ray background. The bound (3.89) applies if the intergalactic magnetic fields are strong enough for this process to be efficient; otherwise the bound may be significantly relaxed. This issue requires further study.

3.5 An illustrative example

The expressions for the neutrino flux that we obtained in the preceding section, combined with the cascade bound, can be compared with the expected sensitivity of detectors like JEM-EUSO. This would yield the range of the parameters α, m and $G\mu$ for which detectable UHE neutrino fluxes can be obtained. This analysis, however, turns out to be rather tedious, mainly because the neutrino flux is given by different expressions, depending on the relative magnitude of z_ν, z_* and z_b. We also find that, for JEM-EUSO sensitivity, the resulting allowed parameter space is rather small, due to the conflicting constraints imposed by the detectability conditions and the cascade bound. In order to simplify the discussion, we will restrict the analysis to an illustrative example of a string theory inspired model.

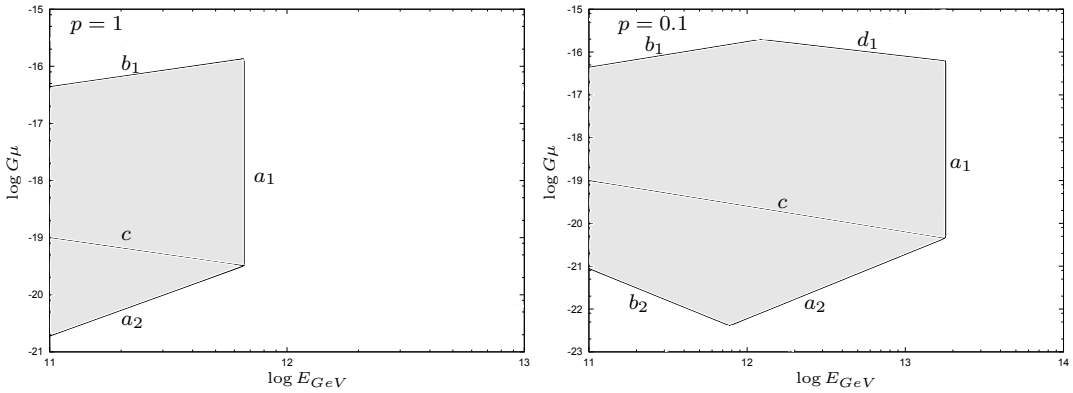

Figure 3.1: $\log G\mu$ vs. $\log E_{GeV}$ for the heavy modulus in the large volume scenario. The figure on the left is for ordinary cosmic strings with reconnection probability $p = 1$, and the one on the right is for cosmic F- and D-strings with $p = 0.1$. The lines represent (a): $E^2 J_\nu(E) = E^2 J_\nu(E)_{JEM}$, (b): $E_{min} = E$, (c): $z_\nu = z_*$, (d): $z_b = z_\nu$ and the subscripts $1, 2$ denote the regimes $z_\nu \lesssim z_*$ and $z_\nu \gtrsim z_*$, respectively. The shaded regions correspond to observable neutrino events that can be detected by JEM-EUSO in the tilted mode. The other constraints that do not interfere with the shaded regions are not shown in the figures.

Specifically, we will consider the large volume string compactification model [32], which is characterized by an intermediate string scale $m_s \sim 10^{11}\ GeV$ and a TeV-scale supersymmetry (SUSY) breaking. The hierarchy between the Planck and the SUSY breaking scales in this model is due to an exponentially large volume of the compact extra dimensions, $V_{comp} \equiv \mathcal{V} l_s^6$, where $\mathcal{V} \sim 10^{15}$ and $l_s \sim m_s^{-1}$ is the string length scale.

Apart from the volume modulus, which has gravitational strength couplings to ordinary matter, the other Kahler moduli have large couplings of the order [33]

$$\alpha \sim \sqrt{\mathcal{V}}. \tag{3.90}$$

With $\mathcal{V} \sim 10^{15}$, we have $\alpha \sim 10^{7.5}$.

	$z \lesssim z_*$	$z \gtrsim z_*$
$\dot{N}_b/(yr^{-1})$	$1.8 \times 10^{15}\, p^{-1} \mu_{-20}^{-7/2} \alpha_{7.5}^{2} (z/z_\nu)^{15/4}$	$1.4 \times 10^{14} p^{-1} \mu_{-20}^{-7/3} \alpha_{7.5}^{-5} (z/z_\nu)^{2}$
$E^2 J_\nu(E)/(GeV/cm^2\, s\, sr)$	$3.0 \times 10^{-8}\, p^{-1} \alpha_{7.5}^{3} (z/z_\nu)^{1/2}$	$3.0 \times 10^{-9}\, p^{-1} \mu_{-20}^{2/3} \alpha_{7.5}^{-1} (z/z_\nu)^{-1/2}$

Table 3.1: Formulae for the heavy modulus of the large volume scenario. $z_\nu = 220$ has been used as the neutrino horizon.

	$z_\nu \lesssim z_*$ $G\mu \gtrsim 9.2 \times 10^{-20}\, E_{11}^{-0.6} \alpha_{7.5}^{6}$	$z_\nu \gtrsim z_*$ $G\mu \lesssim 9.2 \times 10^{-20}\, E_{11}^{-0.6} \alpha_{7.5}^{6}$
$E^2 J_\nu(E) \gtrsim E^2 J_\nu(E)_{JEM}$	$E_{11} \lesssim 6.6\, p^{-10/7} \alpha_{7.5}^{30/7}$	$G\mu \gtrsim 1.9 \times 10^{-21}\, p^{3} \alpha_{7.5}^{-3} E_{11}^{1.5}$
$E_{min} < E$	$G\mu \lesssim 4.5 \times 10^{-17}\, \alpha_{7.5}^{2} E_{11}^{0.6}$	$G\mu \gtrsim 9.0 \times 10^{-22}\, \alpha_{7.5}^{9} E_{11}^{-1.5}$

Table 3.2: Detectability conditions for the heavy modulus of the large volume scenario. E_{min} is evaluated at z_ν for $z_\nu < z_*$ regime and, it is evaluated at z_* for $z_* < z_\nu$ regime.

The modulus masses are given by [33]

$$m \sim \frac{ln\mathcal{V}}{\mathcal{V}} m_p. \tag{3.91}$$

It is useful to parametrize m in terms of α. Since we are interested in $\alpha \sim 10^{7.5}$, the factor $ln\mathcal{V}$ can be replaced by 35. Hence, we obtain for the mass

$$m \sim 35 m_p \alpha^{-2}. \tag{3.92}$$

For $\alpha \sim 10^{7.5}$, we have $m \sim 4.3 \times 10^5$ GeV. The formulae and detactability constraints for this specific case are given given in Table 3.1 and Table 3.2, respectively.

For observable neutrino events, Eqs. (3.78) and (3.79) should be greater than the flux sensitivity limit of JEM-EUSO in the tilted mode given by Eq. (3.84). Since the particles come as bursts, we should make sure $z_b < z_\nu$ in the regime $z_\nu < z_*$ and, $z_b < z_*$ in the regime $z_* < z_\nu$, which yield

the conditions $G\mu \lesssim 3.4 \times 10^{-16}\, p^{-2/7} \alpha_{7.5}^{4/7} (T/yr)^{2/7} E_{11}^{-0.43}$ and $G\mu \lesssim 2.9 \times 10^{-8}\, p^{-1} \alpha_{7.5}^{-13} (T/yr)$, respectively.

The cascade upper bound (3.89) can be expressed using Eqs. (3.87) and (3.88) as $\alpha \lesssim 8.4 \times 10^{7}\, p^{1/3}$ for $z_{cas} \lesssim z_*$, and $G\mu \lesssim 9.0 \times 10^{-17} p^3 \alpha_{7.5}^{-3}$ for $z_* \lesssim z_{cas}$.

There are some additional constraints that need to be considered. The modulus mass m cannot exceed the mass scale of the string, i.e., $m \lesssim m_p (G\mu)^{1/2}$, which yields a bound on the string tension,

$$G\mu \gtrsim 10^{-32} \alpha_{7.5}^{-4}. \tag{3.93}$$

Using all the constraints that are discussed above, we obtained Fig. 3.1 that shows the range of string tension $G\mu$ corresponding to observable events at JEM-EUSO as a function of observed neutrino energy E. The range for the string tensions that give rise to observable neutrino events at JEM-EUSO tilted mode can be summarized as follows. For ordinary cosmic strings (reconnection probability $p = 1$), we get detectable neutrino events for the range of string tension

$$10^{-21} \lesssim G\mu \lesssim 10^{-16}, \tag{3.94}$$

and for cosmic F- and D-strings with reconnection probability $p = 0.1$,

$$10^{-22} \lesssim G\mu \lesssim 10^{-16} \tag{3.95}$$

for energies $E \gtrsim 10^{11}$ GeV. The allowed range of $G\mu$ can be significantly enlarged for future, more sensitive detectors. Note also that although it is easier to detect the signal for $p \lesssim 0.1$, the cascade upper bound may be violated, hence, such high neutrino fluxes are constrained from above and the

parameter space shrinks considerably. On the other hand, if the intergalactic magnetic fields are not strong enough to disperse the electromagnetic cascade from the bursts, this constraint may be relaxed, hence, there would be a larger parameter space for observable neutrino events from cosmic superstrings with $p \lesssim 0.1$.

3.6 Conclusions

We consider moduli produced by cosmic string cusps as a source of UHE neutrinos. Moduli are scalar particles predicted by superstring theory and supersymmetric field theories. Of particular interest to us are the moduli that couple to matter stronger than gravitational strength [32, 33, 34, 35, 30, 31]. We show that unlike gravitationally coupled ones, they can lead to observable UHE cosmic rays. Since the number density of loops is larger in earlier epochs, we get the most numerous events from higher redshifts. Therefore, we are interested in neutrinos produced by modulus decays since they can travel over large cosmological distances without being absorbed much. We treat the string tension $G\mu$, modulus mass m and modulus coupling constant α as free parameters and show that for reasonable values of these parameters, i.e., the values anticipated by theoretical arguments and restricted by detectability conditions, observable UHE neutrino events can be expected at the space based neutrino observatory JEM-EUSO.

We calculate emission of moduli from a cosmic string cusp and find that the spectrum dies out at small energies; there is a minimum energy cutoff given by $k_c \sim m\sqrt{mL}/4$. This is basically because of the fact that moduli are

produced by strings only when the oscillation frequency of a loop $\omega \sim 1/L$ is greater than the mass of a modulus, i.e., $L \lesssim 1/m$, which for large loops only occur around a region called cusp where extremely high frequencies can be reached for a brief period of time. We further show that the number of moduli decrease as their energy increases. Since moduli are emitted with very large Lorentz factors from cusps, $\sqrt{mL} >> 1$, the number of particles emitted by a cusp is dominated by this minimum energy cutoff k_c. Therefore, most of the particles have a Lorentz factor of order $\gamma_c \sim \sqrt{mL}/4$. Actually, there is a distribution of Lorentz factors in the vicinity of a cusp. As we go near the tip of the cusp it increases up to a maximum value set by cusp annihilation, which is given by $\gamma_{max} \sim \eta\sqrt{\eta L}$, where $\eta \equiv m_p(G\mu)^{1/2}$ is the mass scale of the string [105]. However, note that for larger Lorentz factors, number of particles decrease substantially. Therefore, most of the moduli have $\gamma \sim \gamma_c$.

We consider modulus decay into gluons and hadronic cascade initiated by these gluons as the way to generate the UHE neutrinos. We assume that the number of neutrinos produced by the decay of a single modulus has energy dependence $\sim E^{-2}$, where E is the neutrino energy at present epoch. Actually, the energy dependence is given by $E^{-1.92}$ [143] for masses $m \sim 10^{12}$ GeV, and $E^{-1.7}$ for $m \sim 10^6$ GeV [144]. The actual spectrum introduces a weak dependence on the parameters of the model and can be ignored within our order of magnitude estimates. We also assume a flat matter dominated universe when carrying out our analysis which helps expressing the dependence of the calculations on the parameters of the model analytically.

In Fig. 3.1 we show our results for a string theory inspired model. The allowed range for the string tension that give rise to observable neutrino events

that can be detected at JEM-EUSO tilted mode is roughly $10^{-21} \lesssim G\mu \lesssim 10^{-16}$ for ordinary cosmic strings ($p = 1$), and $10^{-22} \lesssim G\mu \lesssim 10^{-16}$ for cosmic F- and D-strings with $p = 0.1$. It is easier to observe strings with $p \lesssim 0.1$ because of enhanced number density of the loops, hence, larger neutrino fluxes. However, the cascade upper bound may be violated badly for such strings and the parameter space becomes too small. The parameter space for such cosmic superstrings can significantly increase if the intergalactic magnetic fields are not strong enough the disperse the electromagnetic cascade particle bursts accompanying the neutrinos so that the upper bound on the cascade radiation is relaxed.

These moduli are subject to the constraints that we discussed in Chapter 2. We showed in Chapter 2 that for large enough values of the modulus coupling constant, the cosmological constraints on such moduli are relaxed significantly. In particular, the anticipated values of the parameters used in this chapter are free from these constraints [28].

The main conclusion of this chapter is that moduli which couple to matter stronger than gravitational strength, i.e., $\alpha >> 1$, may give rise to observable UHE neutrino fluxes with energies $E \gtrsim 10^{11}$ GeV that can be detected at the space based neutrino detector JEM-EUSO, which is scheduled to operate in a few years. This model can be realized in a string theory inspired scenario, e.g., large volume compactification model, where observable neutrino events can be achieved with the anticipated values of the parameters.

Chapter 4

Superconducting loops

4.1 Introduction

In a wide class of particle physics models, cosmic strings can be superconducting, in which case they respond to external electromagnetic fields as thin superconducting wires [86]. String superconductivity arises when a condensate of charged particles (which can be either bosons or fermions) is bound to the string. These particles have zero mass in the bound state, whereas away from the string they have some mass m_X. Loops of superconducting string develop electric currents as they oscillate in cosmic magnetic fields. Near a cusp, a section of string acquires a large Lorentz boost γ_c, and simultaneously the string current is increased by a factor γ_c. If the current grows to a critical value J_{max} charge carriers rapidly scatter off each other and are ejected from the string. The decay products of these particles can then be observed as cosmic rays. This model will be the subject of this chapter.

We consider superconducting string loops as a source of UHE neutrinos.

We consider a simple model in which a magnetic field of magnitude B, occupying a fraction of space f_B, is generated at some epoch $z_{max} \sim 2$–3. The strings are characterized by two parameters: the fundamental symmetry breaking scale η and the critical current J_{max}. We take the mass per unit length of string to be $\mu = \eta^2$.

As was assumed in the previous chapters, we use for the characteristic length of loops formed at cosmic time t

$$L \sim \beta t, \tag{4.1}$$

with $\beta \sim 0.1$. For simplicity and transparency of the formulae obtained in this paper we use several simplifications. We assume cosmology without Λ term with $\Omega_{cdm} + \Omega_b = 1$, the age of the universe $t_0 = (2/3)H_0^{-1} = 3 \times 10^{17}$ s, $t_{eq} \sim 1 \times 10^{12}$ s, and $(1+z)^{3/2} = t_0/t$ for the connection of age t and redshift z in the matter era.

We also assume the fragmentation function for the decay of superheavy X particle into hadrons is

$$dN/dE \propto E^{-2}, \tag{4.2}$$

while Monte Carlo simulation and the DGLAP method give closer to $E^{-1.92}$ [143].

These simplifications give us a great advantage in understanding the dependence of calculated physical quantities on the basic parameters of our model, in particular on fundamental string parameter η. Our aim in this paper is to obtain the order of magnitude of the flux of UHE neutrinos and to indicate the signatures of the model. We believe our simplified model assumptions are justified, given the uncertainties of string evolution and of the evolution of

cosmic magnetic fields.

4.2 Particle emission from superconducting strings

4.2.1 Particle bursts from cusps

As first shown by Witten [86], cosmic strings are superconducting in many elementary-particle models. As they oscillate in cosmic magnetic fields, such strings develop electric currents. Assuming that the string loop size is smaller than the coherence length of the field $L \lesssim L_B \sim 1Mpc$, the electric current can be estimated as [86, 1]

$$J \sim 0.1 e^2 BL. \tag{4.3}$$

Particles are ejected from highly accelerated parts of superconducting strings, called cusps, where large electric currents can be induced [145, 19]. The current near a cusp region is boosted as

$$J_{cusp} \sim \gamma_c J, \tag{4.4}$$

where J is the current away from the cusp region and γ_c is the Lorentz factor of the corresponding string segment. Particles are ejected from portions of the string that develop Lorentz factors

$$\gamma_c \sim J_{max}/J, \tag{4.5}$$

where the current reaches the critical value J_{max}. This maximum current is model-dependent, but is bounded by $J_{max} \lesssim e\eta$, where η is the symmetry breaking scale of the string and $e \sim 0.1$ is the elementary electric charge in Gaussian units, renormalized to take into account self-inductance [1].

One may parametrize J_{max} by introducing the parameter $i_c < 1$:

$$J_{max} = i_c e\eta, \tag{4.6}$$

If the charge carrier is a superheavy particle X with mass m_X, the case which will be considered here, one may use ϵ_X^r for the energy of X-particle in the rest system of the cusp and ϵ_X in the laboratory system. Then $\epsilon_X^r = \gamma m_X = i_c\eta$ and

$$\epsilon_X \sim i_c\gamma_c\eta, \tag{4.7}$$

respectively, where γ is the average Lorentz factor of X-particle in the rest system of the cusp. In Eq. (4.7) we took into account that the energy of X-particle in the laboratory system is boosted by the Lorentz factor of the cusp γ_c.

The number of X particles per unit invariant length of the string is $\sim J/e$, and the segment that develops Lorentz factor γ_c includes a fraction $1/\gamma_c$ of the total invariant length L of the loop. Hence, the number of X particles ejected in one cusp event (burst) is

$$N_X^b \sim (J/e)(L/\gamma_c) \sim J^2 L/eJ_{max}\ . \tag{4.8}$$

The oscillation period of the loop is $L/2$, so assuming one cusp per oscillation, the average number of X particles emitted per unit time is

$$\dot{N}_X \sim 2J^2/eJ_{max}, \tag{4.9}$$

and the luminosity of the loop is

$$\mathcal{L}_{tot} \sim \dot{N}_X\epsilon_X. \tag{4.10}$$

The X particles are short-lived. They decay producing the parton cascade which is developed due to parton splitting in the perturbative regime, until at the confinement radius the partons are converted into hadrons, mostly pions and kaons, which then decay producing gamma rays, neutrinos, and electrons. These particles together with less numerous nucleons give the observational signatures of superconducting cusps.

The neutrino spectrum at present epoch $z = 0$, produced by the decay of one X-particle with energy $\epsilon_X \sim i_c \gamma_c \eta$ at epoch z can be calculated using the fragmentation function (4.2) for an X-particle at rest:

$$\xi_\nu(E) \approx \frac{i_c \eta \gamma_c}{2(1+z)\ln(E_{max}^{rest}/E_{min}^{rest})} \frac{1}{E^2}, \tag{4.11}$$

where E_{max}^{rest} and E_{min}^{rest} are the maximum and minimum neutrino energies in the rest system of X-particle.

Particle emission from a cusp occurs within a narrow cone of opening angle

$$\theta_c \sim \gamma_c^{-1} \sim J/J_{max}. \tag{4.12}$$

4.2.2 Superconducting loops in the universe

In any horizon-size volume of the universe at arbitrary time there are a few long strings crossing the volume and a large number of small closed loops. As loops oscillate under the force of string tension, they lose energy by emitting gravitational waves at the rate

$$\dot{E}_g \sim \Gamma G \mu^2, \tag{4.13}$$

where $\mu \sim \eta^2$ is the string mass per unit length, $G = 1/m_p^2$ is the gravitational constant and $\Gamma \sim 50$ is a numerical coefficient.

The number density of loops with lengths in the interval from L to $L+dL$ at time t can be expressed as $n(L,t)dL$. Of greatest interest to us are the loops that formed during the radiation era $t < t_{eq}$ and still survive at $t > t_{eq}$. The density of such loops at time t is given by [1]

$$n(L,t)dL \sim t_{eq}^{1/2} t^{-2} L^{-5/2} dL, \tag{4.14}$$

in the range from the minimum length L_{min} to the maximum length $L \sim \beta t_{eq}$, where

$$L_{min} \sim \Gamma G\mu t \sim 3 \times 10^{11} \eta_{10}^2 (1+z)^{-3/2} \mathrm{cm}, \tag{4.15}$$

and $\eta_{10} = \eta/10^{10}$ GeV. Here and below we assume that the loop length parameter in (4.1) is $\beta \sim 0.1$, as suggested by simulations [84]. Loops of the minimum length are of most importance in our calculations because they are the most numerous.

For a loop of length L at redshift z, the Lorentz factor at the cusp γ_c can be expressed as

$$\gamma_c = \frac{J_{cusp}}{J} = \frac{i_c e \eta}{0.1 e^2 B L} = \gamma_c(L_{min}) \frac{L_{min}}{L}, \tag{4.16}$$

where $\gamma_c(L_{min}) = \gamma_0 (1+z)^{3/2}$ and

$$\gamma_0 = \frac{10 i_c \eta}{e B t_0 \Gamma G \mu} = 1.1 \times 10^{12} i_c B_{-6}^{-1} \eta_{10}^{-1}, \tag{4.17}$$

where B_{-6} is the magnetic field in microgauss.

4.2.3 Limits on η

The string motion is overdamped at early cosmic times, as a result of friction due to particle scattering on moving strings. The friction-dominated epoch

ends at

$$t_d \sim (G\mu)^{-2} t_p, \tag{4.18}$$

where t_p is the Planck time. In the above analysis we have assumed that loops of interest to us are formed at $t > t_d$. The corresponding condition,

$$\Gamma G\mu t_0/\beta \gtrsim t_d, \tag{4.19}$$

yields

$$\eta \gtrsim 10^9 \text{ GeV}. \tag{4.20}$$

For strings with $\eta < 10^9$ GeV, loops of the size given by (4.15) never form. Instead, the smallest loops are those that form at time t_d with length

$$L_{min} \sim \beta t_d \,, \tag{4.21}$$

and then survive until the present day.

We should also verify that energy losses due to particle emission and to electromagnetic radiation in recent epochs (after magnetic fields have been generated) are sufficiently small, so the lifetimes of the loops (which we estimated assuming that gravitational radiation is the dominant energy loss mechanism) are not significantly modified.

The average rate of energy loss due to particle emission is

$$\dot{E}_{part} \sim f_B \dot{N}_X \epsilon_X \sim 2 f_B J J_{max}/e^2, \tag{4.22}$$

where we have used Eqs. (4.9) and (4.7). The electromagnetic radiation power is smaller by a factor $e^2 \sim 10^{-2}$.

The factor f_B in Eq. (4.22) is the filling factor – the fraction of space filled with the magnetic field. It gives the fraction of time that cosmic string loops

spend in magnetized regions. We assume that loop velocities are sufficiently high that they do not get captured in magnetized cosmic structures (such as galaxy clusters or LSS filaments). To justify this assumption, we note that particle emission can start only after the cosmic magnetic fields are generated, that is, at $z \sim 3$ or so. Before that, gravitational radiation is the dominant energy loss mechanism, and the loops are accelerated to high speeds by the gravitational rocket effect [146, 147]. The smallest loops of length (4.15) have velocities $v \sim 0.1$, certainly large enough to avoid capture.

The particle emission energy rate (4.22) should be compared to the gravitational radiation rate (4.13).

The ratio of the two rates is zero at $z > z_{max}$, where $z_{max} \sim 2$–3 is the red-shift of magnetic field production. At $z < z_{max}$ it is given by

$$\dot{E}_{part}/\dot{E}_g \sim 50 f_{-3} B_{-6} i_c \eta_{10}^{-1} \left(\frac{L}{L_{min}}\right) (1+z)^{-3/2}. \tag{4.23}$$

where $f_{-3} = f_B/10^{-3}$ and L_{min} is given by (4.15).

If particle emission is the dominant energy loss mechanism, then the lifetime of a loop is

$$\tau_{part} \sim \frac{\mu L}{\dot{E}_{part}} \sim \frac{5\eta}{e i_c f_B B} \sim 0.025 \frac{t_0 \eta_{10}}{f_{-3} B_{-6} i_c}. \tag{4.24}$$

Note that τ is independent of L. This means that all loops surviving from the radiation era decay at about the same time.

For the time being, we shall assume that particle radiation is subdominant. We shall discuss the opposite regime in Section 4.2.7.

4.2.4 Rate of cusp events

The rate of observable cusp bursts (i.e., the bursts whose spot hits the Earth) is given by

$$d\dot{N}_b = f_B \frac{d\Omega}{4\pi} \nu(L,z) dL \frac{dV(z)}{1+z} \tag{4.25}$$

where, as before, f_B is the fraction of space with magnetic field B, $d\Omega = 2\pi\theta d\theta$ is the solid angle element, with θ limited by the angle of cusp emission $\theta_c \sim 1/\gamma_c$; $\nu(L,z) = n(L,z)/(L/2)$ is the frequency of the bursts with $n(L,z)$ given by Eq. (4.14), and $dV(z)$ is a proper volume of space limited by redshifts z and $z + dz$,

$$dV(z) = 54\pi t_0^3 [(1+z)^{1/2} - 1]^2 (1+z)^{-11/2} dz. \tag{4.26}$$

Integrating Eq. (4.25) over θ, l and z, we obtain

$$\dot{N}_b = \frac{54}{100\pi\Gamma^{1/2}} \left(\frac{e}{i_c}\right)^2 \left(\frac{t_{eq}}{t_0}\right)^{1/2} \frac{t_0 m_p}{\eta^3} \int_0^{z_{max}} \frac{dz\,[(1+z)^{1/2} - 1]^2}{(1+z)^{11/4}} f_B(z) B^2(z), \tag{4.27}$$

where z_{max} is the redshift at which the magnetic fields are generated. Since the earth is opaque to neutrinos with the energies we are considering, only half of these bursts can actually be detected by any given detector at the surface of the earth or using the atmosphere.

The value of the integral in (4.27) depends on one's assumptions about the evolution of the magnetic field B and of the volume fraction f_B. This evolution is not well understood. If we take these values out of the integral in Eq. (4.27) as the average and characterize them by the effective values of parameters B_{-6} and f_{-3} in the range $0 < z < z_{max}$, then Eq. (4.27) reduces to

$$\dot{N}_b = 2.7 \times 10^2 B_{-6}^2 f_{-3} i_c^{-2} \eta_{10}^{-3} \frac{I}{0.066}\ yr^{-1}, \tag{4.28}$$

where the integral

$$I = \int_0^{z'} dz \frac{[(1+z)^{1/2} - 1]^2}{(1+z)^{11/4}}, \tag{4.29}$$

can be calculated as

$$I = \frac{4}{3}[1 - (1+z')^{-3/4}] - \frac{8}{5}[1 - (1+z')^{-5/4}] + \frac{4}{7}[1 - (1+z')^{-7/4}], \tag{4.30}$$

and it is equal to 0.015, 0.042 and 0.066 for $z' = z_{max} = 1$, 2 and 3, respectively.

The integrand in Eq. (4.27) includes the product $f_B(z)B^2(z)$. In the calculations of other physical quantities below, similar integrals will have different combinations of $f_B(z)$ and $B(z)$. Nevertheless, we shall assume that the average values taken out of the integral are characterized by approximately the same values of f_{-3} and B_{-6}.

All cosmic structures –galaxies, clusters, and filaments of the large-scale structure– are magnetized and contribute to the rate of cusp bursts. In the recent epoch, $z \lesssim 1$, the dominant contribution is given by clusters of galaxies with $B_{-6}^2 f_{-3} \sim 1$. The magnetic fields of galaxies have about the same magnitude, but the corresponding filling factor f_B is orders of magnitude smaller. We shall assume that this holds in the entire interval $0 < z < z_{max}$. The sources in our model are then essentially clusters of galaxies.

4.2.5 Diffuse flux of UHE neutrinos

The diffuse differential neutrino flux, summed over all produced neutrino flavors, is given by the formula

$$J_\nu(E) = \frac{1}{4\pi} \int d\dot{N}_b N_X^b \xi_\nu(E) \frac{1}{\Omega_{jet} r^2(z)}, \tag{4.31}$$

where $d\dot{N}_b$ is the rate of cusp bursts (4.25), N_X^b is the number of X particles produced per burst, given by Eq. (4.8), $\xi_\nu(E)$ is the neutrino spectrum

produced by the decay of one X-particle, given by (4.11),

$$\Omega_{jet} = \pi\theta_c^2 = \frac{\pi}{\gamma_c^2}, \tag{4.32}$$

$$r(z) = 3t_0[1 - (1+z)^{-1/2}] \tag{4.33}$$

is the distance between a source at redshift z and the observation point at $z = 0$, and $\Omega_{jet} r^2$ is the area of the burst spot at the Earth from a source at redshift z.

Using expressions (4.14) and (4.26), and assuming that the product $f_B(z)B(z)$ does not change much in the interval $0 < z < z_{max}$, we obtain[1]

$$E^2 J_\nu(E) = \frac{0.3 i_c (t_{eq}/t_0)^{1/2} (eBt_0^2) f_B}{7\pi(\Gamma)^{1/2} \ln(E_{max}^{rest}/E_{min}^{rest})} \frac{m_p}{t_0^3} [1 - (1+z_{max})^{-7/4}]. \tag{4.34}$$

Numerically, this gives for the neutrino flux summed over neutrino flavors

$$E^2 J_\nu(E) = 6.6 \times 10^{-8} i_c \, B_{-6} \, f_{-3} \;\; GeV/(cm^2 \, s \, sr), \tag{4.35}$$

where we have set $z_{max} = 3$ and estimated the logarithmic factor as ~ 30.

For $i_c \sim 1$, the flux (4.35) is close to the cascade upper limit shown in Fig. 1.2. Notice that the diffuse neutrino flux (4.34) does not depend on η. The neutrino flux must correlate with clusters of galaxies.

To detect this flux, we need to monitor a target with some large mass M. The effective cross-section of the detector is then

$$\Sigma = \sigma_{\nu N} M/m_N \tag{4.36}$$

where $\sigma_{\nu N} \sim 3 \times 10^{-32} \; cm^2$ is the neutrino-nucleon cross section at $E \gtrsim 10^{10}$ GeV and m_N the mass of a nucleon. Because of the opacity of the earth,

[1]We note that numerical simulations of the magnetic field evolution performed by Ryu et al. [148] do indicate that the space average of the magnetic field $\langle B(z)\rangle = f_B(z)B(z)$ remains roughly constant at $\sim 10^{-9}$ G for $0 < z \lesssim 3$ and decreases at larger values of z. The effective values B_{-6} and f_{-3} could be different from those in Eq. (4.28) for the rate of bursts, but we neglect the possible difference.

the detector will see solid angle about 2π sr. The detection rate of particles with energy above E is

$$2\pi E J_\nu(E)\Sigma \approx 23 \left(\frac{M}{10^{18}g}\right)\left(\frac{10^{10}\ GeV}{E}\right) i_c\, B_{-6}\, f_{-3}\, yr^{-1} \tag{4.37}$$

In the case of JEM-EUSO in tilt mode, $M \sim 5 \times 10^{18}g$, and thus we expect about $100 i_c$ detections per year, so events can be expected for $i_c \gtrsim 0.01$.

4.2.6 Neutrino fluence and the number of neutrinos from a burst

The fluence of neutrinos incident on the detector from a burst at redshift z can be calculated as

$$\Phi(>E) = \frac{N_X^b \xi_\nu(>E)}{\Omega_{jet} r^2(z)} \tag{4.38}$$

Consider a neutrino burst from a loop of length l at redshift z. Using N_X^b from (4.8), L_{min} from (4.15) and $\xi_\nu(>E)$ from (4.11), we obtain for a loop of any length l,

$$\Phi(>E) \approx \frac{10 i_c^3}{18\pi e (B t_0^2)\, \ln(E_{max}^{rest}/E_{min}^{rest})[(1+z)^{1/2}-1]^2}\, \frac{\eta^3}{E}, \tag{4.39}$$

which numerically results in

$$\Phi(>E) \approx 1.2 \times 10^{-2} i_c^3\, \eta_{10}^3\, B_{-6}^{-1} \left(\frac{10^{10}\ GeV}{E}\right) \frac{1}{[(1+z)^{1/2}-1]^2}\ km^{-2} \tag{4.40}$$

The number of neutrinos detected in a burst is

$$N_\nu^{det} \sim \Phi(>E)\Sigma \tag{4.41}$$

With $M \sim 5 \times 10^{18}g$ as above,

$$N_\nu^{det}(>E) \approx 0.11 \frac{10^{10}\ \mathrm{GeV}}{E}\ i_c^3\, \eta_{10}^3\, B_{-6}^{-1}\, \frac{1}{[(1+z)^{1/2}-1]^2} \tag{4.42}$$

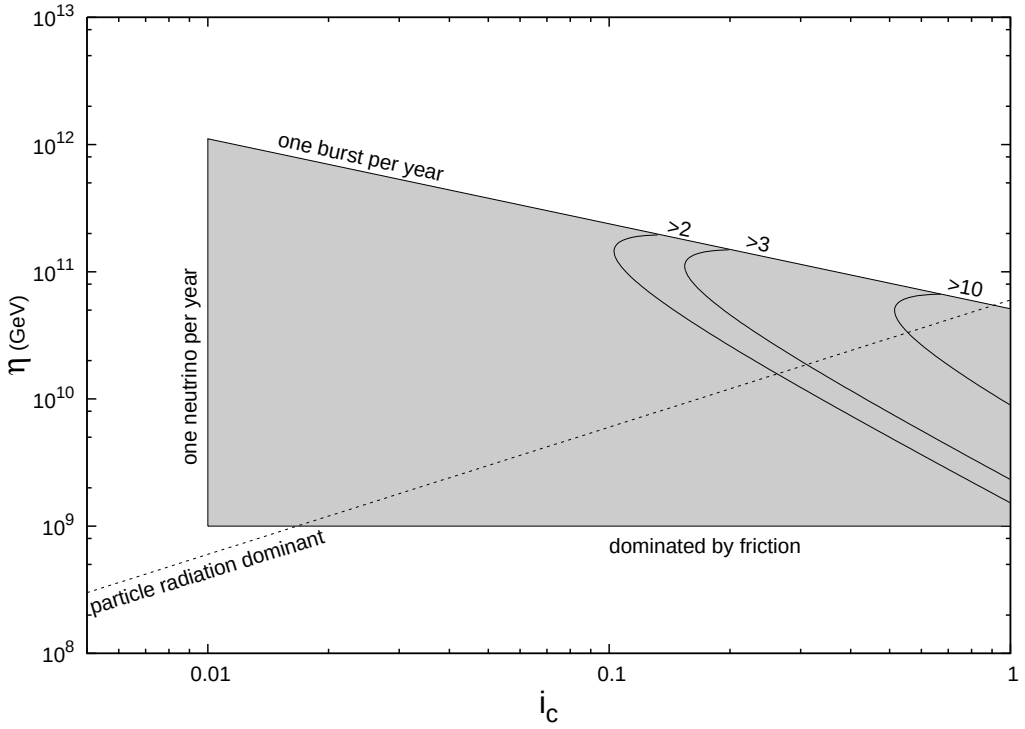

Figure 4.1: The region of parameter space where neutrinos can be seen by a detector with the parameters of JEM-EUSO. The curved lines show the left edges of the regions in which bursts containing at least 2, 3, and 10 neutrinos can be expected at least once per year. Below the dotted line, particle radiation is the dominant channel of energy loss from loops.

Therefore, for a certain range of $i_c\eta_{10}$ values and source redshifts z, multiple neutrinos can be detected as parallel tracks from a single burst. For example, for $i_c\eta_{10} \sim 3$, and $z \sim 1$, $N_\nu^{det} \sim 17$.

For neutrino energies of interest, $E_\nu \gtrsim 1 \times 10^{20}$ eV, the neutrino Lorentz factor is so large that there is practically no arrival delay for neutrinos with smaller energies. All neutrinos from a burst arrive simultaneously and produce atmospheric showers with parallel axes, separated by large distances.

For other sets of parameters $N_\nu^{det} < 1$, i.e. only one neutrino from a burst (or no neutrino) is detectable. As η increases, the rate of bursts (4.28)

diminishes while the number of neutrinos per burst increases, so that the total neutrino flux remains unchanged.

The rate of detected neutrino bursts with the number of detected neutrinos $N_\nu^{det} > \zeta$ for each burst, is given by Eqs (4.28) and (4.30), with z_{max} determined by $N_\nu^{det}(> E, z_{max}) = \zeta$. Using Eq. (4.42) we obtain for $x_{max} \equiv (1 + z_{max})$:

$$x_{max}(> E, \zeta) = \left[1 + \left(\frac{0.11}{\zeta}\frac{i_c^3\eta_{10}^3}{B_{-6}}\frac{10^{10}\ \mathrm{GeV}}{E}\right)^{1/2}\right]^2, \tag{4.43}$$

if (4.43) is less than 4, and $x_{max} = 4$ if (4.43) is larger than 4. Introducing in Eq. (4.28) coefficient 1/2 which approximately takes into account the absorption of UHE neutrinos crossing the Earth we obtain for the rate of detected bursts with $N_\nu^{det} \geq \zeta$

$$\dot{N}_b^{det}(\geq \zeta) = 2.1 \times 10^3 \frac{f_{-3}B_{-6}^2}{i_c^2\eta_{10}^3} I(z_{max})\ \ \mathrm{yr}^{-1}, \tag{4.44}$$

where $I(z_{max})$ is given by Eq. (4.30) with z_{max} from Eq. (4.43).

In Fig. 4.1, we have shaded the region of the parameter space (η, i_c) corresponding to a detectable flux of neutrinos. Curved lines in the figure mark the regions where we expect a burst with a given multiplicity of neutrinos, $\zeta = 2$, 3 or 10, detected simultaneously by a detector with the parameters of JEM-EUSO tilted. To the left of the 2-neutrino-burst line, only a diffuse flux of single neutrinos can be observed. This flux depends only on i_c, and the vertical left boundary of the shaded region marks the value of i_c at which it drops below one particle detected per year.

Note that the regions shown for multiple events are those where we expect at least one burst per year whose average multiplicity is the given ζ or more.

But it is possible even if the parameters are to the left of the $\zeta = 2$ line that we would happen to observe multiple neutrinos from a single burst, which would give a clear signature of neutrino-jet emission from cusps.

Another quantity of interest is the rate of detected neutrinos $f_\nu(\geq \zeta)$ in the events with neutrino multiplicity greater than ζ. It is given by

$$f_\nu(\geq \zeta) = \frac{1}{2} \int \frac{f_B}{2} \frac{1}{\gamma_c^2} \frac{n(L,z)dL}{L} \frac{dV(z)}{1+z} N_\nu^{det}(> E, z, L). \tag{4.45}$$

The important feature of the calculations is the independence of $N_\nu^{det}(> E, z, L)$ from L. This allows us to integrate over L in Eq. (4.45) to obtain

$$f_\nu(\geq \zeta) = 2.1 \times 10^3 \frac{f_{-3} B_{-6}^2}{i_c^2 \eta_{10}^3} \int_0^{z_{max}(\zeta)} dz \frac{\left[(1+z)^{1/2} - 1\right]^2}{(1+z)^{11/4}} N_\nu^{det}(> E, z), \tag{4.46}$$

where $z_{max}(\zeta)$ is given by Eq. (4.43). Using Eq. (4.42) for $N_\nu^{det}(> E, z)$ results in

$$f_\nu(\geq \zeta) = 1.3 \times 10^2 i_c f_{-3} B_{-6} [1 - x_{max}^{-7/4}(i_c, \eta_{10})] \text{ yr}^{-1}. \tag{4.47}$$

for $E > 1 \times 10^{19}$ eV. The asymptotic expression at $0.11 i_c^3 \eta_{10}^3 / B_{-6} \zeta \ll 1$ gives

$$f_\nu(\geq \zeta) = \frac{1.5 \times 10^2}{\sqrt{\zeta}} i_c^{5/2} \eta_{10}^{3/2} B_{-6}^{1/2} \text{ yr}^{-1}. \tag{4.48}$$

4.2.7 Neutrino fluxes in the particle-emission dominated regime

So far we have assumed that gravitational radiation is the dominant energy loss mechanism of strings. In the opposite regime, where the particle emission energy losses dominate, the loop's lifetime τ_{part} is independent of its length and is given by Eq. (4.24). We shall analyze this regime in the present section.

As before, we shall adopt the idealized model where the magnetic field B is turned on at time $t = t_B$, corresponding to redshift z_{max},

$$t_B \sim t_0(1 + z_{max})^{-3/2}. \tag{4.49}$$

The loops decay at the time $t_{dec} \sim t_B + \tau_{part}$. The rate of observable bursts $\dot{N}_b$ is given by Eq. (4.28) with I from Eq. (4.30), where the integration is taken between z_{dec} and z_{max} and z_{dec} is the redshift corresponding to the time t_{dec}.

If $\tau_{part} \gtrsim t_B$, the redshift z_{dec} is significantly different from z_{max}, with $\Delta z = z_{max} - z_{dec} \gtrsim 1$, and the value of I is not much different from that evaluated in Sec. 4.2.4. This is an intermediate regime, in which the results we obtained in Sections 4.2.4 and 4.2.5 for the rate of bursts and for the diffuse flux can still be used as order of magnitude estimates.

For $\tau_{part} \ll t_B$, the loops lose all their energy to particle emission in less than a Hubble time. The condition $\tau_{part} \sim t_B$ can also be expressed as $\dot{E}_{part}/\dot{E}_g(z_{max}) \sim 1$. Using Eq. (4.23) with $z_{max} \sim 3$, we find this condition is met for the smallest loops when

$$\eta \sim 6 \times 10^{10} i_c f_{-3} B_{-6} \ \text{GeV}. \tag{4.50}$$

It marks the boundary of the strong particle-emission domination regime and is shown by the inclined dotted line in Fig. 4.1. Below this line, the results of the preceding sections do not apply even by order of magnitude, but as we shall see, detectable neutrino fluxes can still be produced.

The redshift interval $\Delta z = z_{max} - z_{dec}$ for $\tau_{part} \ll t_B$ can be estimated as

$$\Delta z \approx \frac{2}{3}\frac{\tau_{part}}{t_B}(1 + z_{max}) \ll 1, \tag{4.51}$$

and the integral I in Eq. (4.30) is given by

$$I \approx \Delta z \frac{[(1+z_{max})^{1/2}-1]^2}{(1+z_{max})^{11/4}}. \tag{4.52}$$

With $z_{max} \sim 3$, we have $t_B \sim t_0/8$, and

$$\frac{\tau_{part}}{t_B} \sim 0.2 \frac{\eta_{10}}{f_{-3} B_{-6} i_c}. \tag{4.53}$$

The rate of bursts that are actually detected, $\dot{N}_b^{det}$, can be expressed as a product of $\dot{N}_b$ and the probability p_ν^{det} that at least one neutrino from the burst will be detected. This probability is simply related to the average number of detected neutrinos per burst N_ν^{det}, given by Eq. (4.42),

$$p_\nu^{det} = 1 - \exp(-N_\nu^{det}). \tag{4.54}$$

For $N_\nu^{det} \ll 1$, we have

$$p_\nu^{det} \approx N_\nu^{det} \tag{4.55}$$

and again taking $E > 1 \times 10^{19}$ eV,

$$\dot{N}_b^{det} \sim \dot{N}_b N_\nu^{det} \sim \frac{60\eta_{10}}{(1+z_{max})^{7/4}}\ yr^{-1} \sim 5\eta_{10}\ yr^{-1}, \tag{4.56}$$

where in the last step we have used $z_{max} \sim 3$. Requiring that $\dot{N}_b^{det} \gtrsim 1\ yr^{-1}$, we obtain the condition

$$\eta \gtrsim 10^9\ GeV. \tag{4.57}$$

Note that at the boundary of detectability, where $\eta \sim 10^9$ GeV, we always have $N_\nu^{det} \ll 1$, and thus the approximation (4.55) is justified. This boundary is the lower horizontal line bounding the observable parameter range in Fig. 4.1. Note also that Eq. (4.57) coincides with with the condition (4.20) for the burst-producing loops to be unaffected by friction.

It is interesting to note that the detection rate (4.56) in the particle-emission dominated regime is independent of i_c and depends only on the symmetry breaking scale η. This is in contrast with Eq. (4.37) for the case of gravitational radiation dominance, where the rate is proportional to i_c and independent of η.

4.2.8 Cascade upper limit on neutrino flux

In this section, we calculate the energy density of the cascade radiation in our model and compare it with $\omega_{cas} = 5.8 \times 10^{-7}\ eV/cm^3$ allowed by FERMI-LAT measurements [113].

The cascade energy density can be calculated as

$$\omega_{cas} = \int_0^{z_{max}} \frac{dz}{(1+z)^4} \int_{L_{min(z)}}^{L_{max(z)}} dL f_B n(L,t) \mathcal{L}_{em}(L,t) \tag{4.58}$$

where $\mathcal{L}_{em}(L,t) \sim \frac{1}{2}\mathcal{L}_{tot}(L,t)$ is the loop luminosity in the form of UHE electrons and photons produced by pion decays. The standard calculation (for $z_{max} = 3$) results in

$$\omega_{cas} \approx \frac{1.2 i_c (eBt_0^2)(t_{eq}/t_0)^{1/2} f_B}{7\Gamma^{1/2}} \frac{m_p}{t_0^3} \left[1 - (1+z_{max})^{-7/4}\right], \tag{4.59}$$

which numerically gives

$$\omega_{cas} \approx 8.3 \times 10^{-7}\, i_c\, f_{-3}\, B_{-6}\ \ eV/cm^3. \tag{4.60}$$

The energy density (4.60) does not depend on η and since $\omega_{cas} < \omega_{Fermi}$ for $i_c \lesssim 0.7$, it respects the general upper limit (1.38). For $i_c \sim 1$, the predicted neutrino flux (4.35) is close to the upper limit shown in Fig. 1.2.

4.3 UHE protons from superconducting strings

The cusps of superconducting strings in clusters of galaxies produce UHE nucleons at fragmentation of parton jets with a fraction of nucleons $\epsilon_N = 0.12$ [149] relative to the total number of hadrons. The generation rate $Q_p(\Gamma_p)$ of UHE protons with Lorentz factor Γ_p per unit comoving volume and unit time can be expressed through emissivity,

$$\mathcal{E}_0 = \int_{\Gamma_p^{min}}^{\Gamma_p^{max}} d\Gamma_p m_N \Gamma_p Q_p(\Gamma_p)\,, \tag{4.61}$$

where the emissivity $\mathcal{E}_0$ is the energy released in UHE protons at $z = 0$ per unit comoving volume per unit time, Γ_p^{max} and $\Gamma_p^{min} \sim 1$ are the maximum and minimum Lorentz factors of the protons, respectively, and m_N is the nucleon mass. For a power-law generation spectrum $Q_p(\Gamma_p) \sim \Gamma_p^{-2}$, we have

$$Q_p(\Gamma_p) = \frac{\mathcal{E}_0}{m_N \ln \Gamma_p^{max}} \Gamma_p^{-2}. \tag{4.62}$$

The emissivity is calculated as

$$\mathcal{E}_0 = \epsilon_N f_B \int_{L_{min}}^{L_{max}} dL n(L) \mathcal{E}_{tot}^{cusp}(L), \tag{4.63}$$

where L_{min} is given by (4.15), while $n(L)$ and $\mathcal{L}_{cusp}$ are given by (4.14) and (4.10), respectively. For $\mathcal{L}_{tot}^{cusp}$ one readily obtains

$$\mathcal{L}_{tot}^{cusp} = \frac{J^2 l}{eJ_c} \frac{i_c \gamma_c \eta}{l/2} = 0.2 i_c e B l \eta, \tag{4.64}$$

and after a simple calculation we have

$$\mathcal{E}_0 \approx 0.4 \frac{i_c \epsilon_N f_B (t_{eq}/t_0)^{1/2} e(Bt_0^2)}{\Gamma^{1/2}} \frac{m_p}{t_0^4}, \tag{4.65}$$

which numerically yields

$$\mathcal{E}_0 \approx 1.4 \times 10^{45} i_c f_{-3} B_{-6} \ erg/(Mpc^3\, yr). \tag{4.66}$$

One more parameter relevant for the calculation of $Q_p(\Gamma_p)$ is $\Gamma_p^{\max} = E_p^{max}/m_N$. It can be estimated using $E_p^{max} \sim 0.1\epsilon_X$, where $\epsilon_X = i_c\gamma_c\eta$ is the energy of the boosted X particles in the laboratory system, which being estimated for loops of length l_{min}, gives

$$\Gamma_p^{max} = 1 \times 10^{10} \eta_{10} i_c^2 \frac{1}{\Gamma G\mu} \frac{\eta}{eBt_0} \left(\frac{1\ GeV}{m_N}\right). \tag{4.67}$$

Notice that Γ_p^{max} does not depend on η and that it enters $Q_p(\Gamma_p)$ through $\ln \Gamma_p^{max}$.

Now we can calculate the space density of UHE protons using the generation rate $Q_p(\Gamma_p)$ given by (4.62) and taking into account propagation through CMB radiation with the help of the kinetic equation [150, 151]

$$\frac{\partial}{\partial t} n_p(\Gamma_p, t) - \frac{\partial}{\partial_{\Gamma_p}} [b(\Gamma_p, t) n_p(\Gamma_p, t)] = Q_p(\Gamma_p, t), \tag{4.68}$$

where $b(\Gamma_p, t) = -d\Gamma/dt$ describes energy losses of UHE protons interacting with CMB photons. For $\Gamma \geqslant 3 \times 10^{10}$, the proton energy losses become large and one can neglect the first term in the lhs of equation (4.68). Then Eq. (4.68) becomes stationary and its solution for $t = t_0$ reads

$$n_p(\Gamma_p) = \frac{1}{b(\Gamma_p)} \int_{\Gamma_p}^{\Gamma_p^{max}} Q_p(\Gamma_p) d\Gamma_p \approx \frac{\mathcal{E}_0}{m_N \Gamma_p\, b(\Gamma_p)\, \ln \Gamma_p^{max}}. \tag{4.69}$$

In terms of the proton energy $E = m_N\Gamma_p$ and the diffuse flux $J_p(E) = (1/4\pi) n_p(E)$, we have, in the standard form of presentation,

$$E^3 J_p(E) \approx \frac{1}{4\pi} \frac{\mathcal{E}_0}{\ln \Gamma_p^{max}} \frac{E^2}{b(E)}, \tag{4.70}$$

where $b(E) = dE/dt$. With $b(E)$ taken from [151] a numerical estimate at $E = 3 \times 10^{19}\ eV$ gives

$$E^3 J_p(E) \approx 1.3 \times 10^{24} i_c f_{-3} B_{-6}\ eV^2/(m^2\, s\, sr). \tag{4.71}$$

With $i_c \sim 1$, the calculated flux (4.71) coincides well with the measurements at the same energy, e.g., with the HiRes [109] flux $E^3 J_p(E) = 2.0 \times 10^{24}\ eV^2\, m^{-2}\, s^{-1}\, sr^{-1}$, so the cusp emission may account for the observed events at the highest energies. For $i_c \lesssim 0.1$ the UHE proton flux from superconducting strings is subdominant.

The UHE proton spectrum from superconducting strings has a sharper GZK cutoff than the standard spectrum for homogeneously distributed sources. This is due to the absence of clusters of galaxies in the vicinity of our galaxy. The nearest cluster, Virgo, is located at 18 Mpc from the Milky Way; other clusters are located at much larger distances. Nearby sources affect the spectrum at $E \geqslant 1 \times 10^{20}$ eV, where the proton spectrum from superconducting strings is predicted to be steeper than the standard one. The experimental data at present have too low statistics to distinguish the two cases.

In contrast, homogeneously distributed sources such as necklaces [152], give the dominant contribution at $E \geqslant (7-8) \times 10^{19}$ eV in the form of UHE photons, coming from nearby sources. In the case of superconducting strings such component is absent. The UHE photon component from superconducting strings is not dominant at energy lower than 5×10^{19} eV, because absorption of photons at these energies is stronger than for protons.

4.4 Conclusions

Superconducting cosmic strings produce high energy particles in the decay of charge carriers, X particles, ejected from the string cusps. The large Lorentz factor γ_c of the cusp boosts the energies of these particles and collimates them in a narrow beam with opening angle $\theta \sim 1/\gamma_c$. The basic string parameter is η, the scale of symmetry breaking, which we parametrize as $\eta = \eta_{10} 10^{10}\ GeV$. Another free parameter $i_c \lesssim 1$ determines the critical electric current in the cusp, $J_{max} = i_c e \eta$, and the mean energy of the charge carriers X escaping from the string, $\epsilon_X = i_c \gamma_c \eta$.

The astrophysical parameter which determines the electric current induced in the string is the magnitude of the magnetic field B in the relevant cosmic structures. The fraction f_B of the universe occupied by magnetic field B determines the flux of high-energy particles produced by superconducting strings. The most favorable values of B and f_B for the generation of a large flux of UHE neutrinos are $B \sim 10^{-6}\ G$ and $f_B \sim 10^{-3}$. They correspond to clusters of galaxies.

The main uncertainties of our model are related to the uncertainties in our understanding of the evolution of cosmic strings and of the origin and evolution of cosmic magnetic fields. On the cosmic string side, the key unknown quantity is the parameter β which sets the characteristic length of string loops in Eq. (4.1). Here, we used the value of $\beta \sim 0.1$, as suggested by numerical simulations in Refs. [82, 83, 84].

On the astrophysical side, basically unknown is the cosmological evolution of the magnetic field parameters $f_B(z)$ and $B(z)$ in the redshift interval $0 <$

$z < z_{max}$, where $z_{max} \sim 2 - 3$ is the redshift when the magnetic field was generated. For the space average value $\langle f_B(z)B(z)\rangle$ we use the numerical simulation by Ryu et al. [148], according to which this value remains roughly constant at $0 < z < 3$. Some important quantities, such as the diffuse neutrino flux $J_\nu(E)$, the cascade energy density ω_{cas}, and the UHE proton emissivity are determined by the evolution of the product $f_B(z)B(z)$. However, some other quantities, such as the rate of neutrino bursts and fluence depend on the evolution of $f_B(z)$ and $B(z)$ in other combinations. In these cases we consider the parameters f_{-3} and B_{-6} as effective values, using $f_{-3} \sim B_{-6} \sim 1$.

In addition, we adopted the following simplifying assumptions. The Lorentz factor of the cusp is characterized by a single fixed value γ_c, while in reality there is a distribution of Lorentz factors along the cusp. The spectrum of particles in a jet is approximated as E^{-2}, while a QCD calculation [143] gives a spectrum which is not a power law, with the best power-law fit as $E^{-1.92}$. We use cosmology with $\Lambda = 0$. The diffuse spectrum of UHE protons is calculated using very rough approximations. Given the uncertainties of string and magnetic field evolution, these simplifications are rather benign. On the other hand, they have the advantage of yielding analytic formulae, which allow us to clearly see the dependence of the results on the parameters involved in the problem. In particular, with the assumed particle spectrum $\sim E^{-2}$, the diffuse flux of neutrinos, the cascade upper limit and the diffuse flux of UHE protons do not depend on η. Since the realistic spectrum is very close to E^{-2}, this means that the quantities listed above depend on η very weakly.

We summarize the results obtained in this chapter as follows.

As our calculations show, among different sources, such as galaxies, group

of galaxies, filaments, etc., the largest diffuse flux is produced by clusters of galaxies with $B \sim 10^{-6}\ G$ in a cluster core and $f_B \sim 10^{-3}$. The calculated diffuse neutrino flux for three neutrino flavors and for $z_{max} = 3$ is

$$E^2 J_\nu(E) \sim 6.6 \times 10^{-8}\, i_c\, f_{-3}\, B_{-6}\ \ GeV/(cm^2\, s\, sr). \tag{4.72}$$

This flux respects the cascade upper limit, provided by the energy density of electrons, positrons and photons, which initiate electromagnetic cascades in collisions with CMB photons. The cascade energy density is calculated from Eq. (4.72) as

$$\omega_{cas} \approx 8.3 \times 10^{-7}\, i_c\, f_{-3}\, B_{-6}\ \ eV/cm^3. \tag{4.73}$$

and is close to the cascade limit for $i_c \sim 1$. It is the same as given by Eq. (4.60).

At energies $E \lesssim 10^{22}$ eV, the flux (4.72) is detectable by future detectors JEM-EUSO and Auger (South + North). The signature of the superconducting string model is the correlation of neutrinos with clusters of galaxies. We note, however, that the neutrino flux from the nearest cluster, Virgo, is undetectable by the above-mentioned detectors.

Another signature of the model is the possibility of multiple events, when several showers appear simultaneously in the field of view of the detector, e.g. JEM-EUSO. They are produced by neutrinos from the same jet. The time delay in arrival of neutrinos with different energies is negligibly small. Such multiple events are expected to appear for a certain range of parameters, as indicated in Fig. 4.1.

As an illustration, in Table 4.1 we show, for a representative value $\eta = 5 \times 10^{10}$ GeV, the diffuse neutrino flux, in units of the cascade upper limit J_ν^{max}, the rate of bursts, and the average shower multiplicity for several values

of i_c. Note that the bottom row in the table is the *average* multiplicity, that is, the average number of neutrinos detected per burst. For example, the low multiplicity at $i_c = 0.1$ indicates that only a small number (about 5) out of the 220 bursts per year will actually be detected. For $i_c = 1/3$, the average multiplicity is below 1, but Fig. 4.1 shows that we can expect at least one 2-neutrino burst per year.

i_c	1.0	1/2	1/3	0.1
J_ν/J_ν^{max}	0.42	0.21	0.14	0.042
rate of bursts	2.2 yr^{-1}	8.7 yr^{-1}	19.6 yr^{-1}	220 yr^{-1}
multiplicity	26	3.2	0.95	0.026

Table 4.1: The diffuse flux $J_\nu(E)$ in units of the cascade upper limit J_ν^{max} for 3 neutrino flavors, found from (1.38), the rate of neutrino bursts, and the shower multiplicity (the average number of neutrinos detected in one bursts), for $\eta = 5 \times 10^{10}$ GeV, $z_{max} = 3$ and different values of i_c. The multiplicity is shown for neutrinos with $E \gtrsim 10^{10}$ GeV from a burst at $z = 2$.

The diffuse flux of UHE protons is suppressed by the small fraction of nucleons produced at decay of X particles (the factor $\epsilon_N = 0.12$ is obtained in MC and DGLAP calculations [143]), and by energy losses of protons interacting with the CMB during propagation. The calculated flux at energy $E \geqslant 3 \times 10^{19}\ eV$ is given by the approximate formula

$$E^3 J_p(E) \approx \frac{1}{4\pi} \frac{\mathcal{E}_0}{\ln \Gamma_p^{max}} \frac{E^2}{b(E)} \tag{4.74}$$

where $b(E) = -dE/dt$ is the energy loss rate of protons, Γ_p^{max} is the maximum Lorentz factor of a proton at production, and $\mathcal{E}_0$ is the emissivity (energy in the form of protons emitted per unit comoving volume per unit time), given

by

$$\mathcal{E}_0 \approx 1.4 \times 10^{45}\, i_c\, f_{-3}\, B_{-6}\ \ erg/(Mpc^3\, yr) \tag{4.75}$$

For $i_c \sim 1$ and $E \sim 3 \times 10^{19}\ eV$, the proton flux can reach the value $1.3 \times 10^{24}\ eV^2\, m^{-2}\, s^{-1}\, sr^{-1}$, which can be compared for example with $2 \times 10^{24}\ eV^2\, m^{-2}\, s^{-1}\, sr^{-1}$ measured by HiRes [109]. Thus, radiation from cusps may account for observed events at the highest energies. The predicted spectrum at $E > 8 \times 10^{19}\ eV$ is steeper than the standard UHECR spectrum with homogeneous distribution of sources. The accompanying UHE gamma radiation is very low, due to large distances between the sources (clusters of galaxies).

As already mentioned, practically all predicted quantities, such as the diffuse neutrino flux (4.72), the cascade energy density (4.73), the diffuse flux of UHE protons (4.74) and the proton emissivity (4.75), do not depend on the basic string parameter η. There are only two observable quantities that do, the rate of neutrino bursts $\dot{N}_b$ and the neutrino fluence $\Phi(> E)$:

$$\dot{N}_b \sim 3 \times 10^2 \frac{B_{-6}^2 f_{-3}}{i_c^2 \eta_{10}^3}\ yr^{-1} \tag{4.76}$$

$$\Phi(> E) \approx 1 \times 10^{-2} \frac{i_c^3 \eta_{10}^3}{B_{-6}} \left(\frac{10^{10}\ GeV}{E}\right) \frac{1}{[(1+z)^{1/2} - 1]^2}\, km^{-2}, \tag{4.77}$$

As η decreases (at a fixed i_c), the rate of neutrino bursts goes up and the number of neutrinos detected in a burst,

$$N_\nu^{det}(> E) \approx 0.11 \frac{10^{10}\ \mathrm{GeV}}{E} \frac{i_c^3 \eta_{10}^3}{B_{-6}} \frac{1}{[(1+z)^{1/2} - 1]^2} \tag{4.78}$$

goes down, while the product $\dot{N}_b N_\nu^{det}$ remains η-independent.

We have considered here only ordinary field theory cosmic strings. Recent developments in superstring theory suggest [94, 153, 134] that the role of

cosmic strings can also be played by fundamental F-strings and by D-branes. Such strings may be superconducting, in which case they will also emit bursts of relativistic particles from their cusps. The main difference from the case of ordinary strings is that the probability for two intersecting strings to reconnect, which is $p = 1$ for ordinary strings, can be $p < 1$ and even $p \ll 1$ for F or D-strings. A low reconnection probability results in an enhanced density of loops; the particle production by loops is increased correspondingly.

UHE neutrinos from superconducting strings may have the following important signatures: correlation with clusters of galaxies and multiple neutrino-induced showers observed simultaneously in the field of view of a detector, e.g., JEM-EUSO.

Chapter 5

Conclusions

In this dissertation, we presented two new mechanisms for producing particles from cosmic (super)string loops and discussed their cosmological and observational effects. The first mechanism relies on the existence of moduli and the second one requires superconductivity.

Moduli are emitted by oscillating loops of cosmic strings provided that the frequency of oscillation is greater than the modulus mass m. This occurs when the loop sizes are very small, i.e., $L \lesssim 1/m$, hence moduli produced by this mechanism can have effects on the early universe cosmology. There are very stringent constraints on string tension for gravitationally coupled moduli. We showed that for moduli coupling to matter stronger than gravitational strength these constraints are significantly relaxed.

Moduli can also be produced from cusps with very large Lorentz boosts of order $\gamma_c \sim \sqrt{mL}$. This occurs for the loops of size $L \gtrsim 1/m$. We studied UHE neutrinos produced via hadronic decays of such moduli. We presented our results for a specific string theory inspired model, namely, the large volume

compactification scenario. We found that observable UHE neutrino fluxes can be achieved for the anticipated values of the modulus mass and coupling constant. For a wide range of string tension $G\mu$, UHE neutrino events with energies $E \gtrsim 10^{11}$ GeV are expected at sensitive neutrino detectors such as JEM-EUSO.

Superconducting cosmic strings can emit superheavy charge carriers from their cusps. Similar to the mechanism discussed above, these particles can decay via hadronic cascade and produce observable UHE neutrino fluxes. We showed that this can be realized with reasonable assumptions about the cosmic magnetic fields. This model predicts correlation with the clusters of galaxies and multiple neutrino-induced showers observed simultaneously in the field of view of a detector such as JEM-EUSO.

Bibliography

[1] E.P.S. Shellard and A. Vilenkin, "*Cosmic Strings and Other Topological Defects*", Cambrigde University Press (1994).

[2] M. B. Hindmarsh and T. W. B. Kibble, "*Cosmic strings*", Rept. Prog. Phys. **58**, 477 (1995) arXiv: hep-ph/9411342.

[3] E. J. Copeland and T. W. B. Kibble, "*Cosmic Strings and Superstrings*", Proc. Roy. Soc. Lond. **A 466**, 623 (2010) arXiv : hep-th/0911.1345.

[4] M. Sakellariadou, "*Cosmic Strings and Cosmic Superstrings*", Nucl. Phys. Proc. Suppl. **192-193**, 68-90 (2009) arXiv: hep-th/0902.0569.

[5] J. P. Preskill, "*Cosmological production of superheavy magnetic monopoles*", Phys. Rev. Lett. **43**, 1365 (1979).

[6] Ya. B. Zel'dovich, I. Yu. Kobzarev and L. B. Okun, "*Cosmological consequences of the spontaneous breakdown of a discrete symmetry*", Sov. Phys. JETP **40**, 1 (1975).

[7] A. Vilenkin, "*Gravitational field of vacuum domain walls and strings*", Phys. Rev **D 23**, 852 (1981).

[8] V. Berezinsky, P. Blasi and A. Vilenkin, "*Signatures of topological defects*", Phys. Rev. D **58**, 103515 (1998) arXiv: astro-ph/9803271.

[9] P. Bhattacharjee and G. Sigl, "*Origin and propagation of extremely high-energy cosmic rays*", Phys. Rept. **327**, 109 (2000) arXiv: astro-ph/9811011.

[10] T. Vachaspati, "*Cosmic Rays from Cosmic Strings with Condensates*", Phys. Rev. **D 81**, 043531 (2010) arXiv: astro-ph.CO/0911.2655.

[11] V. Berezinsky, K. D. Olum, E. Sabancilar, A. Vilenkin, "*UHE neutrinos from superconducting cosmic stings*", Phys. Rev. **D 80**, 023014 (2009) arXiv: astro-ph.CO/0901.0527.

[12] E. Morganson, P. Marshall, T. Treu, T. Schrabback and R. D. Blandford, "*Direct Observation of Cosmic Strings via their Strong Gravitational Lensing Effect: II. Results from the HST/ACS Image Archive*", MNRAS, **Vol. 406**, 2452 (2010) arXiv : astro-ph.CO/0908.0602.

[13] N. Kaiser and A. Stebbins, "*Microwave anisotropy due to cosmic strings*", Nature **310**, 391 (1984).

[14] M. Wyman, L. Pogosian and I. Wasserman, "*Bounds on Cosmic Strings from WMAP and SDSS*", Phys. Rev. **D 72**, 032513 (2005), Erratum: Phys. Rev. **D 73**, 089905 (2006) arXiv:astro-ph/0503364.

[15] N. Bevis, M. Hindmarsh, M. Kunz and J. Urestilla, "*Fitting CMB data with cosmic strings and inflation*", Phys. Rev. Lett. **100**, 021301 (2008) arXiv: astro-ph/0702223.

[16] L. Pogosian, S-H. H. Tye, I. Wasserman and M. Wyman, "*Cosmic strings as the source of small-scale microwave background anisotropy*", JCAP **0902**, 013 (2009) arXiv: astro-ph/0804.0810.

[17] A. A. Fraisse, "*Limits on defects formation and hybrid inflationary models with three-year WMAP observations*", JCAP **0703**, 008 (2007) arXiv: astro-ph/0603589.

[18] L. Pogosian and M. Wyman, "*B-modes from cosmic strings*", Phys. Rev. **D 77**, 083509 (2008) astro-ph/0711.0747.

[19] A. Babul, B. Paczynski and D.N. Spergel, "*Gamma-ray bursts from superconducting cosmic strings at large redshifts*", Ap. J. Lett. **316**, L49 (1987).

[20] V. Berezinsky, B. Hnatyk and A. Vilenkin, "*Gamma ray bursts from superconducting cosmic strings*", Phys. Rev. **D 64**, 043004 (2001) arXiv: astro-ph/0102366.

[21] K. S. Cheng, Y. W. Yu and T. Harko, "*High Redshift Gamma-Ray Bursts: Observational Signatures of Superconducting Cosmic Strings?*", Phys. Rev. Lett. **104**, 241102 (2010) [arXiv : astro-ph.HE/1005.3427].

[22] T. Vachaspati, "*Cosmic Sparks from Superconducting Strings*", Phys. Rev. Lett. **101**, 141301 (2008) arXiv: astro-ph/0802.0711.

[23] T. Damour and A. Vilenkin, "*Gravitational wave bursts from cusps and kinks on cosmic strings*", Phys. Rev. **D 64**, 064008 (2001) arXiv: gr-qc/0104026.

[24] T. Damour and A. Vilenkin, "*Gravitational radiation from cosmic (super)strings: bursts, stochastic background, and observational windows*", Phys. Rev. **D71**, 063510 (2005) arXiv: hep-th/0410222.

[25] T. Damour and A. Vilenkin, "*Cosmic strings and the string dilaton*", Phys. Rev. Lett. **78** 2288 (1997) arXiv: gr-qc/9610005.

[26] M. Peloso and L. Sorbo, "*Moduli from cosmic strings*", Nucl. Phys. **B 649** 88 (2003) hep-ph/0205063.

[27] E. Babichev and M. Kachelriess, "*Constraining cosmic superstrings with dilaton emission*", Phys. Lett. **B 614**, 1 (2005) arXiv: hep-th/0502135.

[28] E. Sabancilar, "*Cosmological Constraints on Strongly Coupled Moduli from Cosmic Strings*", Phys. Rev. **D 81**, 123502 (2010) arXiv: hep-ph/0910.5544.

[29] L. Randall and R. Sundrum, "*A Large Mass Hierarchy from a Small Extra Dimension*", Phys. Rev. Lett. **83**, 3370 (1999) arXiv: hep-ph/9905221.

[30] W. D. Goldberger and M. B. Wise, "*Phenomenology of a Stabilized Modulus*", Phys. Lett. **B 475**, 275 (2000) arXiv: hep-ph/9911457.

[31] F. Brummer, A. Hebecker and E. Trincherini, "*The Throat as a Randall-Sundrum Model with Goldberger-Wise Stabilization*", Nucl. Phys. **B 738**, 283 (2006) arXiv: hep-th/0510113.

[32] J. P. Conlon, F. Quevedo and Kerim Suruliz, "*Large-volume Flux Compactifications: Moduli Spectrum and D3/D7 Soft Supersymmetry Breaking*", JHEP **08**, 007 (2005) arXiv: hep-th/0505076.

[33] J. P. Conlon and F. Quevedo, "*Astrophysical and Cosmological Implications of Large Volume String Compactifications*", JCAP **08**, 019 (2007) arXiv: hep-ph/0705.3460.

[34] A. R. Frey and A. Maharana, "*Warped Spectroscopy: Localization of Frozen Bulk Modes*", JHEP **08**, 021 (2006) arXiv: hep-th/0603233.

[35] C. P. Burgess et al., "*Warped Supersymmetry Breaking*", JHEP **04**, 053 (2008) arXiv: hep-th/0610255.

[36] WMAP Collaboration, "*Seven-Year Wilkinson Microwave Anisotropy Probe (WMAP) Observations: Cosmological Interpretation*", Astrophys. J. Suppl. **192**, 18 (2011) arXiv: astro-ph.CO/1001.4538.

[37] A. Friedman, "*Uber die Krummung des Raumes*". Z. Phys **10**, 377 (1922) [English translation: "*On the Curvature of Space*", Gen. Rel. Grav. **31**, 1991 (1999)].

[38] G. Lemaitre, Ann. Soc. Sci. Bruxelles **47**, 49 (1927) [English translation: "*A homogeneous universe of constant mass and increasing radius accounting for the radial velocity of extra-galactic nebulae*", Mon. Not. R. Astron. Soc. **91**, 483 (1931)].

[39] E. Hubble,"*A Relation between Distance and Radial Velocity among Extra-Galactic Nebulae*", Proc. Nat. Acad. Sci. **15**, 168 (1929).

[40] H. P. Robertson,"*Kinematics and World-Structure*", Astrophys. J. **82**, 284 (1935).

[41] A. G. Walker, "*On Milnes theory of world structure*", Proc. London Math. Soc. **42**, 90 (1936).

[42] W. de Sitter, "*On the curvature of space*", Proc. Kon. Ned. Acad. Wet. **20**, 229 (1917); "*Einstein's theory of gravitation and its astronomical consequences*", Mon. Not. R. Astron. Soc. **78**, 3 (1917).

[43] A. Penzias and R. Wilson, "*A Measurement of Excess Antenna Temperature at 4080 Mc/s*", Ap. J. **142**, 419 (1965).

[44] G. F. Smoot et al., "*Structure in the COBE differential microwave radiometer first-year maps*", Ap. J. **396**, L1 (1992).

[45] J. C. Mather et al., "*Measurement of the cosmic microwave background spectrum by the COBE FIRAS instrument*", Ap. J. **420**, 439 (1994).

[46] A. H. Guth, "*The Inflationary Universe: A Possible Solution to the Horizon and Flatness Problems*", Phys. Rev. **D 23**, 347 (1981).

[47] A. D. Linde, "*A New Inflationary Universe Scenario: A Possible Solution of the Horizon, Flatness, Homogeneity, Isotropy and Primordial Monopole Problems*", Phys. Lett. **B 108**, 389 (1982).

[48] A. Albrecht and P. J. Steinhardt, "*Cosmology for Grand Unified Theories with Radiatively Induced Symmetry Breaking*", Phys. Rev. Lett. **48**, 1220 (1982).

[49] V. F. Mukhanov and G. V. Chibisov,"*Quantum Fluctuation and Nonsingular Universe*", JETP Lett., **33**, 532 (1981).

[50] A. Linde, "*Particle physics and inflationary cosmology*", Harwood (1990) hep-th/0503203.

[51] S. Weinberg, "*Cosmology*", Oxford University Press (2008).

[52] A. D. Sakharov, "*Violation of CP Invariance, c Asymmetry, and Baryon Asymmetry of the Universe*", Pisma Zh. Eksp. Teor. Fiz. **5**, 32 (1967).

[53] J. Goldstone, "*Field Theories with Superconductor Solutions*", Nuovo Cim. **19**, 154 (1961).

[54] P. W. Higgs, "*Broken Symmetries, Massless Particles and Gauge Fields*", Phys. Lett. **12**, 132 (1964).

[55] F. Englert and R. Brout, *Broken Symmetry and the Mass of Gauge Vector Mesons*, Phys. Rev. Lett. **13**, 321 (1964).

[56] G. S. Guralnik, C. R. Hagen, and T. W. B. Kibble, "*Global Conservation Laws and Massless Particles*", Phys. Rev. Lett. **13**, 585 (1964).

[57] C. N. Yang and R. L. Mills, "*Conservation of Isotopic Spin and Isotopic Gauge Invariance*", Phys. Rev. **96**, 191 (1954).

[58] S. L. Glashow, "Partial-symmetries of weak interactions", Nucl. Phys. **22**, 579 (1961).

[59] S. Weinberg, "*A model of leptons*", Phys. Rev. Lett. **19**, 1264 (1967).

[60] A. Salam, In "*Elementary Particle Theory*", ed. N. Svartholm (Almquist and Wiksells, 367 (1969).

[61] UA1 Collaboration-CERN, "*Experimental Observation of Isolated Large Transverse Energy Electrons with Associated Missing Energy at* $\sqrt{s} =$ 540 *GeV*", Phys.Lett. **B 122**, 103 (1983); "*Experimental Observation of Lepton Pairs of Invariant Mass Around* 95 GeV/c^2 *at the CERN SPS Collider*", Phys. Lett. **B 126**, 398 (1983).

[62] UA2 Collaboration-CERN, "*Observation of Single Isolated Electrons of High Transverse Momentum in Events with Missing Transverse Energy at the CERN anti-p p Collider*", Phys. Lett. B 122, 476 (1983); "*Evidence for* $Z^0 \to e^+e^-$ *at the CERN anti-p p Collider*", Phys. Lett. **B 129**, 130 (1983).

[63] H. Georgi and S. L. Glashow, "*Unity of All Elementary Particle Forces*", Phys. Rev. Lett. **32**, 438 (1974).

[64] S. Coleman and J. Mandula, "*All Possible Symmetries Of The S Matrix*", Phys. Rev. **159**, 1251 (1967)

[65] P. West, *Introduction to Supersymmetry and Supergravity*, World Scientific (1986).

[66] J. L. Gervais and B. Sakita, "*Field Theory Interpretation Of Supergauges In Dual Models*", Nucl. Phys. **B34**, 632 (1971).

[67] S. Weinberg, *The Quantum Theory of Fields Vol. III Supersymmetry*, Cambridge University Press (1995).

[68] K. Becker, M. Becker and J. H. Schwarz, "*String Theory and M-Theory: A Modern Introduction*", Cambridge University Press (2007).

[69] D. A. Kirzhnits, "*Weinberg model and the 'hot' universe*", JETP Lett. **15**, 745 (1972).

[70] D. A. Kirzhnits and A. D. Linde, "*Macroscopic consequences of the Weinberg model*", Phys. Lett. **B 42**, 471 (1972).

[71] H. B. Nielsen and P. Olesen, "*Vortex Line Models for Dual Strings*", Nucl. Phys. **B 61**, 45 (1973).

[72] E. B. Bogomol'nyi, "*The stability of classical solutions*", Sov. J. Nucl. Phys. **24**, 449 (1976).

[73] T. W. B. Kibble, "*Topology of Cosmic Domains and Strings*", J. Phys. **A A9**, 1387 (1976).

[74] E. P. S. Shellard, "*Cosmic String Interactions*", Nucl. Phys.**B 283**, 624 (1987).

[75] R. A. Matzner, "*Interaction of U(1) Cosmic Strings: Numerical Intercommutation*, Comput. Phys. **2**, 51 (1988).

[76] K. J. M. Moriarty, E. Myers and C. Rebbi, "*Dynamical Interactions Of Flux Vortices In Superconductors*", Phys. Lett. **B 207**, 411 (1988).

[77] L. M. A. Bettencourt and T. W. B. Kibble, "*Nonintercommuting configurations in the collisions of type I U(1) cosmic strings*", Phys. Lett. **B 332**, 297 (1994) arXiv: hep-ph/9405221.

[78] N. D. Mermin, "*The topological theory of defects in ordered media*", Rev. Mod. Phys. **51**, 591 (1979).

[79] M. G. Jackson, N. T. Jones and J. Polchinski, "*Collisions of cosmic F- and D-strings*", JHEP **10**, 013 (2005)[arXiv : hep-th/0405229].

[80] J. Polchinski, "*Introduction to Cosmic F- and D-Strings*", arXiv: hep-th/0412244.

[81] J. Polchinski and J. V. Rocha, "*Analytic study of small scale structure on cosmic strings*", Phys. Rev. **D 74**, 083504 (2006).

[82] V. Vanchurin, K. D. Olum and A. Vilenkin, "*Scaling of Cosmic String Loops*", Phys. Rev. **D 74**, 063527 (2006).

[83] K. D. Olum and V. Vanchurin, "*Cosmic String Loops in the Expanding Universe*", Phys. Rev. **D 75**, 063521 (2007).

[84] J.J. Blanco-Pillado, K. D. Olum and B. Shlaer, "*Large parallel cosmic string simulations: New results on loop production*", [arXiv : astro-ph.CO/1101.5173].

[85] J. Polchinski and J. V. Rocha, "*Cosmic string structure at the gravitational radiation scale*", Phys. Rev. **D 75**, 123503 (2007).

[86] E. Witten, "*Superconducting Strings*", Nucl. Phys. **B 249**, 557 (1985).

[87] A. Everett, "*New Mechanism For Superconductivity In Cosmic Strings*", Phys. Rev. Lett. **61**, 1807 (1988).

[88] C. T. Hill, H. M. Hodges and M. S. Turner, "*Bosonic Superconducting Cosmic Strings*", Phys. Rev. **D 37**, 263 (1988).

[89] D. Haws, M. Hindmarsh and N. Turok, "*Superconducting Strings Or Springs?*", Phys. Lett. **B 209**, 255 (1988).

[90] R. L. Davis and E. P. S. Shellard, "*The Physics Of Vortex Superconductivity*", Phys. Lett. **B 207**, 404 (1988); "*The Physics Of Vortex Superconductivity 2*", Phys.Lett. **B 209**, 485 (1988).

[91] E. Witten, "*Cosmic Superstrings*", Phys. Lett. **B 153**, 243 (1985).

[92] A. Vilenkin and A. E. Everett, "*Cosmic strings and domain walls in models with Goldstone and pseudogoldstone bosons*", Phys. Rev. Lett. **48**, 1867 (1982).

[93] G. R. Dvali and S.H. Henry Tye, "*Brane Inflation*", Phys. Lett. **B 450**, 72 (1999) arXiv: hep-ph/9812483.

[94] S. Sarangi and S. H. Henry Tye, "*Cosmic string production towards the end of brane inflation*", Phys. Lett. **B 536**, 185 (2002) arXiv: hep-th/0204074.

[95] A. Linde, "*Hybrid Inflation*", Phys. Rev. **D 49**, 748 (1994) arXiv: astro-ph/9307002.

[96] M. Sakellariadou, "*A note on the evolution of cosmic string/superstring networks*", JCAP 0504, 003 (2005).

[97] G. B. Hobbs et al., "*Gravitational wave detection using pulsars: status of the Parkes Pulsar Timing Array project*", PASA **26**, 103 (2009) arXiv: astro-ph/0812.2721.

[98] A. Vilenkin, "*Cosmological Density Fluctuations Produced by Vacuum Strings*", Phys. Rev. Lett. **46**, 1169 (1981).

[99] T. W. B. Kibble and N. Turok, "*Selfintersection of Cosmic Strings*", Phys. Lett. **B 116**, 141 (1982).

[100] P. Bhattacharjee, T. W. B. Kibble and N. Turok, "*Baryon Number From Collapsing Cosmic Strings*", Phys. Lett. **B 119**, 95 (1982).

[101] P. Bhattacharjee and N. C. Rana, "*Ultrahigh-energy Particle Flux From Cosmic Strings*", Phys. Lett. **B 246**, 365 (1990).

[102] A. J. Gill and T. W. B. Kibble, "*Cosmic rays from cosmic strings*", Phys. Rev. **D 50**, 3660 (1994) arXiv: hep-ph/9403395.

[103] J. H. MacGibbon and R. H. Brandenberger, "*High-energy Neutrino Flux From Ordinary Cosmic Strings*", Nucl. Phys. **B 331**, 153 (1990).

[104] P. Bhattacharjee, "*Cosmic Strings and Ultrahigh-Energy Cosmic Rays*", Phys. Rev. **D 40**, 3968 (1989).

[105] J. J. Blanco-Pillado and K. D. Olum, "*The form of cosmic string cusps*", Phys. Rev. **D 59**, 063508 (1999) arXiv: gr-qc/9810005.

[106] M. Nagano,"*Search for the end of the energy spectrum of primary cosmic rays*", New J. Phys. **11**, 065012 (2009).

[107] K. Greisen, "*End to the Cosmic-Ray Spectrum?*", Phys. Rev. Lett. **16**, 748 (1966).

[108] G. T. Zatsepin and V. A. Kuz'min, "*Upper Limit of the Spectrum of Cosmic Rays*", JETP Lett. **4**, 78 (1966).

[109] R. U. Abbasi et al. [HiRes Collaboration], "*First observation of the Greisen-Zatsepin-Kuzmin suppression*", Phys. Rev. Lett. **100**, 101101 (2008) arXiv: astro-ph/0703099.

[110] J. Abraham et al. [Pierre Auger Collaboration], "*The Cosmic Ray Energy Spectrum and Related Measurements with the Pierre Auger Observatory*", arXiv: astro-ph.CO/0906.2189.

[111] V. S. Berezinsky, "*Neutrino astronomy and massive longlived particles from big bang*", Nucl. Phys. **B 380**, 478 (1992).

[112] P. Sreekumar et al. (EGRET Collaboration), "*EGRET Observations of the Extragalactic Gamma Ray Emission* , Astrophys. J. **494**, 523 (1998).

[113] A. A. Abdo et al. [FERMI-LAT Collaboration], "*The Spectrum of the Isotropic Diffuse Gamma-Ray Emission Derived From First-Year Fermi Large Area Telescope Data*", Phys. Rev. Lett. **104**, 101101 (2010) arXiv: astro-ph.HE/1002.3603.

[114] V. Berezinsky and A. Smirnov, "*Cosmic neutrinos of ultra-high energies and detection possibility*", Ap. Sp. Sci., **32**, 461 (1975).

[115] V. S. Berezinsky, S. V. Bulanov, V. A. Dogiel, V. L. Ginzburg and V. S. Ptuskin, "*Astrophysics of Cosmic Rays*", North-Holland 1990.

[116] V. Berezinsky, "*Ultra High Energy Neutrino Astronomy*", Nucl. Phys. B Proc. Suppl. **151**, 260 (2006).

[117] V. S. Berezinsky and G. T. Zatsepin, "*Cosmic rays at ultra high energies (neutrino?)*", Phys. Lett **B 28**, 423 (1969); V. S. Berezinsky and G. T. Zatsepin, Soviet Journal of Nuclear Physics **11**, 111 (1970).

[118] O. E. Kalashev, V. A. Kuzmin, D. V. Semikoz and G. Sigl, "*Ultrahigh-energy neutrino fluxes and their constraints*", Phys. Rev. D **66**, 063004 (2002).

[119] H. Takami, K. Murase, S. Nagataki and K. Sato, "*Cosmogenic neutrinos as a probe of the transition from Galactic to extragalactic cosmic rays*", Astropart. Phys. **31**, 201 (2009).

[120] C. T. Hill, D. N. Schramm and T. P. Walker, "*Ultra-high-energy cosmic rays from superconducting cosmic strings*", Phys. Rev. D **36**, 1007 (1987).

[121] V. Berezinsky, M. Kachelriess and A. Vilenkin,"*Ultrahigh Energy Cosmic Rays without Greisen-Zatsepin-Kuzmin Cutoff*", Phys. Rev. Lett. **79**, 4302 (1997).

[122] V. A. Kuzmin and V. A. Rubakov, "*Ultrahigh-energy cosmic rays: A Window to postinflationary reheating epoch of the universe?*", Phys. Atom. Nucl. **61** 1028 (1998) [Yad. Phys. **61**, 1122 (1998)].

[123] E. W. Kolb, D. J. H. Chung and A. Riotto, "*Nonthermal Supermassive Dark Matter*", Phys. Rev. Lett. **81**, 4048 (1998).

[124] V. A. Kuzmin and I. I. Tkachev, "*Ultrahigh-energy cosmic rays, superheavy long-lived particles, and matter creation after inflation*", JETP Lett. **68** (1998) 271-275.

[125] C. D. Anderson, "*The Positive Electron*", Phys. Rev. **43**, 491(1933).

[126] C. D. Anderson and S. H. Neddermeyer, "*Cloud Chamber Observations of Cosmic Rays at 4300 Meters Elevation and Near Sea-Level*", Phys.Rev. **50**, 263 (1936).

[127] J. C. Street and E. C. Stevenson, "*New Evidence for the Existence of a Particle Intermediate Between the Proton and Electron*", Phys. Rev. **52**, 1003 (1937).

[128] C.M.G.Lattes, H. Muirhead, G. P. S. Occhialini, C. F. Powell, "*Processes Involving Charged Mesons*", Nature **159**, 694 (1947).

[129] Y. Takahashi, JEM-EUSO Collaboration, "*The Jem-Euso Mission*", [arXiv : astro-ph/0910.4187].

[130] S. B. Giddings, S. Kachru and J. Polchinski, "*Hierarchies from fluxes in string compactifications*", Phys. Rev. **D 66**, 106006 (2002).

[131] M. R. Douglas, "*The statistics of string/M theory vacua*", JHEP **03**, 046 (2003).

[132] S. Kachru, R. Kallosh, A. Linde and S. P. Trivedi, "*De Sitter Vacua in String Theory*", Phys. Rev. **D 68**, 046005 (2003).

[133] S. Kachru, R. Kallosh, A. Linde, J. M. Maldacena, L. P. McAllister and S. P. Trivedi, "*Towards Inflation in String Theory*", JCAP **10**, 013 (2003).

[134] G. Dvali and A. Vilenkin, "*Formation and Evolution of Cosmic D Strings*", JCAP **03**, 010 (2004).

[135] M. Kawasaki, K. Kohri and T. Moroi, "*Hadronic Decay of Late-Decaying Particles and Big-Bang Nucleosynthesis*", Phys. Lett. **B 625**, 7 (2005) arXiv: astro-ph/0402490.

[136] K. Jedamzik, "*Big Bang Nucleosynthesis Constraints on Hadronically and Electromagnetically Decaying Relic Neutral Particles*", Phys. Rev. **D 74**, 103509 (2006).

[137] J. Ellis, K. A. Olive and E. Vangioni, "*Effects of Unstable Particles on Light-element Abundances: Lithium versus Deuterium and He-3*", Phys. Lett. **B 619**, 30 (2005).

[138] C. D. Hoyle, et al., "*Sub-milimeter Tests of the Gravitational Inverse-square Law* ", Phys. Rev. **D 70**, 042004 (2004).

[139] F. Dubath, J. Polchinski and J. V. Rocha, "*Cosmic String Loops, Large and Small*", Phys. Rev. **D 77**, 123528 (2008).

[140] V. Vanchurin, "*Cosmic String Loops: Large and Small, but not Tiny*", Phys. Rev. **D 77**, 063532 (2008).

[141] C. J. A. Martins and E. P. S. Shellard, "*Fractal Properties and Small-scale Structure of Cosmic String Networks*", Phys. Rev. **D 73**, 043515 (2006).

[142] C. Ringeval, M. Sakellariadou and F. Bouchet, "*Cosmological Evolution of Cosmic String Loops*", JCAP **02**, 023 (2007).

[143] V. Berezinsky and M. Kachelriess, "*Monte Carlo simulation for jet fragmentation in SUSY QCD*", Phys. Rev. **D 63**, 034007 (2001); R. Aloisio, V. Berezinsky and M. Kachelriess, "*Fragmentation functions in supersymmetric QCD and ultrahigh energy cosmic ray spectra produced in top-down models*", Phys. Rev. **D 69**, 094023 (2004); S. Sarkar and R. Toldra, "*Production of ultra-energetic cosmic rays through the decay of super-heavy X particles*", Nucl. Phys. **B 621**, 495 (2002); C. Barbot

and M. Drees, "*The high energy cosmic ray spectrum from relic particle decay*", Phys. Lett. **B 533**, 107 (2002).

[144] M. Kachelriess, *Private communication.*

[145] D. N. Spergel, W. H. Press and J. Goodman, "*Dynamics of superconducting cosmic strings*", Nucl. Phys. **B291**, 847 (1987).

[146] T. Vachaspati and A. Vilenkin, "*Gravitational radiation from cosmic strings*", Phys. Rev. **D31**, 3052 (1985).

[147] C.J. Hogan and M.J. Rees, "*Gravitational interactions of cosmic strings*", Nature **311**, 109 (1984).

[148] D. Ryu, H. Kang, J. Cho and S. Das, "*Turbulence and Magnetic Fields in the Large-Scale Structure of the Universe*", Science **320**, 909 (2008).

[149] R. Aloisio, V. Berezinsky, M. Kachelriess, "*Fragmentation functions in supersymmetric QCD and ultrahigh energy cosmic ray spectra produced in top-down models*", Phys. Rev. D, **69**, 094023 (2004)

[150] M.S. Longaire, "*High Energy Astrophysics*", Cambridge University Press, (1987).

[151] V. Berezinsky, A. Gazizov and S. Grigorieva, "*On astrophysical solution to ultrahigh energy cosmic rays*", Phys. Rev. D **74** 043005 (2006).

[152] V. Berezinsky and A. Vilenkin, "*Cosmic Necklaces and Ultrahigh Energy Cosmic Rays*", Phys. Rev. Lett. **79**, 5202 (1997).

[153] E. J. Copeland, R. C. Myers and J. Polchinski, "*Cosmic F- and D-strings*", JHEP 0406, 013 (2004).